Evolution of Pile Shaft Capacity over Time in Soft Clays (Case Study: Leda Clay)

by

Mohammadamin Hosseini

A thesis submitted to the Faculty of Graduate and Postdoctoral Affairs in partial fulfillment of the requirements for the degree of

Master of Applied Science

in

Civil Engineering

Carleton University
Ottawa, Ontario

ABSTRACT

This thesis presents a comprehensive experimental investigation to examine the evolution of pile shaft capacity over time. This phenomenon is observed in pile foundations that are driven into soft clays, and is referred to as pile set-up and/or freeze. This research consists of two phases which the first phase investigates the behavior of pile-soil interface over time using a modified direct shear test at two different loading rates of slow (0.05 mm/min.) and fast (2.5 mm/min.). These laboratory tests were used to understand the concept of pile-soil interface in relation with pile set-up. The second phase of this research involved a series of pile load testing which was performed on steel and concrete piles driven into Leda clay in a test site located in southeast of Ottawa region, called the Canadian Geotechnical Research Site No.1. The piles were tested immediately after driving to measure their initial bearing capacities, and were tested repeatedly over different elapsed time to study the change in pile shaft capacity over time. Meanwhile, the excess pore water pressure around the pile was also monitored by a pore water pressure sensor. The average pile capacity measurements for both steel and concrete piles indicated that there is approximately 4.5-5.5 times increase in the pile capacity after 30 days from the initial day depending on the type of the piles used.

Dedicated

To My Parents

Acknowledgements

First and foremost, I would like to express my very great appreciation to my supervisor, Dr. Mohammad Rayhani, for his guidance, valuable suggestions and supports during the development of this research work. I gratefully thank my thesis committee and for their constructive clarifications on my thesis work. I would like to offer my special thanks to my colleagues for their invaluable support through my research program. I would also like to extend my thankfulness to the Civil and Environmental Engineering laboratory technicians for their help in providing information in proceeding the research program.

Last but not the least, I would like to thank my family: mom and dad and to my brothers for supporting me spiritually throughout completing this thesis and encouraging me to continue my studies. Words may not express how thankful I am to my parents because their prayer for me was what supported me thus far.

Table of Contents

List of Figures

List of Tables

List of Appendices

Chapter 1: Introduction

1.1 Overview: Pile Capacity Increase over Time

A pile is a slender member made of steel, concrete, timber, plastic, or composites, installed in the ground to transfer the superstructure loads to soils at specific depths under the base of the structure. Typically, pile foundations are used when the soil does not have a sufficient bearing capacity to support the structural loads, when the estimated settlement exceeds the limits, and other elements that may make the pile foundation a suitable option. Piles are categorised based on the type of load transfer as end-bearing piles and friction piles. While an end-bearing pile transfers loads to an end-bearing layer, friction piles resist most loads through the skin friction, which is developed along the pile shaft. The resistance of friction piles are dependent on the interaction of the pile shaft and adjacent soils. The method of installation also affects the load transfer behaviour of the pile and includes driving, boring, cast-in-place, and screw piling. In the driving method, the pile is normally driven into the ground using a hammer system (e.g., drop hammers, pneumatic hydraulic hammers, diesel hammers, and vibratory hammers), while cast-in-place piles are formed by concrete fill in an excavated borehole in the site. The method of installation may affect the soil stress and strain states, and therefore, particular techniques are utilized to drive the piles based on the pile properties and the type of the soil.

Piles driven into various types of soil, specifically in clay, may experience an increase in capacity as a function of time, due to the dissipation of excess pore water pressure generated

around the pile during pile driving. This phenomenon of increase in pile capacity over time is referred to as set-up or freeze, and recently, it has been called side shear set-up (Bullock et al. 2005). Pile set-up is of critical importance in the design of piles and occurs in almost all types of soils, including organic or inorganic clay, loose to medium dense silt, sandy silt, and fine sand (Astedt and Holm, 1992; Hannigan et al., 1997). In the past several years, a number of mechanisms have been suggested to help understand pile set-up and the influential parameters that can affect the rate of set-up. In clay soils, the set-up is related to reconsolidation of the disturbed soil around the pile and aging (Randolph et al., 1979).

During pile driving, high excess pore water pressure is normally developed in the surrounding soil near the pile. This excess pore water pressure will cause a reduction in the effective stresses and, hence, the shear strength of the soil for a specific period of time after driving. The amount of excess pore water pressure can approach up to twice the in-situ vertical effective stress, although there is much higher pore water pressure at the toe of the pile, and this pressure can reach up to 3 to 4 times the effective stress (Randolph et al., 1979). In the case of sensitive soils such as Leda clay, the result of pore water pressure may be greater, up to 8 times the effective stress (Poulos and Davis 1980). The concept of pore water pressure dissipation was used to explain the gain in pile capacity over time after driving by Seed and Reese (1955).

Many researchers investigated the pile set-up in different types of soils during last decades. Although, this rich literature provides an insight to the subject of the pile set-up, but the exact mechanism of set-up is not fully clear. Furthermore, most of the suggested empirical relationships that were developed through data from lab/field tests and modeling the pile set-up have only provided information for specific regions with particular soil characteristics. In this study, the rate of set-up specifically in sensitive clay is investigated as there is a need to develop a dependable

set-up rate for driven piles in sensitive clay due to lack of proper investigation and understanding. Thus, this research aims to investigate and evaluate the pile set-up by performing medium-scale pile load tests in sensitive clay, while monitoring the pore water pressure, in order to use the aftermath for future practice. Due to lack of full understanding of the pile set-up, most designers use conservative approaches to design driven piles in sensitive soils by relying the pile load test results after installation of the pile. Proper monitoring and accurate approximation of set-up rates would reduce the cost of construction and still provide satisfactory performance from the pile.

1.2 Objective and Scope of Research

This research is aimed at developing a prediction system that can be used to estimate the pile capacity increase in sensitive clays and to develop a relationship between the pile capacity and elapsed time after initial installation. The research involves a series of laboratory tests that will examine the evolution of pile-soil interface strength over time, as well as field scale pile load tests to study the rate of set-up along with monitoring the pore water pressure around the pile. The following approaches were adopted to understand the set-up mechanism and investigate the controlling factors:

1. Investigating the shearing behaviour of typical pile-soil interface (clay-steel and clay-concrete) in fast and slow loading rates;
2. Developing an understanding of the rate of increase in pile capacity over time in sensitive clay through monitoring change in pore water pressure that is caused by disturbance of the soil.

The outcome of this research can be used to aid designers in proper design of piles in sensitive clay. Incorporating the set-up into pile design is expected to reduce the general cost of pilling projects by reducing pile diameter, pile length, size of driving equipment, and subsequently piling duration. The results can also be used to choose proper relevant time for pile load testing during construction.

1.3 Structure of the Thesis

This thesis is divided into five sections. The first chapter is a general overview of the pile set-up and a deliberation of this concept in the design of pile foundations. It also acknowledges the objective and preparation of this thesis. The second chapter includes the evaluation of pile set-up in clay, description of effective factors of pile capacity, and an analysis of several past studies that referred to the concept of pile set-up. The third chapter presents laboratory experiments which present the interaction of pile-soil performance over time by using a modified direst shear test. The fourth chapter consists of the performance of the field experiment of medium-scale piles driven into sensitive clay at the site. This chapter also includes a discussion of the rate of pile set-up, and the results are compared and justified with past studies. Finally, the last chapter contains a summary, conclusion, and recommendation for future studies.

Chapter 2: Literature Review

2.1 Introduction

Pile foundations are widely used to support high load structures in compressible and weak ground strata throughout the world. Piles are relatively long elements with generally slender geometry and structural foundations that transfer structural loads to firmer soil layers. The term "pile" is often used to refer to all types of deep foundations, including driven piles, drilled shafts, and caissons. A deep foundation is used where the soil is not strong enough to handle a design load and physical constraints. The pile foundations are classified according to the composition of piles (timber, concrete, steel, and composite piles), methods of installation, and other properties. Based on the nature of support provided by the surrounding soil, piles may be classified as end-bearing piles and friction piles; while, the end bearing pile transfer loads to the end-bearing layer whereas the friction piles resist most of the loads through the skin friction which is developed along the pile shaft. The resistance of the friction piles are dependent on the interaction of pile shaft and adjacent soils. Piles are also classified based on the level of displacement they induce during their installation process. Large-displacement pile is a pile that displaces a large volume of the soil within the adjoining soil mass (e.g., closed-end pipe piles), while small-displacement piles stated as sectional displacement of the surrounding soil such as open-ended pipe pile, and H-piles. Non-displacement pile is formed by excavation or boring method such as drilled shafts.

The bearing capacity of a pile depends on different parameters, including the type of the pile, method of installing pile, soil properties, and loading conditions. Piles driven into various types of soil, specifically in clay, experience an increase in capacity as a function of time due to dissipation of excess pore water pressure generated around the pile during pile driving. This phenomenon of time-dependant capacity increase is referred to as set-up or freeze. Pile set-up occurs in almost all types of soils including organic or inorganic clay, loose to medium dense silt, sandy silt, and fine sand (Astedt and Holm, 1992; Hannigan et al., 1997). It is important to evaluate the performance of the driven pile over time due to the pile set-up. This section of the thesis concentrates on the behaviour of the friction piles driven into soft clay over time. Friction piles in clay soils typically resist the superstructure load through the adhesion developed along the pile shaft. It is essential to review the pile behavior at driving stage and during loading applications.

2.2 Pile Capacity

The bearing capacity of a single pile shows the maximum load a pile can withstand under different modes of loading (compression, tension, lateral, etc.). The axial bearing capacity of a pile, q, is normally derived from frictional shaft capacity developed along the pile surface, q_s, and toe capacity derived from soil resistance under the toe of the pile, q_t. The contribution of each of these bearing capacity components depends on the type of the soil as well as pile characteristics. The unit shaft resistance, q_s, is a function of the adhesion, c_a, and interface friction angle between the soil and the pile surface (δ). In cohesionless soils the interface friction angle plays a major role in developing the pile shaft capacity, while adhesion is the governing parameter in defining the pile

shaft capacity in cohesive soils. The frictional resistance (q_s) in cohesionless soils is calculated by the following empirical expression:

$$q_s = \sigma_v' K_s \tan \delta \qquad (2.1)$$

where, K_s, is the coefficient of lateral earth pressure acting perpendicular to the pile surface, and σ_v', is the vertical effective stress that is dependent on pore water pressure along the shaft of the pile. The coefficient of lateral earth pressure (K_s) is affected by various parameters, including soil compressibility, OCR ratio, primary stress levels, and method of pile installation. Also, the soil-pile interface friction angle (δ) is affected by additional parameters including soil grain size, pile material, surface roughness, and normal stress at pile-soil interface.

Equation 2.1 is generally applied to predict the pile shaft capacity of cohesionless soils, though the proper method of determining friction resistance in cohesive soil applies a total stress analysis. This approach is recommended based on the undrained shear strength of soil (S_u), and the shaft resistance can be estimated using following expression:

$$q_s = \alpha S_u \qquad (2.2)$$

where α is the adhesion coefficient ranging from 0.5 to 1, which was evaluated based on field test data (Tomlinson, 1957; Fleming et al., 1992). This empirical equation presents a magnitude for unit shaft resistance, though the actual pile capacity is affected by pile geometry, installation method, soil properties, and pile set-up.

The toe bearing capacity of piles can be estimated using Terzaghi's bearing capacity equation for shallow foundations. As per this expression, the toe bearing capacity is a function of the effective stress and soil properties at the pile toe. The pile toe capacity in cohesive soils in normally determined using undrained shear strength of the soil, Su, and a bearing capacity factor Nc (CGS, 2007):

$$q_t = N_c s_u \quad (2.3)$$

Nc can be determined as a function of pile diameter and is usually ranged from a value of 6-9 (CGS, 2007). Interpolation of the value between 6 and 9 is also suggested based on the undrained shear strength of the soil and the pile embedment depth within the bearing stratum.

For cohesionless soils, the toe bearing capacity can be estimated using the effective stress at the toe of the pile, σ'_v, soil unit weight, γ, and the pile toe diameter, D:

$$q_t = N_q \sigma'_t + 0.5\gamma D N_\gamma \quad (2.4)$$

where, Nq and Nγ are the bearing capacity factors. Design guidelines such as the CFEM (2007) provide typical values for these bearing capacity factors depending on the soil type and pile installation method. The second term in this equation is approximately equal to typical pile weight and is ignored in the design practice.

2.2.1 Uplift Capacity

Uplift capacity is related to the sum of the pile shaft resistance and the weight of the pile resistance. Depending on soil conditions and type of analysis (effective and total stress analysis), the uplift capacity can be estimated using equations 2.1 and 2.2, respectively. Polous and Davis (1980) reported that uplift capacity is usually smaller than pile compressive capacity due to the additional resistance at the pile toe. The result showed the reduction of uplift capacity from 60 to 80% of the frictional capacity of piles in compression. Some researchers discussed the mechanisms relating to the variations in the shaft capacity under compressive and uplift loading modes. For example, De Nicola and Randolph (1993) examined model piles in granular soils under tensile and compressive loading, and the result indicated that one of the fundamental explanations for the inconsistency of the capacities was the Poisson's ratio effect. During uplift, the bearing capacity

at the toe of the pile is lost due to tension. In clays, the ultimate skin friction is typically equal to vertical downward loading (Taylor 1948). However, this is not true in soft clay, since failure may not appear along the boundary of the pile. The pull-out may also cause negative pore water pressure dissipation, and therefore the ultimate capacity of the pile could be much less in a short period of time.

2.2.2 Lateral Capacity

The approximation of ultimate lateral capacity is usually conducted through a static equilibrium method that the theory of lateral earth pressure is applied to measure the forces acting along the pile shaft and evaluate equilibrium conditions (Giraldo, 2014). The conventional static approach described by Poulos and Davis (1980) assumes that the pile is slender, rigid (soil failure appears before pile failure, also indicated as "short piles") and pile head is free to rotate, and there is a point of rotation at an unidentified depth below ground level. The ultimate lateral resistance is referred as a function of the pile diameter, embedment length, lateral load eccentricity and distribution of soil lateral pressure through the pile shaft. A typical approach suggested by Broms (1964a and 1964b), considers soil type, pile type and pile head fixity by implementing simplified assumptions, such as distribution of lateral earth pressure along the pile shaft dependant on soil type (cohesive and/or cohesionless), and failure mechanisms depend on the yield moment of the actual pile. This method is typically used in initial design due to simplicity, though ultimate bearing capacity predicted through static approaches may take place at higher lateral deflections (Giraldo, 2014).

2.3 Pile Load Testing

Load tests are performed to determine the ultimate capacity of representative piles used in a specific project and verify the bearing capacity values estimated through analytical and empirical methods. Generally, piles are designed analytically, based on the load conditions and soil characteristics. Pile load tests are performed to verify the bearing capacity and identify the actual bearing capacity required for the design. To perform pile load tests, one must first drive the model piles. It is recommended to choose a location where soil conditions are known (eg. close to a borehole) and the soil conditions are somewhat poor. It is also important to keep the type of piles and method of driving the similar to the ones that will be used in the construction project. Correspondingly, the driven model piles may be carried out through either static (tension and/or compression) or dynamic pile load testing methods to estimate the axial or lateral pile capacity.

2.3.1 Static Load Testing Method

The standard tests for the axial capacity of pile foundations are typically carried out in both compressive and tensile forms. The compressive load test determines combined shaft and toe resistance, and if this test is conducted with a single strain gauge, the measured ultimate capacity would be an aggregate of the shaft and toe resistance. In order to distinguish the proportion of the shaft and toe resistance, the pile may need to be internally instrumented with multiple strain gauges. This would help to determine the resistance distribution between the shaft and toe segments.

The static load test is typically performed using a reaction dead load or a series of reaction piles surrounding the test pile, where a reaction frame is connected with a capacity higher than the expected pile resistance (Figure 2.1). The test loads are applied using a hydraulic jack and the pile

resistance and displacement through are measured a load cell and a displacement gauge devices such as a linear variable differential transformer (LVDT). This test is usually carried out according to ASTM D1143 for axial compressive loads, while other test methods such as the Statnamic testing and Oestemberg load tests are also common in industry. The static tensile test standardized by ASTM D3689 is another method used to measure the axial shaft capacity of the pile (Figure 2.2).

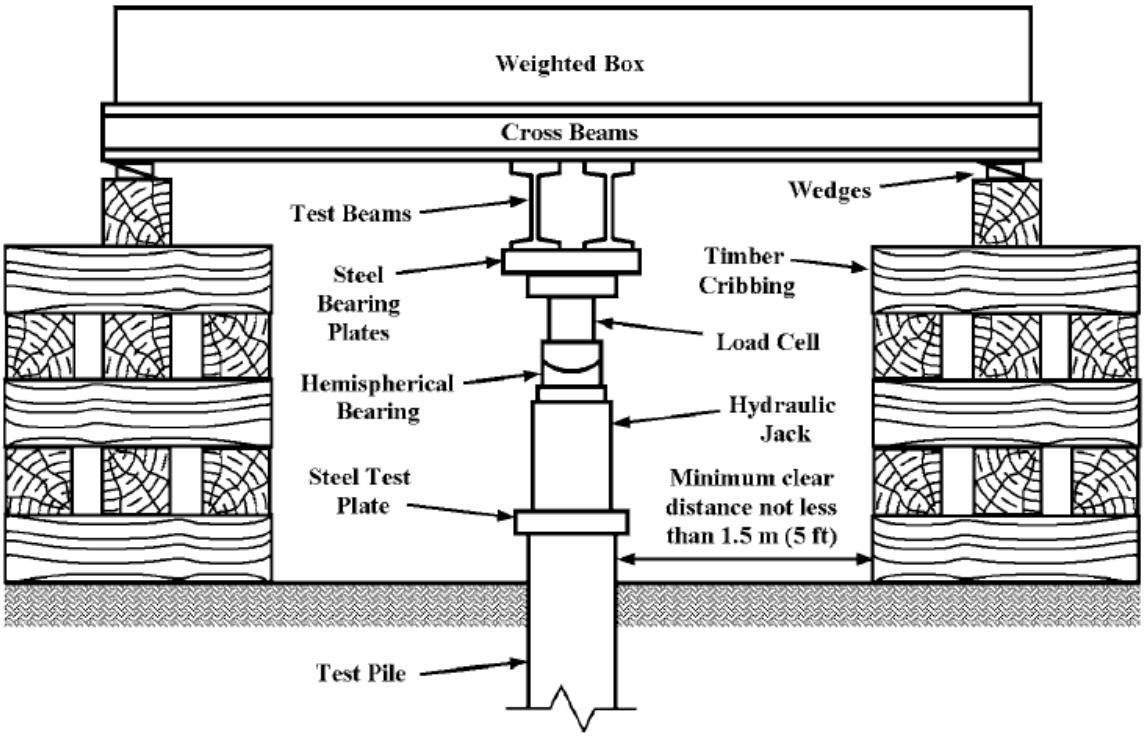

Figure 2.1: Typical setup for axial compressive test using hydraulic jack acting against weighted box (ASTM D1143)

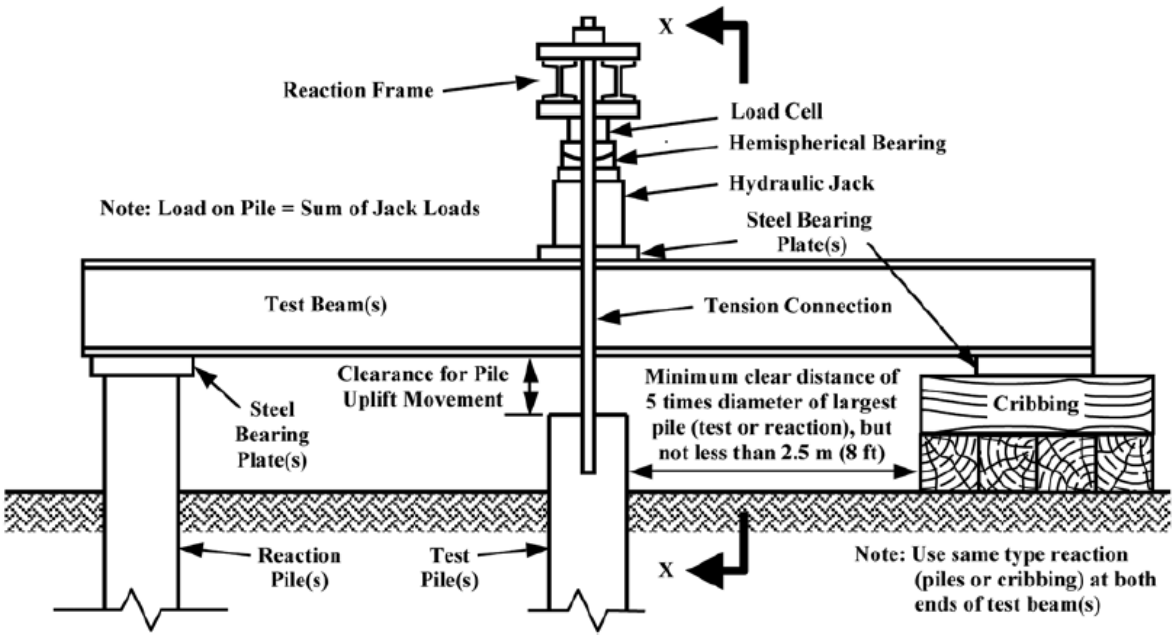

Figure 2.2: Schematic of tensile load test using hydraulic jack supported on beam (ASTM D3689)

2.3.2 Dynamic Load Testing Method

Another alternative pile load test method to measure the ultimate capacity of the pile is dynamic load testing, which is standardized by ASTM-D4945-00. Dynamic load testing is an effective method that requires instrumentation of the pile by accelerometers and strain transducers. This test method involves measuring the pile elastic response to the force of the impact hammer during driving. The pile driving hammer drops and produces compressive waves in the pile and pile-soil interface (Figure 2.3). Any change in these waves is recorded using accelerometers and strain transducers measuring the pile response, and a pile drive analyzer device is used to compute the pile resistance based on a numerical integration of a dynamic wave equation. This test can provide the amount of resistance distributed between shaft and toe. The measured bearing capacity can be correlated with the results of the static load tests on the same pile foundation.

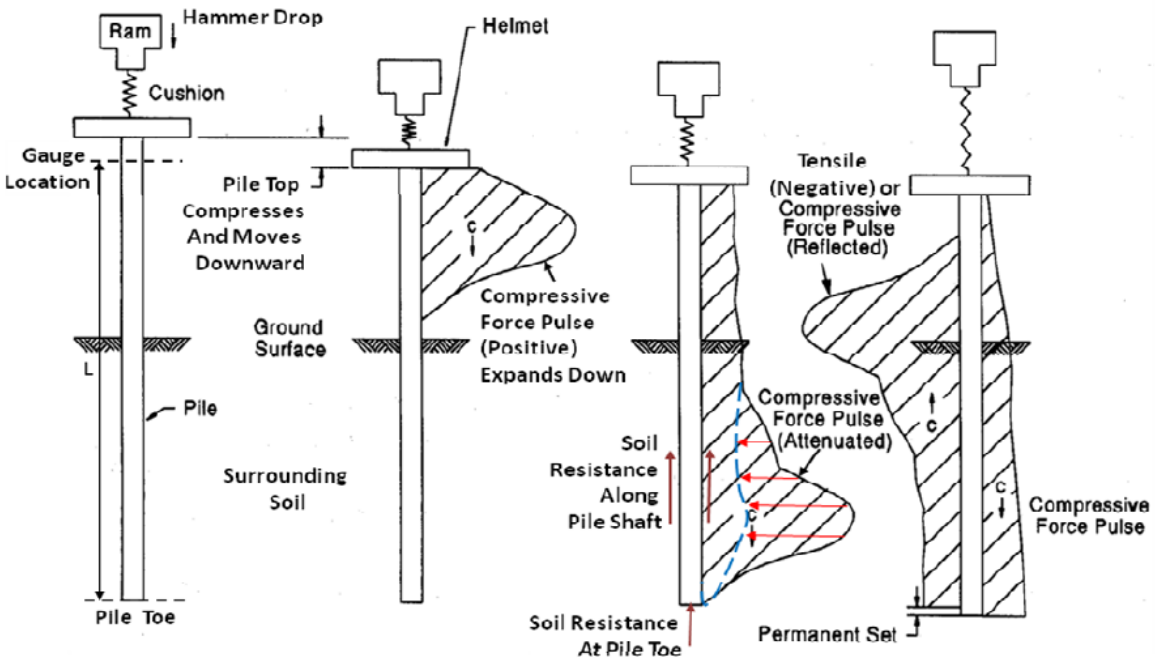

Figure 2.3: Wave propagation in piles during dynamic pile load test (Ng et al., 2011)

2.4 Pile Installation Methods

Piles are typically installed either by driving them using a hammer system or by predrilling the soil and filling it with the pile materials (cast-in-place). Pile driving is normally performed using an impact or vibratory hammer depending on the nature of the soil and design regulations. Different types of pile foundations including precast concrete pile, timbers, steel and composite piles can be installed using driving techniques. However, this technique might generate different levels of soil displacement depending on the geometry of the pile such as diameter during pile driving. This soil displacement may be advantageous in cohesionless soils, as it could densify the surrounding soil and increase the shaft capacity of the pile. In cohesive soils, on the other hand, large displacements could induce excess pore water pressure which, in turn, can reduce the pile capacity. Drilled piles are typically installed by drilling a hole which is then filled with steel

reinforcement and concrete to create a coherent reinforced concrete pile. The excavation hole can be supported by casing or drilling mud to prevent caving of the surrounding soil. However, the gap between the pile and soil generated by the casing of drilling mud may result in lower shaft capacity. Drilled piles can be made with different diameters and depths and can be extended into the bedrock to provide higher resistance.

2.5 Effect of Pile Driving on Bearing Capacity in Clay

The pile driving may induce remoulding and disturbance of the soil surrounding the pile. It is necessary to understand these processes in order to improve the estimation of the bearing capacity of the pile. According to De Mello (1969), the effects of pile driving in clay are divided into four stages. The first stage is the remoulding of the structure of the soil around the pile, which occurs during driving the pile. The second stage is the variations in the state of stress of the soil and the pile, which is referred to as the formation of excess pore water pressure. The third stage is described as the dissipation of excess pore water pressure, which occurs at a certain rate depending on the soil permeability. Lastly, the final stage is the increase of the soil strength over time due to decrease in excess pore water pressure and soil aging. This process is reviewed in the following sections.

2.5.1 Soil Disturbance and Remoulding

When a pile is driven into the soil, the surrounding soil is compressed and remoulded as the driving progress. The effect of this process on soil properties and pile behavior has been broadly studied (Seed and Reese, 1955; Fellenius and Samson, 1976; and many others). As Broms (1966) stated, this remoulded region spreads from one to three diameters laterally, while the extent of disturbance

at the pile toe would be only one pile diameter (Figure 2.4). Other researchers reported remoulding and disturbance zone of up to five times the pile diameter (e.g., Cooke and Price, 1973). The soil remoulding has shown to decrease the undrained shear strength of the soil surrounding the pile. This reduction typically appeared in the soil surrounding the pile at a distance up to three to five times the pile diameter from the surface of the pile (Afshin, 2015; Tomlinson, 1994; Franke, 1988). Seed and Reese (1955) investigated the behavior of friction piles driven into San Francisco Bay mud, and observed that the water content of the soil around the pile decreased after pile driving.

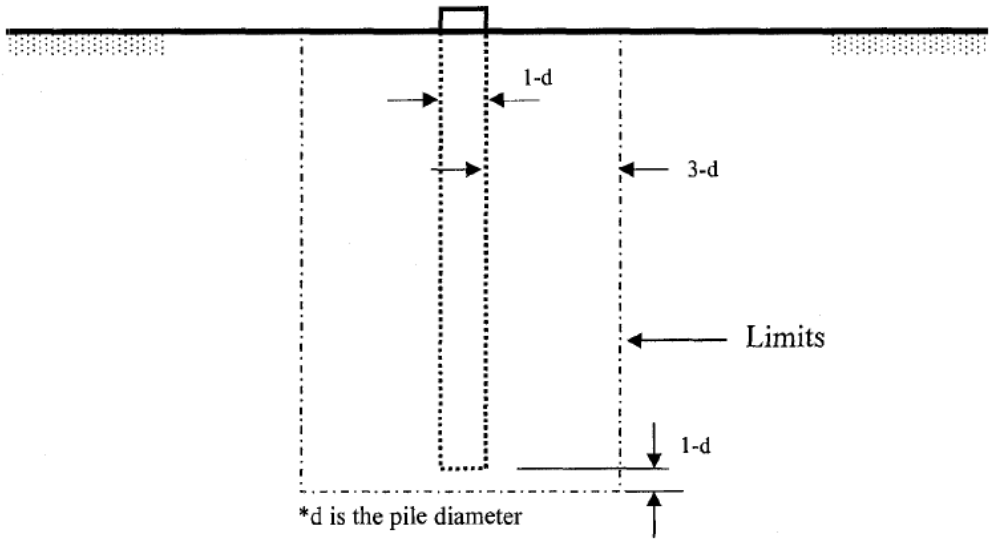

Figure 2.4: Regions of the compression and remoulding during pile driving (Broms, 1966)

2.5.2 Change in Pore Water Pressure

Excess pore water pressure develops due to the remoulding and disturbance of soil by driven piles. According to the relationship between effective stress and pore water pressure, when a pile is driven into the soil, total stress is increased as the pile pushes the soil away and alters the structure

of the soil. This may decrease or increase the effective stress of the soil depending on soil properties. In cases where the soil dilates, the effective stress increases, and if the soil shrinks under shearing, the effective stress decreases. The normal or slightly over-consolidated clays tend to remould and compress during the pile driving.

Many researchers have attempted to measure the excess pore water pressure as it is developed in the pile surrounding soil as the pile is driven into the soil. The development of this pore water pressure for a specific period after pile driving has been reported by many researchers including Seed and Reese (1955); Yang(1956); Bjerrum et al. (1958); Lo and Stermec (1965); Lambe and Horn (1965); Koizumi and Ito (1967); Orrje and Brom 1967; Flaate (1968); McCammon and Golder (1970); D'Appolonia and Lambe (1971); Flaate (1972); Clark and Meyerhof (1972, 1973); Bozozuk et al. (1978); Sutton and Rigden (1979); Thorburn and Rigden (1980); Konard and Roy (1987); Azzouz and Marrison(1988); Skov and Denver (1988); Fellenius (1989); Orrje and Chung (1988); Azzouz et al (1990); Bogard and Matlock (1990); Leung et al. (1991); Bond and Jardine (1991); Ng (2011) and many others. Previous results indicated that the excess pore water pressure at the pile surface may become equal to or even greater than the overburden pressure (Lambe and Horn, 1965; D'Appolonia and Lambe, 1971; Poulos and Davis, 1980). Poulos and Davis (1980) reported that the excess pore water pressure can approach up to twice the in-situ vertical effective stress, although there is much more pressure at the toe of the pile. This pressure can be up to 3 to 4 times greater than the effective stress.

Several researchers introduced analyses to predict the process and magnitude of the excess pressure around the pile. Nishida (1964) proposed a prediction approach based on elasto-plasticity analysis. Lo and Stermac (1965) and D'Appolinia and Lambe (1971) suggested similar analyses that estimate the maximum pore water pressure generated by pile driving. Their solutions were

shown to be valid for normally consolidated and over-consolidated clays. Randolph et al. (1979) proposed an empirical equation to estimate the excess pore water pressure induced around the pile. This equation illustrated a relationship between the excess pore water pressure and the change in the average effective stress and undrained shear strength of the soil due to remoulding, disturbance, and shearing.

2.5.3 Dissipation and Stabilization of Pore Water Pressure

The next stage in behaviour of pore water pressure in the pile-soil interface zone is dissipation of the excess pore pressure which starts immediately after excess pore water pressure build up. This process is accompanied by changes in the stress field of the soil around the pile, where the effective stress of the soil increases as the pore water dissipation proceeds. The dissipation rate is dependent on soil permeability, pile spacing and material, and thickness of the clay layer. Figure 2.5 shows the rate of dissipation of excess pore water pressure in marine clay. In this figure, the excess pore water pressure is shown by Δu and expressed as $\frac{\Delta u}{\sigma'_{v0}}$, where σ'_{v0} is the vertical effective stress, and s is the radial distance, which is expressed as $\frac{s}{r_0}$, and r_0 is the pile radius. In case of sensitive soils, such as Leda clay, the resulting pore water pressure could be greater and may reach up to 8 times the effective stress. The concept of change in pore water pressure over time is used to explain the increase in pile capacity over time (Seed and Reese, 1955).

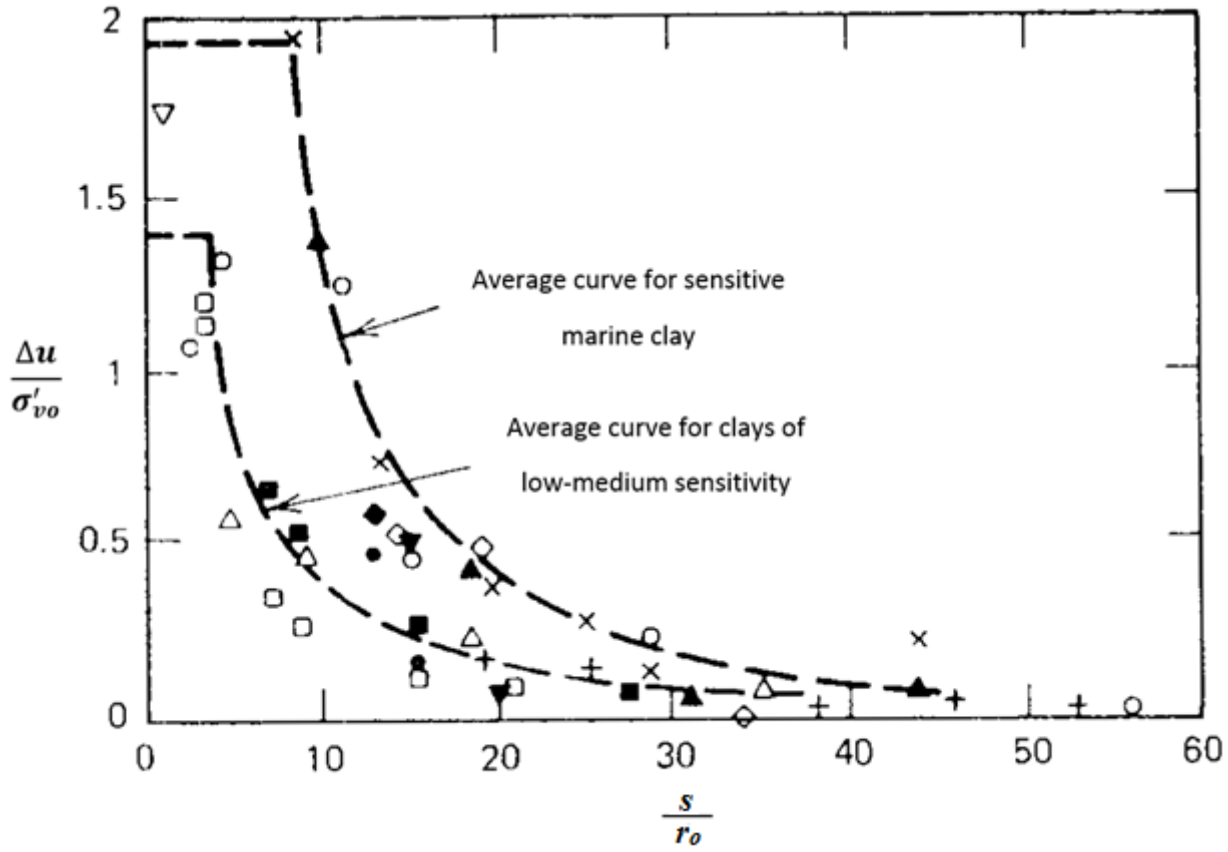

Figure 2.5: Summary of measured pore water pressures (after Poulos and Davis 1980)

Along with the dissipation of excess pore water pressure around the pile, the shear strength of the disturbed soil increases. This is related to increase in the effective stress of the soil due to dissipation of excess pore water pressure which, in turn, leads to reconsolidation of the soil and, hence, increase in shear strength of the affected soil. The shear strength of the reconsolidated soil around driven piles after dissipation was reported to be higher than the soil's initial undisturbed shear strength (Randolph et al., 1979). A similar behaviour was reported by Flaate (1972) where the shear strength of reconsolidated soils around the piles at the Nitsund Bridge was significantly higher than their initial values prior to pile driving. Seed and Reese (1955) proposed a relationship between the reduction in soil moisture content due to excess pore water pressure dissipation and the increase in shear strength of the soil.

2.5.4 Cavity Expansion Theory for Simulating Pile Driving

Analytical models have been suggested to describe the behavior of the soil around a pile when it experiences expansion due to pile driving. The theory of cavity expansion has been established to simulate the in-situ behaviour of the soil, in relation to various material properties, and loading conditions. Pandit et al. (1983) stated that there are three independent factors which may be determined to explain the cavity expansion problems. The first is the shape of the cavity, which represents the field states, and includes spherical and cylindrical shapes. The second is the properties of the soil surrounding the cavity, which in most cases (except strain softening behaviour) is assumed to be a homogenous linear elastic-plastic material. The last factor is related to loading conditions, which has not been studied in detail. The syllogism of cylindrical cavity development to model the installation of displacement piles that evaluates the stress changes due to pile installation was proposed by Randolph et al. (1979). In addition, Baligh (1985, 1986) explored the strain and stress changes from the strain path method at the instant vicinity of the pile, specifically at the zone of large stress gradients ahead of and behind the toe of the pile and the change to quasi steady-state conditions through the pile shaft. These two approaches were compared by Randolph (2003), and it was found that both theories disregard the few diameters close to the toe of the pile, and the radial displacement fields are very comparable aside from the one immediately adjacent to the pile shaft.

Satibi et al. (2007) studied cavity expansion in sand using both stress-controlled and displacement-controlled expansion analyses. Satibi et al. (2007) used K-pressure method (stress-controlled expansion) to explore the increase in radial stress due to pile installation which is the main concern in the study of the displacement piles. On the other hand, Satibi et al. (2007) also investigated displacement-controlled cavity expansion, in which the radial stress increase was

induced by applying a prescribed horizontal displacement on a cavity wall. The result of the stress field after cavity expansion showed small difference with the K-pressure method. However, both methods showed reasonable results.

2.6 Pile Set-up

Piles driven into various types of soil, especially in clay, experience an increase in capacity as a function of time due to dissipation of excess pore water pressure generated around the pile during pile driving, and reconsolidation and aging of the remoulded soil near the piles. This phenomenon of time-dependent capacity increase is referred to as "set-up" or "freeze". Recently, it has been also referred to "side shear set-up" by several researchers (e.g., Randolph, 2003; Bullock et al., 2005). The set-up value is related to two important factors, soil characteristics and pile type as well as the installation technique. The mechanisms for pile set-up are mostly ingrained, but these theories are still under debate, which requires further studies to understand the concept accurately.

The phenomenon of pile set-up was reported by a significant number of researchers, including Seed and Reese (1955), Housel (1948), Eide et al. (1961), Yang (1956), McClelland (1969), McCammon and Golder (1970), Flaate (1972), Randolph et al. (1979), Thorbum and Rigdan (1980), McManis et al. (1988), Chung (1988), Skov and Denver (1988), Coop and Wroth (1989), Bogard and Matlock (1990), Titi (1996), Randolph (2003), Bullock et al. (2005), and Fellenius (2008). Many of these investigations illustrated a time-dependent increase of pile capacity for piles driven into cohesive soil. Figure 2.6 illustrates some of the past results in the form of normalized pile capacity summarized by Titi, (1996). Nevertheless, there have been a few researchers who reported a decrease in the bearing capacity of friction piles driving into clay over

time (e.g., Kraft et al., 1981; Fellenius et al., 1989; Bond and Jardine, 1991) as shown in Figure 2.7.

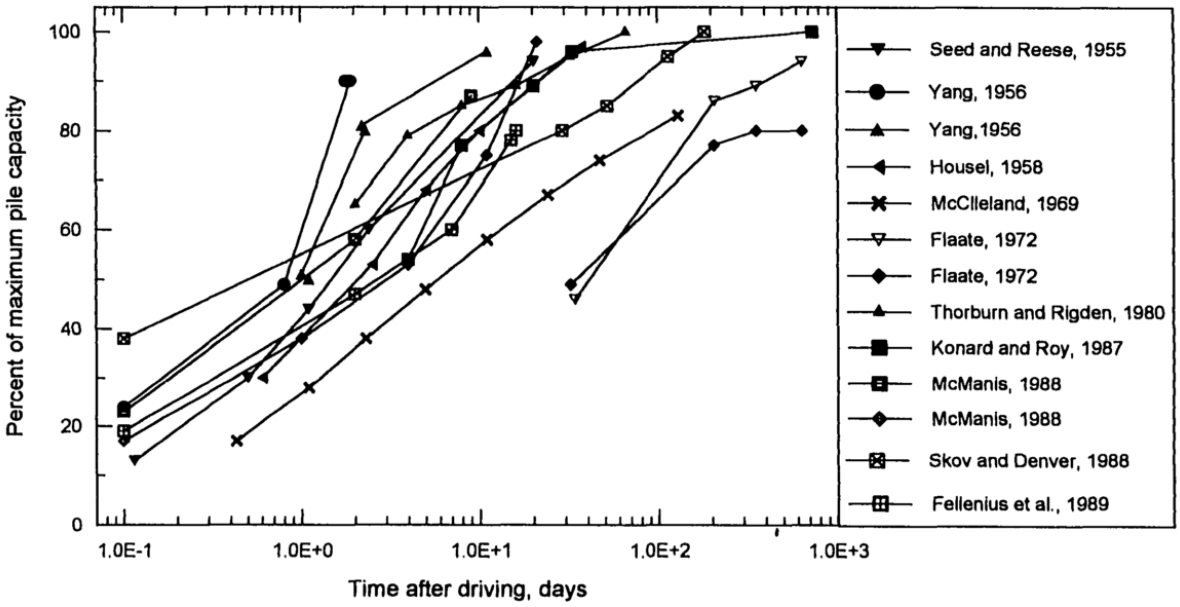

Figure 2.6: Field data on bearing capacity over time for friction piles driven into clay (Titi, 1996)

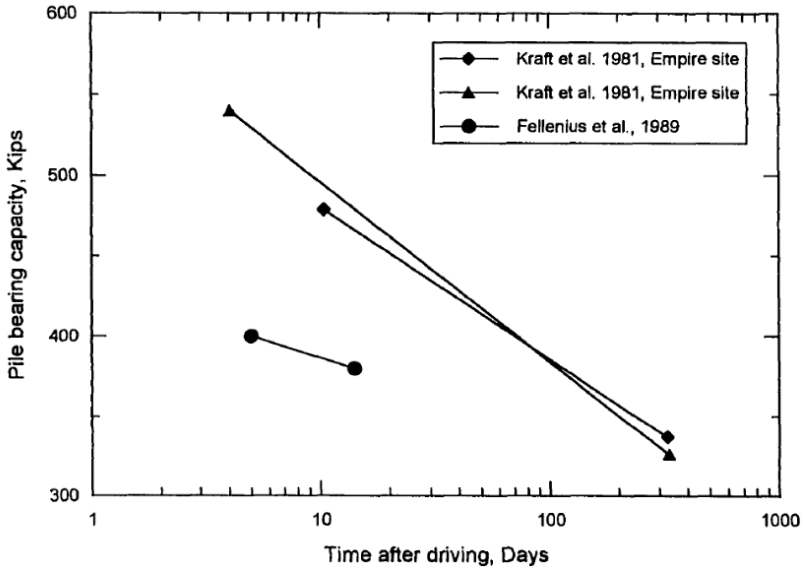

Figure 2.7: Observation of decrease in pile capacity over time (Titi, 1996)

2.6.1 Effect of Soil Type on Pile Set-up

Pile set-up occurs in almost all types of soils, including organic or inorganic clay, loose to medium dense silt, sandy silt, and fine sand (Astedt and Holm, 1992; Hannigan et al., 1997). The set-up occurs due to dissipation of the excess pore water pressure which was initially generated due to disturbance of the soil during pile installation. In cohesive soils such as clay, or with mixture of fine-grained granular (e.g., clayey silt or fine sand), driving piles may generate excess pore water pressure which will gradually dissipates over time. Accordingly, this phenomenon is clarified in form of divided stages in pile set-up mechanism. Long et al. (1999) reported that pile set-up has been found to be higher in soft clays compared to the stiff clays. Randolph et al. (1979) indicated that stress variations around a pile after driving into clay was almost independent of the soil's overconsolidation ratio (OCR). Alternatively, Whittle and Sutabutr (1999) stated that with proper determination of OCR and hydraulic conductivity of the soil, set-up prediction would be reliable for large diameter open-ended pipe piles.

On the other hand, driving piles in fine-grained granular soils (e.g., silts or fine sands) also generates excess pore water pressure that may dissipate much rapidly (i.e., during driving the pile) compared to clayey soils. The rate of set-up in granular soils typically depends on the depth of the ground water table (GWT). Svinkin et al. (1994) stated that the rate of set-up is linear with time above GWT, while the set-up with respect to the time is a power function below GWT. The increase in capacity was reported at approximately 100% over 3 months in non-cohesive soils. Long et al, (1999) observed the largest set-up at first 10 days after pile driving in sand, however the set-up performed to continue for almost 500 days and, in turn, the measured shaft capacity increased approximately twice the initial value.

2.6.2 Effect of Pile Type on Set-up

Pile set-up has been reported for almost all driven pile types. The set-up was shown to be affected by the composition of piles (i.e., timber, concrete, steel, and composite piles) and the level of soil displacement induced during pile installation process which can be a function of pile size and type (H-piles, open-ended pipe piles, and closed-end pipe piles). Camp and Parmer (1999) reported a decrease in set-up rate as the pile size increased, while Long et al. (1999) stated that there is no proper indication of variance between small and large displacement piles. Moreover, Finno et al. (1989) reported that after driving an open-ended pipe pile, higher excess pore water pressure was produced compared to that generated by driving an H-pile. However, the shaft capacities for both piles were the same after 43 days. Preim and Hussein (1989) compared the set-up pre-stressed concrete and steel piles and indicated that there is higher set-up in pre-stressed concrete piles than the steel piles, which was linked to a higher pile-soil interface friction coefficient for the concrete piles.

2.6.3 Magnitude of Pile Set-up

As discussed earlier, the effect of soil characteristics and pile type (i.e., installation method) have shown significant influence on the rate of set-up (Axelsson, 2002; Chow et al., 1998; Svinkin et al., 1994). Several studies were published on pile set-up showing the rate and magnitude of the set-up for different piles installed in different soil strata. The majority of these researchers observed the set-up within 30 days after the pile installation day, and after that, the rate of change was very slow. Ng et al. (2011) investigated pile set-up by performing pile load tests on five piles driven in cohesive soil in Iowa, and the result revealed a 52 to 66% increase in shaft resistance. Blessey and Lee (1980) performed pile load tests in southeast Louisiana, which showed an

approximately 400 to 500% increase in shaft capacity several weeks after initial pile driving. McManis et al. (1988) investigated set-up on full-scale pre-stressed concrete piles in Luling Bridge near New Orleans, Louisiana and reported a 440-1150% increase in bearing capacity five weeks after initial pile driving. Also, Skov and Denver (1988) developed pile load tests and the results indicated 20 to 100% increase in pile bearing capacity over time. Most of these field experiments were performed in different type of soil and/or different pile properties, however the results of these experiments showed set-up with variation in rates which was due to their affective parameters.

2.7 Pile Set-up Mechanisms

Komurka et al. (2003) explained the increase in pile capacity in three phases. At phase 1, the rate of the set-up coincides with the rate of dissipation. The condition of the soil is disturbed, and the rate of the excess pore water pressure dissipation is not constant. Accordingly, the plot shows a non-linear trend with respect to the time log at that specific period after driving (Figure 2.8). In this phase, the effective horizontal stress increases in the distressed soil and the soil is consolidated and its strength is increased. This stage of the set-up presents the increase of the pile capacity just minutes after driving the pile (Bullock, 1999). The period of the non-linear rate of excess pore water pressure dissipation is dependent on the properties of the soil and the pile, including pile type and size, soil type, permeability as well sensitivity of the soil. This logarithmic rate of excess pore water pressure dissipation will continue at a nonlinear rate for certain number of days. This outcome may appear while the soil is permeable and a larger volume of the soil is displaced by the pile.

At phase 2, sometimes after driving the pile, the rate of excess pore pressure dissipation shifts to a consistent and linear trend with respect to time. The period after driving the pile, upon which the rate of excess pore water pressure dissipation turns to logarithmically linear phase is referred to as "initial time". Throughout phase 2, the disturbed soil experiences an increase in effective vertical and horizontal stress, and the soil gains shear strength according to consolidation theory. The duration of phase 2 is a function of soil (type, permeability, and sensitivity) and pile (type, permeability, and size) properties. The duration of the logarithmically linear rate of dissipation could be longer if the soil and pile are less permeable and a larger volume of soil is displaced by the pile. The phase of logarithmically linear pore water pressure dissipation may develop for several weeks, months, and sometimes years (Skov and Denver 1988). Azzouz et al. (1990) reported that complete consolidation for a 380 mm diameter displacement pile occurred in approximately 200 to 400 days. Whittle and Sutabutr (1999) also reported that the time for dissipation of excess pore water pressure due to driving large diameter open-ended piles is a function of the ratio of the pile diameter to the thickness of the wall.

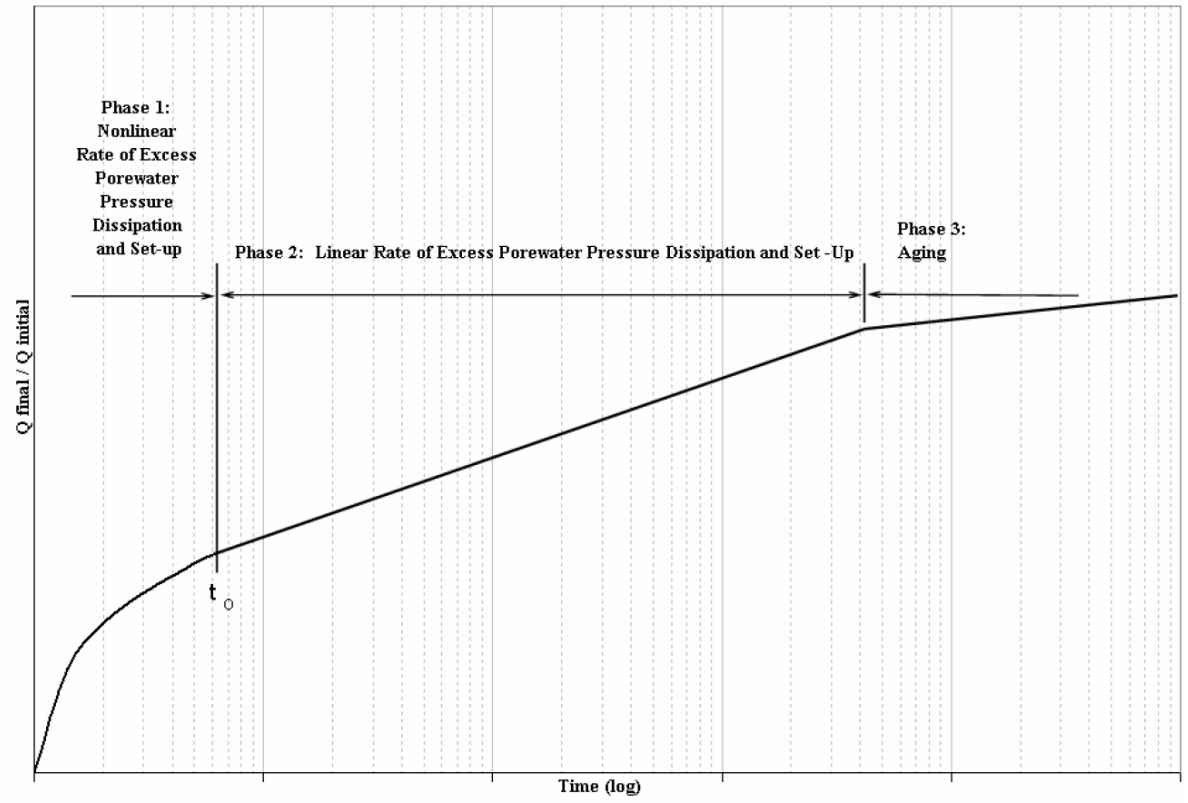

Figure 2.8: Schematic illustration of pile set-up phases (Kumarka et al., 2003)

Based on conventional consolidation theory, a very long time is required for the dissipation of excess pore water pressure to be completed. Essentially, there is a time after which the rate of dissipation is very slow and there would be no additional consequence. At this time, the primary consolidation is typically achieved. However, secondary compression continues immediately after the completion of primary consolidation and is independent of effective stress. Correspondingly, the rate of set-up correlates to the rate of excess pore water pressure dissipation and, as mentioned, there is a period of time after the primary consolidation in which the change in the rate of set-up is very slow (secondary compression). Since, effective stress-related set-up is adequately complete, hence, the rate of set-up is independent of effective stress during this phase. This time-dependent change in soil properties at a constant effective stress is called aging.

At phase 3, aging of the soil will occur which could be related to thixotropy, secondary compression, particle interference, and clay dispersion (Camp et al., 1993; Long et al., 1999; Schmertmann, 1991). Aging effects may increase the shear modulus, stiffness, and dilatancy of the soil, and decrease the compressibility of the soil (Axelsson, 1998; Schmertmann, 1991). In addition, aging may increase the pile–soil interface friction (McVay et al., 1999) at an approximately linear rate with the log of time (Schmertmann, 1991). In clay, thixotropy occurs mainly at very low effective stress under drained conditions (Schmertmann, 1991). The pile set-up mechanisms are illustrated in Figure 2.8. This chart shows a general understanding of pile set-up mechanisms for a given soil type at a given length along the pile shaft. Hence, it is possible to observe overlap among phases, or more than one phase can contribute to set-up at a time due to non-uniform soil conditions along the embedment length of the pile shaft.

2.8 Prediction of Pile Set-up

Pile set-up has been investigated for many years, and researchers have tried to analyze and anticipate pile shaft capacity using a number of empirical and theoretical approaches. Nevertheless, there is no conclusive theory for carrying out the conditions involved in pile set-up. Peck (1958), Woodward et al. (1961), Tomlinson (1971), Flaate (1972), and McClleland (1969) suggested that the behaviour of the pile shaft-soil can be analyzed based on total stress analysis, which corresponds to the strength of the pile-soil interaction with the undrained shear strength of the undisturbed soil. Alternatively, Zeevaert (1959), Eide et al. (1961), Chandler (1968), Burland (1973), Meyerhof (1976), Flaate and Seines (1977), and Parry and Swain (1977) considered the effective stress analysis to understand the pile-soil behaviour and estimate the pile shaft capacity. Both these studies were only estimating the capacity at initial stage, and the effect of time was not

considered. The effect of time in the effective stress analysis of the driven piles was presented by Esrig et al. (1977), and then the shaft capacity of the driven piles was predicted during the different pile service life phases. It is important to monitor the pile capacity over time in order to observe the set-up.

A number of other researchers expanded these studies by using numerical and analytical methods, including cavity expansion methods and other fundamental models, to explain the soil response and then the pile behavior (Carter et al., 1979; Randolph et al., 1979; Randolph et al., 2003). The results of these studies illustrated the significance of effective stress conditions in the soil surrounding driven piles and the analysis of pile-soil interaction behaviour (Banerjee et al., 1982; Roy et al., 1981; Azzouz and Lutz, 1986; Coop and Wroth, 1989; Bogard and Matlock, 1990; Bond and Jardine, 1991; Wathugala et al., 1993; Paikowsky et al., 1995; and many others).

2.8.1 Numerical and Analytical Estimation Methods

Several methods were developed to predict the magnitude of pile capacity over time. Skov and Denver (1988) proposed the most broadly used linear relationship with respect to log of time for estimating the pile set-up. The proposed formula is a semi-logarithmic relationship to predict set-up:

$$\frac{Q_t}{Q_o} = 1 + A[log(\frac{t}{t_o})] \qquad (2.5)$$

where Q_t is the pile capacity at time t, Q_0 is the initial pile capacity immediately after driving, t_o is the initial time at which the rate of excess pore water pressure dissipation turns into a linear trend with respect to the log of time (as shown in Figure 2.5). In the field, it is important to determine multiple capacities with close timing in order to define t_o, which is a function of soil type and pile

size. The initial time (t_o) increases with pile diameter (Camp and Parmar, 1999). Table 2.1 illustrates the results of past studies using Skov's and Denever's (1988) empirical relationship, including variation of pile set-up factor (A) and initial time (t_o) for specific types of soil and pile. Parameter *A* is a function of soil type, pile size, type, material, and capacity (Camp and Parmar, 1999; Svinkin et al., 1994; Svinkin and Skov, 2000); however, it is independent of depth and dissipation of excess pore water pressure (Bullock, 1999; McVay, et al., 1999). The *A* parameter could be assumed or back-calculated from field data. Chow et al. (1998) stated that the results of several researchers specified that the *A* value ranged from 0.25 to 0.75.

Table 2.1: Outline of increase in pile capacity with time parameters (after Paikowsky et al. 2004)

Researcher	**Soil Type**	**A**	**t_o (day)**	**Pile type and Location**
Skov and Denver (1988)	Clay	0.2	0.6	Concrete piles (Denmark)
Svinkin et al. (1994)	Clay	0.36-1.07	1 or 2	Pre-stressed concrete piles and H-piles (Ohio)
Camp and Parmar (1999)	Sandy Clay/ Sandy Silt	0.37-1.31	2	Concrete piles (South Carolina)
Bullock et al. (2005)	Dense fine sand & soft to medium stiff silty clay	0.2	1	Concrete piles (North Florida)
Yang and Liang (2006)	Clay	0.5	1	Steel pipe, HP, concrete, timber

Several researchers used cavity expansion theory to explain pile set-up (Vesic, 1972; Coop and Wroth, 1989; Bond and Jardine, 1991). Randolph et al., (1979) developed a numerical analysis of the behaviour of piles driven into clay. They investigated the variations in stresses and the pore water pressure while driving the piles and during consecutive consolidation of the soil adjacent to the pile. The excess pore water pressure was induced because of cavity expansion and was

expected to dissipate through external radial flow of the pore water pressure. The numerical method was used to simulate the changes in strength and water content of the soil around the pile. The result showed that the increase in the rate of bearing capacity can be measured by using the predicted rate of increase in shear strength of the soil adjacent to the driven pile (Figure 2.9). However, this analysis assumed plane strain and axial symmetry, which made the problem a one-dimensional problem. Consequently, the shear stress acting in the vertical direction and vertical movement as a result of pile driving were not contemplated.

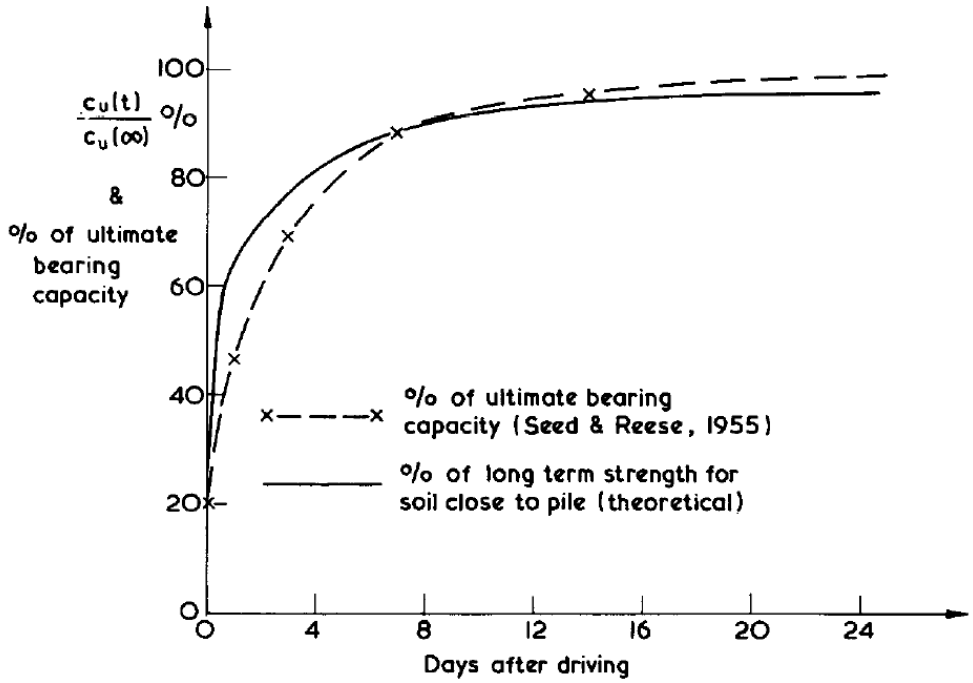

Figure 2.9 (a): Comparison of increase in pile bearing capacity over time and theoretical increase in strength of soil close to pile (after Seed and Reese, 1955)

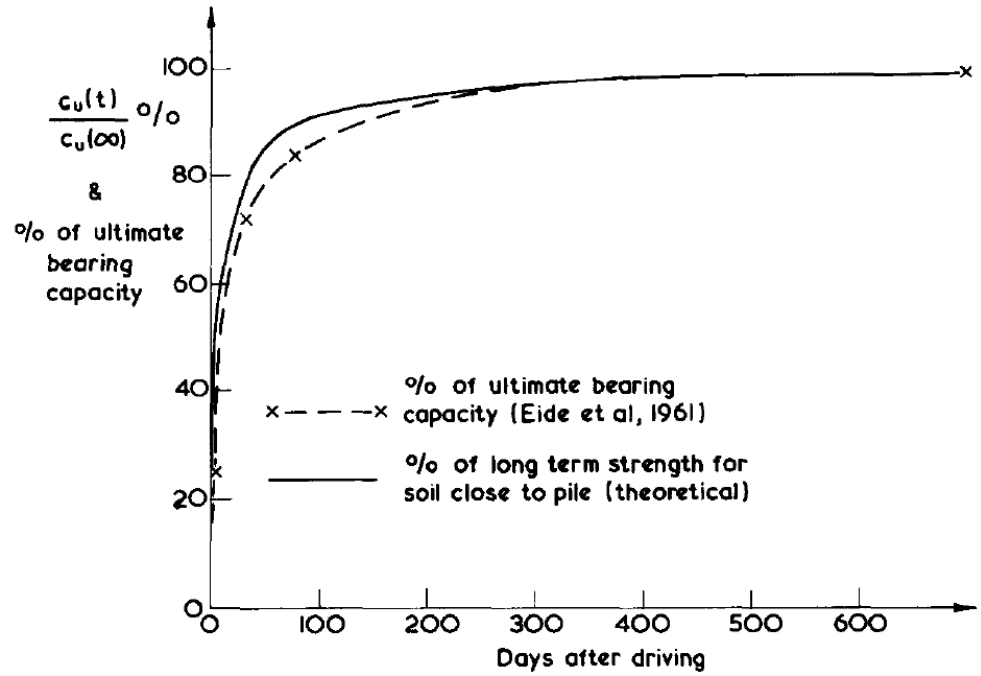

Figure 2.9 (b): Comparison of increase in pile bearing capacity over time and theoretical increase in strength of soil adjacent to pile (after Eide et al., 1961)

Paikowsky et al. (2004) established a summary for the increase in bearing capacity of driven piles over time in case of both static and dynamic load tests. The gradient of the semi-logarithmic relationship between the static and dynamic capacity at a specific elapsed time after driving the pile was indicated as C_{gt} and C_{gtd} respectively. The required time for the 300 mm pile to gain 75% of its maximum capacity is indicated as t_{75}. The following Table 2.2 illustrates the summary of the collected values. Paikowsky et al. (2004) suggested the following empirical formula for any pile size to estimate the time required to gain 75% of maximum capacity:

$$t_{75\ of\ pile} = 4r^2 t_{75} \qquad (2.6)$$

This relationship is established based on normalized maximum capacity of the pile, which used to compare the set-up rate for different types of pile and sizes. This empirical equation is presented based on a logarithmic scale, which is the relationship between the ratio of the initial capacity at

the end of driving (EOD) to the maximum capacity. The time from driving the pile is linear between 40% and 90% maximum capacity. Also, the gradient of the curve is selected as pile capacity parameter C_{gt}, which denotes the rate of the gain in the pile capacity.

Table 2.2: Summary of increase in pile capacity with time parameters (after Paikowsky et al. 2004)

	Static Data Set C_{gt}	Static Data Set t_{75*}	Dynamic Data Set C_{gt}	Dynamic Data Set t_{75*}	All Data C_{gt}	All data t_{75**}
Number of Cases	15	5	7	6	22	11
Average for all piles in set	0.389	385.0	0.48	21.3	0.376	186.6
Standard Deviation	0.119	26.3	0.068	7.9	0.106	237.9

* Closed-end pipe piles only
** t_{75} = time for a standard pile (300 mm diameter) to gain 75% of its maximum capacity
C_{gt} = rate of pile capacity gain with the logarithm of time

Several researchers have established empirical equations using numerical and field data to predict the rate of dissipation of the excess pore water pressure to justify the increase in pile capacity over time (Table 2.3). Soderbeg (1962) proposed that dissipation of pore water pressure may be estimated using the theory of radial consolidation. In addition, Soderberg (1962) suggested the increase in strength with time was related to the non-dimensional time factor T_h, as shown in following expression:

$$T_h = \frac{4\, c_h\, t}{B^2} \qquad (2.7)$$

where c_h= coefficient of horizontal consolidation, t= time since the end of driving, and B=pile width. Several further numerical relationships have been developed for predicting pile capacity. Titi and Wathugala (1999) developed a method to estimate the change in pile capacity over time for friction piles in clay. They introduced a method which was based on the life phases of the tested pile, alternating from installation method to consolidation and consequent loading. Moreover, Randolph et al. (2003) stated that pile shaft capacity depends on the radial effective stress acting around the pile shaft (i.e., according to $\tau_s = \sigma'_{rf}\, tan\delta$; where, σ'_{rf} is effective stress at failure, and δ, is interface friction angle), and this can be predicted by contemplating the following changes while installing the pile, consolidation and loading. Randolph et al. (2003) proposed a potential analytical approach to estimate the radial total stress, σ_{ri}, which is expressed as following:

$$\sigma_{ri} - u_o = \sigma'_{ri} + \Delta U_{max} = (\sigma'_{ri} - P'_i) + P'_o + \Delta P \qquad (2.8)$$

where, ΔU_{max} is the maximum excess pore pressure, and $P'_o$and P'_i are respectively the original in situ mean effective stress and the value instantly after pile installation (adjacent to the pile shaft). In addition, σ'_{ri}, is the radial effective stress just after installation and ΔP, is the mean total stress. Randolph et al. (2003) stated that the estimation of these parameters may not be easy, but this approach is a potential scientific method.

Table 2.3: Suggested empirical relationship to estimate pile set-up

Authors	Equations
Skov and Denver (1988)	$$Q_t = Q_O[A \log\left(t/t_o\right) + 1$$ where Q_t= pile capacity at time t Q_o= pile capacity at time t=t_o Sand: t_o = 0.5, A = 0.2 Clay: t_o = 1.0, A = 0.6
Huang (1988)	$$Q_t = Q_{EOD} + 0.236(1 + log(t)(Q_{max} - Q_{EOD}))$$ where Q_{max} = maximum pile capacity
Guang-Yu (1988)	$$Q_{14} = (0.375\, S_t + 1)Q_{EOD}$$ where Q_{14}= capacity after 14 days S_t= Sensitivity of soil
Svinkin (1996)	$$Q_t = 1.4\, Q_{EOD} t^{0.1} \quad \textbf{Upper Bound}$$ $$Q_t = 1.025\, Q_{EOD} t^{0.1} \quad \textbf{Lower Bound}$$
Long et al. (1999)	$$Q_t = Q_o[A\ log(t/0.01) + 1$$ where A is the same as in Skov and Denver (1988)
Svinkin and Skov (2000)	$$\frac{Q_t}{Q_{EOD}} - 1 = B[log_{10}\,(t) + 1]$$ where B is the same as above Skov and Denver (1988)

2.9 Pile Set-up in Sensitive Clays

The sensitivity of soil is categorized into three levels of low, medium, and high, and it is measured based on the ratio of undisturbed to remoulded undrained shear strength of the clay. There are a number of different variables that can affect the rate of soil sensitivity, including cementation, thixotropy, stable structure and discharge, ion exchange, and change in monovalent or divalent cation ratio (Titi, 1996). Mitchell (1993) explained thixotropy as a time-dependent process during which materials stiffen while at rest and liquefy upon remoulding and disturbance. Mitchel (1960) described the significant controlling factors in thixotropy as the pore water composition, particle size and shape, and the bonding between clay particles.

Several researchers investigated the pile set-up in sensitive soils. Blanchet et al. (1980) have performed pile load tests in sensitive clay, and the results showed that full dissipation of the excess pore water pressure induced by pile driving required 30 days around a single friction pile. Yin et al. (2011) investigated the time dependent behaviour of sensitive clay using numerical analysis and attempted to model the behavior of sensitive clay over time. The model was applied into a finite-element code that considered coupled consolidation analysis, which later was used to justify the experimental result of oedometer tests. Afshin and Rayhani (2015) investigated the pile set-up in sensitive clay (called Champlain Sea clay in Ontario) by performing a series of small-scale pile load tests in the lab. The result showed an average set-up value of 2 after 12 days from initial pile driving. However, the pile set-up has not been incorporated in the current design practice, though set-up in sensitive clay has become considerably important in past decades as more development has appeared on areas that used to be inadequate for construction expansions.

2.10 Previous Studies of Relevance

2.10.1 Behaviour of Pile-Soil Interface over Time

Pile-soil interface characteristics play an important role in the bearing capacity of the pile shaft. Pile resistance is related to the interface shear strength parameters, including interface friction angle and interface adhesion. These properties are used to approximate shaft resistance, q_s, in two conditions of drained and undrained by estimating the β and α coefficients, respectively. A number of researchers have performed tests trying to quantify interface shear strength parameters using direct shear boxes and simple shear devices (Silvestri et al., 1989; Taha, 2013; and many others). They have found that there are a number of factors that may affect interface shear strength, including surface roughness, moisture content, soil composition, and rate of loading (Potyondy, 1961). Surface roughness is normally measured using an LVDT or a displacement sensor as the average of the displacements measured at each data point, known as a centre line average or total roughness $R_{t,}$ and by calculating the root mean square of the same data set to determine the average roughness or $R_{a.}$

The shear strength of saturated clay in undrained conditions is normally affected by a number of parameters, including rate of shearing, overconsolidation ratio (OCR), and soil anisotropy (Silvestri et al., 1989). The shearing failure modes under undrained conditions are categorized into three modes: turbulent, sliding, and transitional. Turbulent failure is described as an increase in the disturbance of the clay structure, while sliding is defined as surface failure due to inadequacy in particle interlocking. In addition, transitional failure is an intermediate type among turbulent and sliding failures (Lupini et al., 1981). Taha (2013) investigated the interface behaviour of marine clay with steel and concrete materials, and identified several factors that affect

the interface shear strength, including surface roughness, OCR, dry density, and degree of saturation. The most influential variable in the interface shear strength was surface roughness (Rouaiguia, 2012). This is due to additional particles interacting with the material surface. Several other researchers studied the interface of soil with variety of materials (e.g., grout, and fibre reinforced polymers) in order to reach better understanding of the surface roughness impact on interface shear strength; and thus find a suitable material that may have higher shear strength (Chu and Yin, 2006, Giraldo 2014).

The time dependent behaviour of pile-soil interface has not been widely investigated. Ovando-Shelley (1994) studied the interface shear strength behaviour of both undisturbed and remoulded specimens of Mexico clay using direct shear apparatus. Interface strength in remoulded clays was initially less than half the interface strength of undisturbed clay specimens but it increased with time. This was related to dissipation of excess pore water pressure and reconsolidation of the soil particles at the interface level. The ultimate interface strength for remoulded clay, however, did not reach the interface strength of undisturbed specimens.

2.10.2 Pile Set-up Investigation using Pile Load Tests

Pile load tests (static and/or dynamic) are typically used to measure the actual capacity of the piles. To understand the concept of pile set-up, pile load tests are performed over time to estimate the rate of change in bearing capacity of the pile. The gradual increase in the pile bearing capacity in clay over time has been reported by a number of researchers (Seed and Reese 1955; Orrje and Broms 1967; Flaate 1972; Fellenius and Samson 1976; Bozozuk et al. 1978; and many others). The maximum pore water pressure was observed immediately after the pile driving, and also the lowest bearing capacity was reported at initial stage (EOD). Seed and Reese (1955) performed static pile load tests on full-scale instrumented pipe piles which were driven into organic silty clay

and estimated about 50 to 60% increase in the shear strength of the soil (from the initial shear strength) thirty days after driving. Seed and Reese (1955) stated that this increase was due to a decrease in water content thirty days after driving the pile. On the other hand, some researchers such as Preim and Hussein (1989) used variety of pile materials to analyse the result of the pile set-up. In comparison, concrete piles were described to achieve higher set-up than steel piles. This is due to higher pile-soil interface friction and concrete's greater material permeability than steel. Alternatively, type of the piles also have shown to affect the rate of set-up due to the extent of remoulding and disturbance of adjacent soils to the pile. Lukas and Bushel (1989) discovered an increase of 50% in the bearing capacity of H-piles driven into soft clay in Chicago, whereas there was only an increase of 25% in the capacity of pipe piles. Afshin and Rayhani (2015) investigated the pile set-up phenomenon by developing a series of small-scale pile load tests in Champlain Sea clay, and the range of set-up value was 1.6 to 3.3. Similar behaviour was reported by Long et al. (1999), that pile shaft capacity was increased in the range of one up to six times from the initial capacity after driving. The change in pile capacity with time is clarified partly by the dissipation of excess pore pressures, while aging may also relate to the gain in capacity over time. Attwooll et al. (1999) investigated nine sets of full-scale pile load tests in clay that were performed in Salt Lake City. The results showed 86 to 117% increase in pile capacity 93 days after installation and a notable increase in shaft resistance that grows with depth.

2.11 Summary of Literature Review

This literature review provides the overview and theories which have been applied to explain the increase in the capacity of a pile over time after driving pile in clay. This phenomenon is called pile set-up or freeze. Driving a pile cause the soil disturbance and remoulding while this

disturbance induces excess pore water pressure, and as a result decrease of the soil shear strength. Immediately after the formation of excess pore water pressure (EOD), the pore water pressure tends to dissipate and stabilize the clay system. In most cases, soil shear strength and the bearing capacity of the pile increased over time.

Widespread investigations were accomplished to understand pile set-up and some of the essential mechanisms and their effect in pile set-up. Throughout the studies, pile set-up was affected by type of soils, pile types and sizes, pile driving methods, rates of loading, and pile-soil interface properties. Different rates of increase in pile capacity have been reported for piles in clay, and at this point the range of change in bearing capacity was approximately 20 to 1150% from the initial pile capacity. In addition, many empirical equations have been suggested to predict the pile set-up. Moreover, some researchers have developed numerical methods to simulate the pile set-up by using consolidation theory and cavity expansion and others.

Although, this published literature provides an insight to the subject of the pile set-up, the exact mechanism of set-up is not well understood. Furthermore, most of the suggested empirical relationships that were developed through data from lab/field tests and modeling the pile set-up have only provided information for specific regions with particular soil characteristics. In this study, the rate of set-up specifically in sensitive clay is investigated as there is a need to develop a dependable set-up rate for driven piles in sensitive clay due to lack of proper investigation and understanding. Thus, this research aims to investigate and evaluate the pile set-up by performing medium-scale pile load tests in sensitive clay, while monitoring the pore water pressure, in order to use the aftermath for future practice.

Chapter 3: Evolution of Pile-Clay Interface Strength over Time

3.1 Introduction

Determination of ultimate pile capacity is significant for proper design and construction of pile foundations. Pile capacity is typically estimated by using several empirical expressions (e.g., Canadian Foundation Engineering Manual, 2007) and then it would be validated by static/dynamic pile load tests. The pile load test is often performed shortly after pile installation, and the result of the pile load test is usually anticipated to be the ultimate pile capacity in most design cases. However, these results might be much less than the actual ultimate pile capacity due to soil disturbance during pile driving. While driving the pile, the soil experiences remoulding and large deformations which cause the generation of the excess pore water pressure, and in turn reduces the shear strength and pile bearing capacity. In cohesive soils, this excess pore water pressure may be much larger than the initial effective overburden stress (Appolonia, 1971). The exact mechanism of pile capacity increase is not fully understood, but the capacity increase is mainly attributed to the dissipation of excess pore water pressure in the soil-pile interface region and subsequent reconsolidation of the soil (Komurka *et al.* 2003). Axelsson (1998) and Schmertman (1991) reported that ageing can also induce additional capacity increase due to an increase in the shear modulus and stiffness of the soil and reducing its compressibility. A general relationship was presented by Skov and Denver (1988), which expresses the increase of the pile capacity with respect to the log of time.

Laboratory testing of soils sheared against other materials may be carried out to develop an understanding into the characteristics of the stress-strain and the frictional behaviour of piles over time. This chapter is focusing on the evolution of pile-soil interface strength over time through interface shear testing of both concrete-soil and steel-soil interactive systems using direct shear tests. The result of the interface shear tests is compared with those achieved during medium-scale pile-load tests in the field.

3.2 Soil Properties

The soil used in this study is a marine sensitive clay called Leda clay which covers Ottawa Valley and south of Province of Quebec. This clay was formed near the end of the most recent glaciation period in the pre-historic Champlain Sea. The soil unit weight was measured to be about 15.3 $kN/m^3$and the water content of the soil was measured at about 52% (referred to ASTM D2216). From the Atterberg limit test, the plasticity index of this Leda clay was determined at approximately 24% with a liquid limit of 51% (referred to ASTM D4318). The particle size distribution of the sensitive clay performing hydrometer test showed a clay fraction of about 40% as shown in Figure 3.1 (ASTM D422). The soil was classified to be highly plastic clay (CH) according to Unified Soil Classification System (referred to ASTM D2487). Vane shear tests were performed at depths of 0.5, 1.0, 1.5, and 2.0 meter according to ASTM D2573 to determine the average undrained shear strength which was estimated to be about 35 kPa. The coefficient of one-dimensional consolidation was measured according to ASTM D2435/2435M and presented a value of 1.4×10^{-8} m^2/s (summarized property index in Table 3.1).

Table 3.1: Index properties of Leda Clay

ρ (Mg/m^3)	w (%)	LL (%)	PI (%)	w_{opt} (%)	$\rho_{d(max)}$ (Mg/m^3)	S_u (kPa)	C' (kPa)	ϕ' (°, deg)	C_v (m^2/s)
1.53	52	51	24	30	1.41	35	8.6	26	1.40×10^{-8}

Notes: ρ, density; w, moisture content; w_{opt}, optimum moisture content; LL, liquid limit; PI, plasticity index; $\rho_{d(max)}$, maximum dry density; S_u, undrained shear strength; C', cohesion; Φ', friction angle; C_v, coefficient of consolidation.

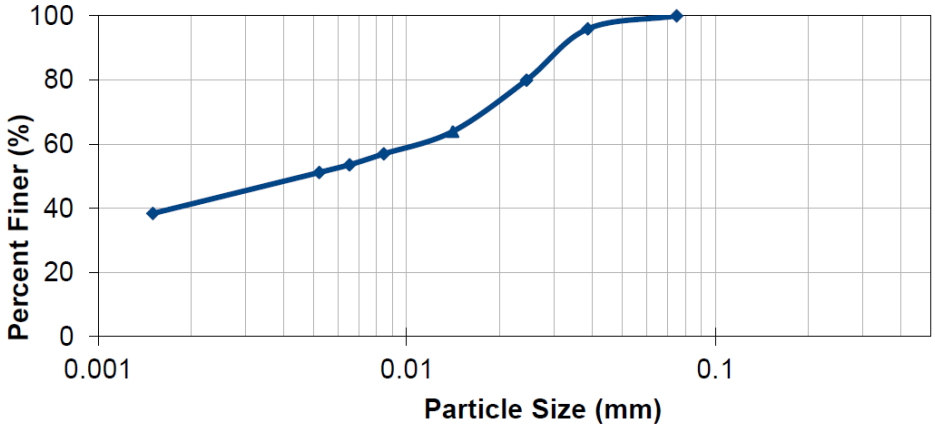

Figure 3.1: Distribution of particle size (Giraldo, 2014)

3.3 Pile Interfaces

The interface between the soil and pile materials plays a critical role in determining the frictional capacity along the pile shaft. In this study, two common pile materials, steel and concrete, are used to study their interface strength along with evaluation of the shear strengths over time in Leda clay (Figure 3.2). A modified interface test (direct shear apparatus) was employed under the procedure specified in ASTM D3080/D3080M.

Pile surface roughness is a major factor that may affect the interface shear strength in cohesive and cohesionless soils (Lemos and Vaughan, 2000; Yoshimi and Kishida, 1981). A number of studies have mentioned the importance of the surface roughness in interface shear strength. For instance, the shear resistance of pile-sand interface was found to be reliant on the

roughness of the plane surface of interface with respect to the size of the sand particles, sand type, normal stress, density and the rate of loading (Lemos and Vaughan, 2000). Uesugi and Kishida (1986) stated that as the surface roughness increases, the shearing occurs more within the sand medium. Alternatively, for the case that the interface surface is very rough, the shear strength of the interface is identical to the shear strength of the sand. In clay, the interface shear strength is dependent on sample preparation technique, water content, clay particle fraction, loading rate, and roughness of the surface. The soil interface shearing strength is typically smaller than the shear strength of the clay alone, and as the surface roughness decreases, the interface shear strength tends to decrease (Kraft et al., 1981). For instance, Tsubakihara & Kishida (1993) stated that for steel with critical roughness of 10 μm and greater, the shear failure occurs within the clay specimen instead of interface sliding. On the other hand, when steel surface has lower than critical roughness, interface sliding may occur at the peak strength.

Surface roughness was measured using a FARO© arm measuring device to scan each interface surface across a linear path and evaluate the vertical tip deviations. In this simplified method, the interface roughness was estimated by calculating the average displacements obtained at each measured point, known as total roughness R_t, and by calculating the root mean square of the same data, known as average roughness, R_a, as shown in following expressions:

$$R_t = \frac{h_1+h_2+\cdots+h_n}{n} \qquad R_a = \sqrt{\frac{h_1^2+h_2^2\ldots+h_n^2}{n}} \tag{3.1}$$

The steel interface used in this study was a piece of square plate with about 25 mm thickness which was fabricated in a way to simulate the interaction of the soil and steel. The total roughness of the steel plate, R_t was 9.70 μm and the average roughness, R_a was calculated to be 11.30 μm. The concrete specimen was prepared by using pre-mixed Portland cement plus fine sand with 1:3 ratio

of fine sand to cement, and 30% water content by weight. The concrete specimen was cast in bottom portion of the shear box, airtight with Plexiglas in order to achieve smooth and flat surface, and allowed to cure for 14 days prior to the interface testing. The total roughness of the concrete specimen, R_t was estimated at about 7.1 μm and the average roughness, R_a was calculated to be 9.1 μm.

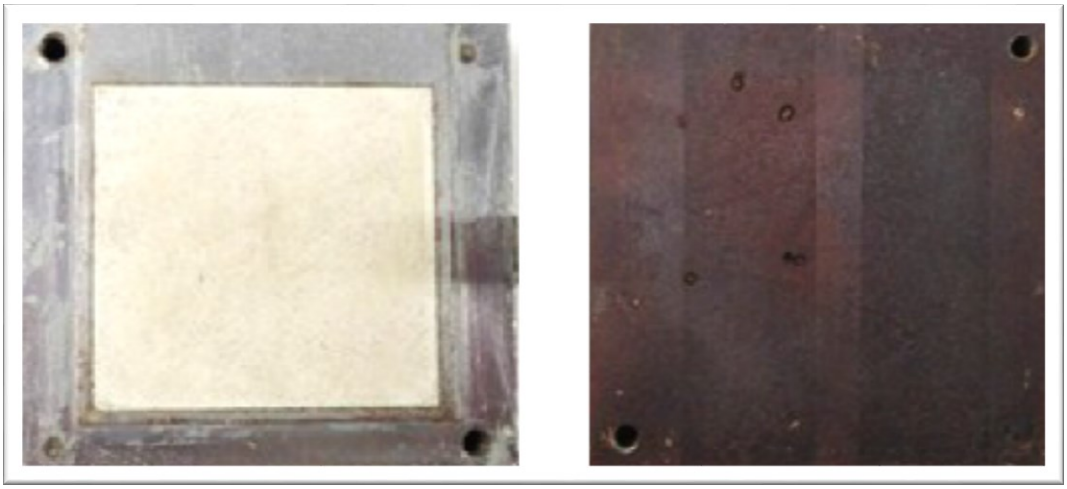

Figure 3.2: Surface interface for concrete (left) and steel (right)

3.4 Procurement of Soil Samples

The soil samples were obtained from "Canadian Geotechnical Site No. 1" located in Gloucester, Ontario. In order to reach the clay layered used for sampling, the top soil was removed upto a depth of 1.2m using an excavator. PVC pipes with 300 mm diameters and height of 150mm were used to obtain relatively undisturbed clay samples. A series of plywood beams were placed on top of sample tubes and the sample tubes were slowly pushed into the ground while ensuring minimal disturbance in all samples. Following the embedment, the sample tubes were carefully extracted by excavating the soil that surrounded the sample tubes. Immediately after extraction, the filled tubes were sealed to avoid desiccation and sustain the in-situ moisture conditions. The undisturbed

samples were transported to the test facility where soil specimens were prepared and the interface test was conducted (as shown in Figure 3.3).

Figure 3.3: Extracting undisturbed soil samples

3.5 Experimental Procedure and Preparation of Test Specimen

The interface test was performed using a modified direct shear test device (ASTM D3080/D3080M) where the interface materials were placed in the lower-half of the box and the soil was placed in the upper-half of the box. The standard shear box has outer dimensions of 90x90 mm and inner dimensions of 60 x60 mm with a specimen height of 25 mm (i.e., bottom section). The normal pressure is applied through a vertical load jig using weights to exert vertical stresses to the specimen. In addition, the shearing stresses are measured through a digital load cell attached horizontally to the shear box. Both horizontal and vertical strain gauges are joined to a digital logging station and measured through a linear variable differential transducer (LVDT) which is viewed on the LabView software.

For the soil-steel interface testing, the square steel plate was placed at the bottom section of the shear box and the undisturbed soil sample was cut and fitted in the top section of the shear box, while ensuring proper interaction between the steel and clay. For the soil-concrete interface tests, the bottom section of the shear box was filled with the prepared concrete specimen and the undisturbed clay sample was cut and fitted in the top section and established full interaction with concrete surface as shown in Figure 3.4 (a) and (b). After interface sample preparation, the shear box was placed in distilled water for 24 hours to achieve sample hydration. Previous research on a similar soil has shown that the specimen attain saturated condition within a period of 24 h (Taha and Fall, 2013). Three sets of normal stresses (30, 60, and 150 kPa) were imposed upon the pile-soil system to recreate the overburden pressure in the field and to consolidate the soil. After consolidation, static horizontal stresses were applied at different shearing rates (0.05 mm/min and 2.5 mm/min) to investigate the effective parameters in shear strength variation over time.

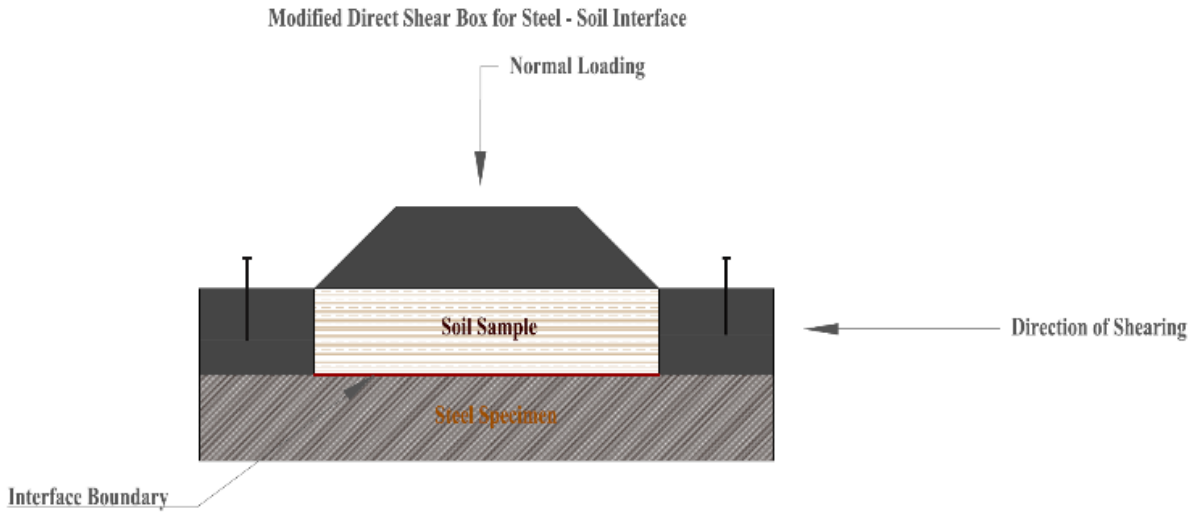

Figure 3.4(a): Modified shear box schematic for steel specimen

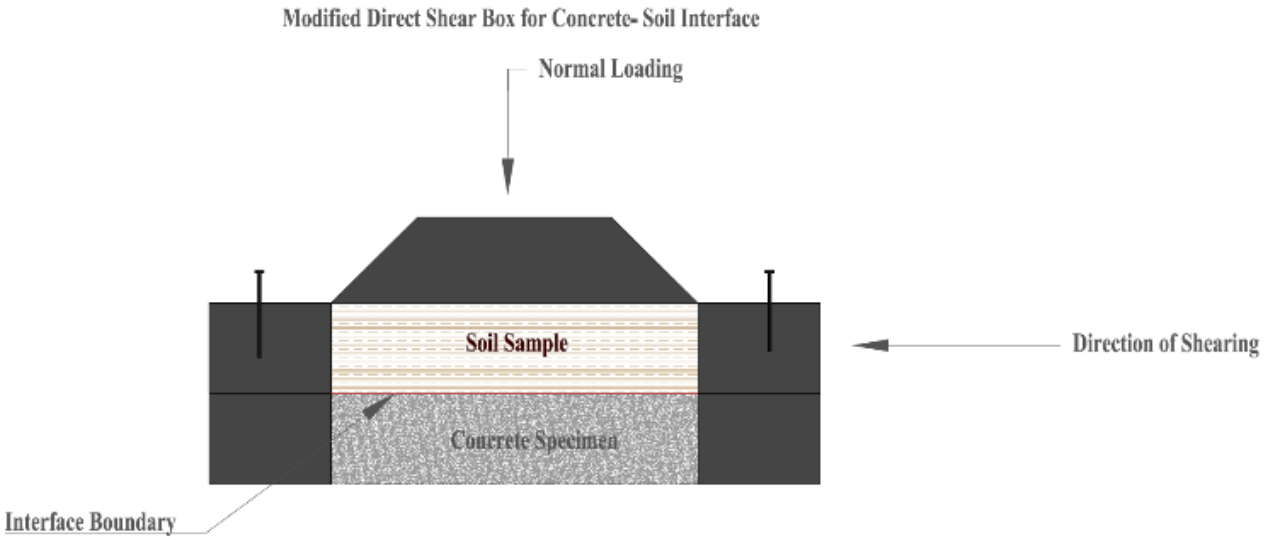

Figure 3.4 (b): Modified shear box schematic for concrete specimen

3.6 Results and Discussion of Initial Interface Properties

3.6.1 Fast Loading Rate

A set of direct shear tests was carried out at a fast loading rate (2.5 mm/min) to determine the soil and interface shear strength properties of concrete and steel. Figure 3.5 demonstrates the shear

stress versus displacement curves for both soil-soil and soil-interface (i.e., concrete and steel) systems at three specific normal stresses (30, 60, and 150 kPa). As presented, the shear stress of the soil and concrete interface is steadied at a horizontal displacement of 2 mm for all normal stresses while the steel interface is stabilized at a small horizontal displacement of about 0.25 mm. The maximum shear stresses for soil-soil shear tests ranged from 36 kPa to 107 kPa under the applied normal stresses. This range was much lower for both the interface specimens. For steel-soil interface tests, the shear stress ranged from about 17 to 43 kPa. Similar shear stress values were achieved for the concrete-soil interface specimens ranging from 19 to 40 kPa.

The Mohr-Coulomb failure criterion is conventionally used in practice to estimate the interface shear strength. For the series of normal stresses deliberated in this study and expected in the field, a linear Mohr-Coulomb failure standard may be used to estimate the shear strength properties of the soil-soil and interface tests. Figure 3.6 shows the failure envelope for initial interface tests including soil-soil, concrete-soil and steel-soil. These envelopes were obtained by fitting linear regression lines through each set of maximum interface shear stress versus normal stress. The overall result of the failure envelope indicates that the soil has much higher friction angle and cohesion at around 21° and 52 kPa, respectively. Comparing these results with the drained shear strength properties shown in Table 3.1 underscores the importance of rate of shearing on shear strength properties. As the rate of loading increases, the soil friction angle decreases while cohesion might slightly increase.

The steel- and concrete interfaces showed relatively similar behaviour in terms of both adhesion and interface friction angle. However, the interface shear strength parameters for both the steel- and concrete-soil specimens were significantly lower than those for the soil-soil tests. This could be related to lower surface roughness of both the steel and concrete specimens as

discussed in section 3.3. Result for the concrete interface indicates the lowest interface friction angle of $\delta=10°$, while the steel interface friction angle was about 12°. On the other hand, concrete interface showed an apparent interface adhesion of 15.6 kPa which is higher than steel adhesion of 11 kPa. This may be related to the slight difference in surface roughness of the steel and concrete surfaces as well as the water absorption potential of the concrete specimen in concrete interface test. However, it can be noticed that the trend in all three figures may not illustrate a consistent change in modulus of elasticity at each normal stress which this may be occurred due to the seating error during setting up the shear box. Table 3.2 summarizes the results of these tests including the friction angle and cohesion/adhesion of the soil and interfaces for fast loading rate.

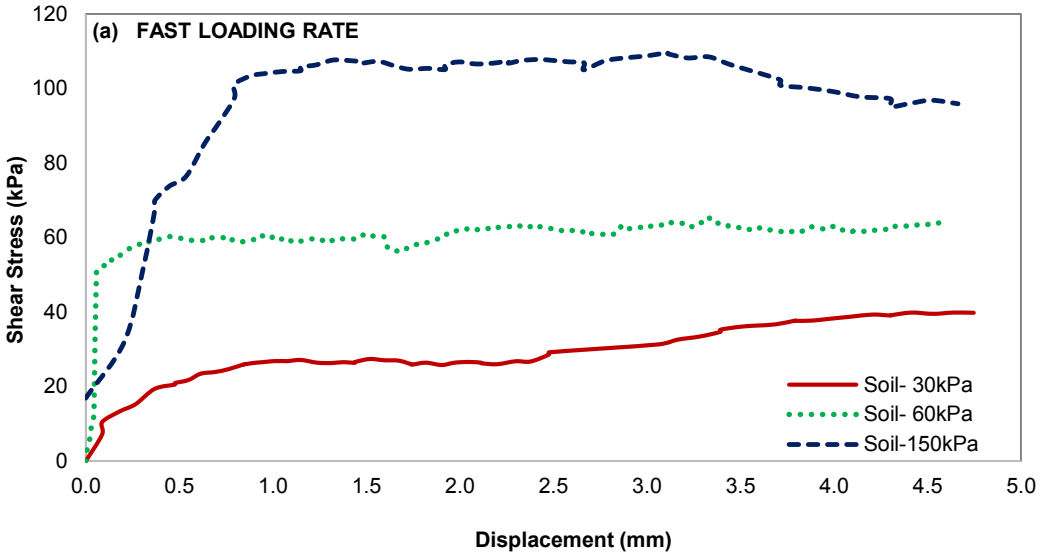

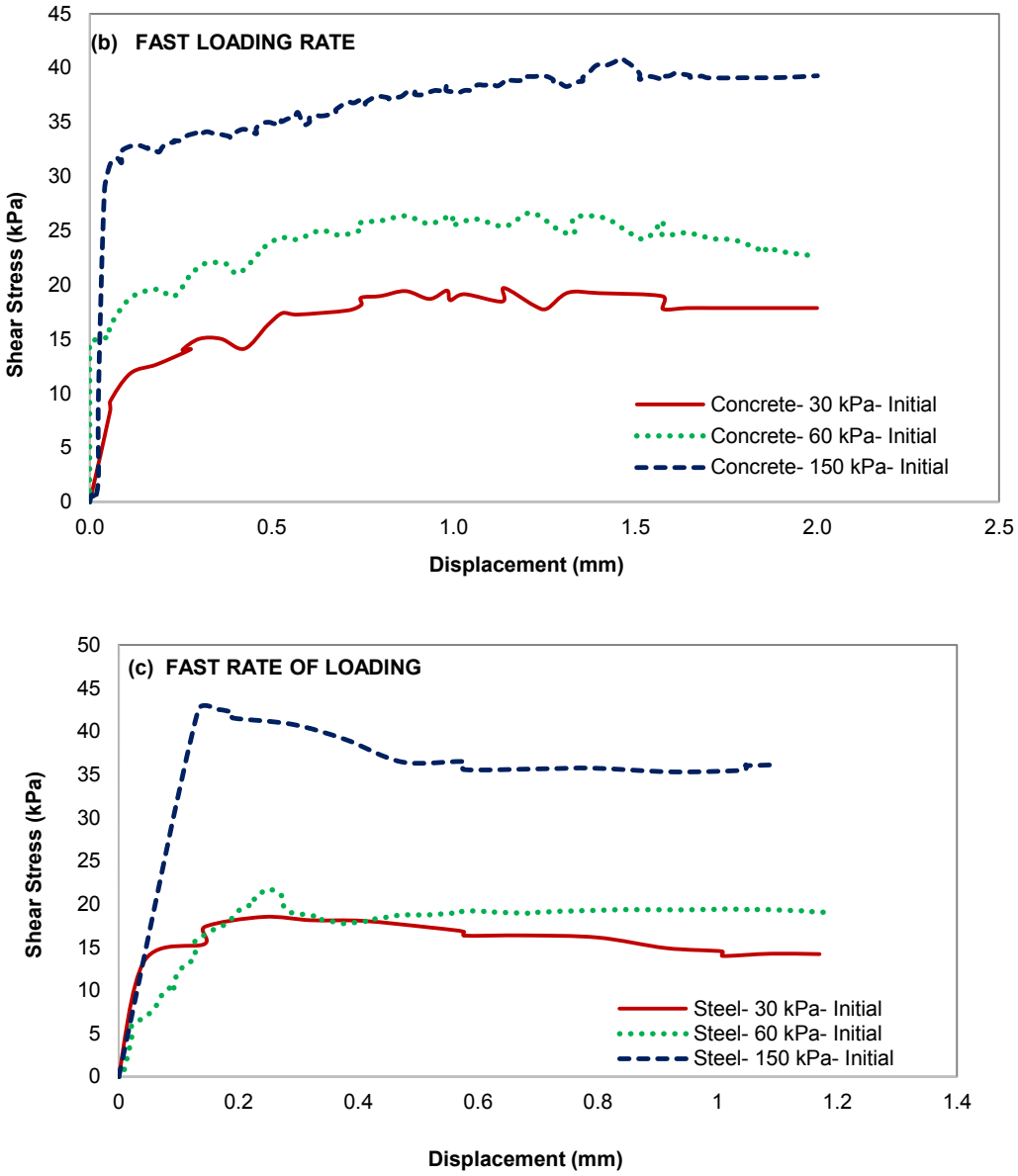

Figure 3.5: Shear Stress vs. displacement curves at initial for fast loading rate a) soil-soil tests, b) soil-concrete, c) soil-steel

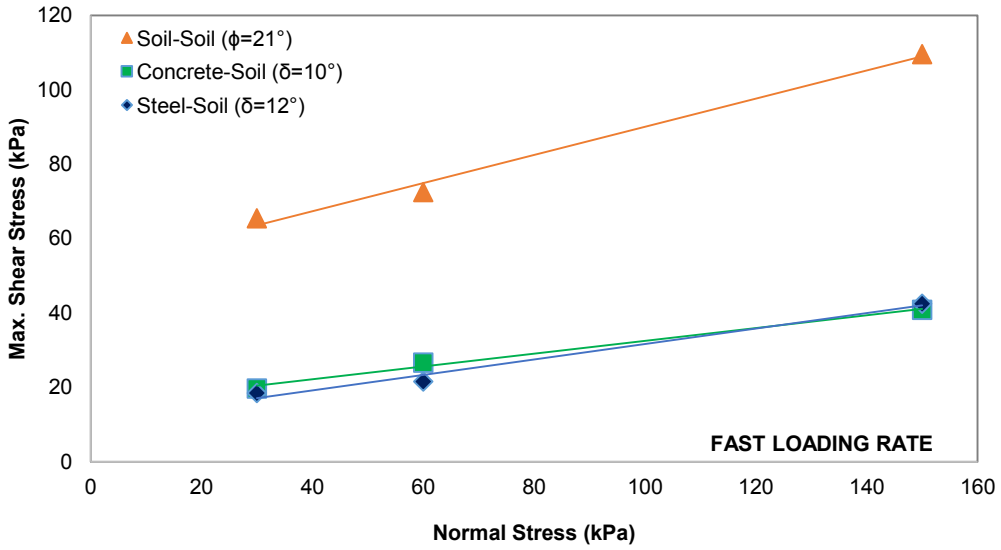

Figure 3.6: Stress envelope for soil-soil and soil-pile shear test (fast loading rate)

3.6.2 Slow Loading Rate

A series of direct shear tests were also performed at much lower shearing rate of 0.05 mm/min to evaluate the interface shear behaviour of Leda clay by comparing steel and concrete against clay under three different normal stresses of 30, 60, and 150 kPa. The shear stress versus horizontal displacement for these tests are plotted for both soil-soil and soil-interface systems in Figure 3.7. The stress-strain plots for soil-soil interface tests are illustrating rather similar behaviour to the concrete-clay; however the interface shear strength may not be the same. The stress-strain curves for soil-soil and concrete-soil interface tests demonstrated a maximum shear stress followed by a constant volume rate residual shear stress. The ultimate shear stress range was also similar for both the soil-soil and concrete-soil tests, demonstrating a shear stress range of about 18 to 70 kPa. On the other hand, the stress-strain curves for steel-soil interface showed a peak shear stress followed by a strain softening until reaching a residual shear stress. The ultimate shear stress

values for the steel-soil are also the lowest maximum shear stress in all three overburden pressures compared to the others (30, 60 and 150 kPa). The maximum shear stress is typically reached at different rate for most interface tests, for instance the steel-soil interface showed the maximum stress at the displacement range of 0.1-0.6 mm, while the concrete-soil interface reached the maximum stress at a horizontal displacement of 0.7 mm (Figure 3.7 b and c). The evaluation of the result shows that the concrete interface specimen carries a slight strain hardening behaviour, and reaches a maximum shear stress gradually (i.e., at higher strain level) before reaching steady state of residual shear stress. In addition, the concrete interface showed slightly higher shear strength compared to the soil-soil interface, whereas the steel interface presented the lowest. This difference is probably attributed to variation of the surface roughness and pile material properties.

According to several researchers (e.g., Lemos and Vaughan, 2000), the shear strength in clay-clay interface may be associated to the type of failure including, sliding shear, turbulent shear, and transitional shear. These failures are classified based on the ratio of rotund to platy particles in the soil. At greater clay fraction, platy particles tend to slide due to the distinct particle orientation leading to poorer shear strength which is known as sliding shear. However, the clay particles may rotate due to high ratio of rotund particles which cause to prevent the placement effect of platy particles; this is called as turbulent shear. In addition, the failure that represents an in-between behaviour of the rotational and sliding shear is defined as transitional shear (Lupini et al., 1981; Lemos and Vaughan, 2000). The shearing mechanism for steel-clay interface here seems to be similar to sliding shear due to smoother surface and high clay fraction, which might have led to lower shear strength.

The typical results of failure envelope (Figure 3.8) using a Mohr-Coulomb failure mechanism show a largest friction angle for soil, then concrete followed by steel interface friction

angle. Table 3.2 summarizes the frictional angle and adhesion of clay and clay interface tests. It can be seen that the interface shear strength parameters of the soil-steel presents the lowest interface friction angle (δ_{steel}=10°) followed by concrete interface friction angle ($\delta_{concrete}$=24°), whereas the apparent adhesion of steel (c_a= 16.8 kPa) is greater than the adhesion of the concrete interface (c_a=9.1 kPa). This variance may be justified by the orientation of clay particles along the shear region and the surface roughness of the plane interface, respectively. Rouaiguia (2012) stated that steel surfaces are typically smooth which may cause the clay particles to be orientated smoothly in the direction of the movement. Consequently, this property reduces the interface shear resistance and the interface friction angle. The inconsistency in modulus of elasticity for normal stresses shown in Fig. 3.7(b) could be related to possible seating error during setting up the shear box specimens.

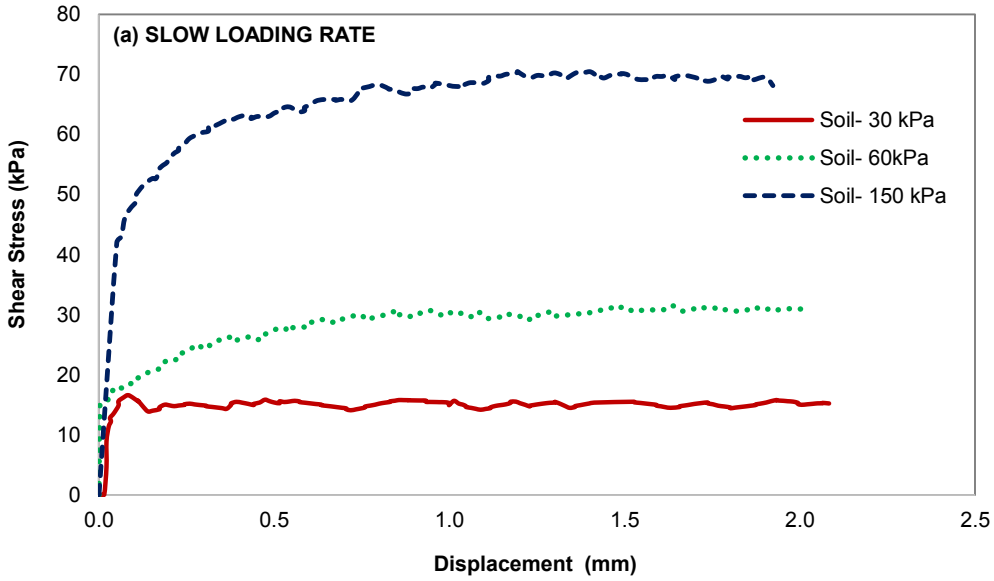

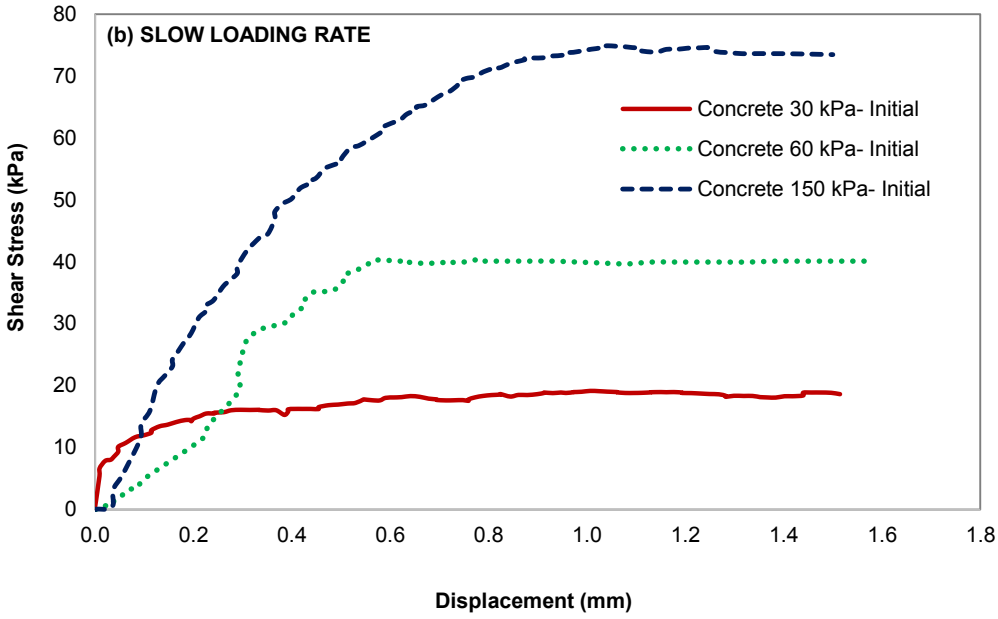

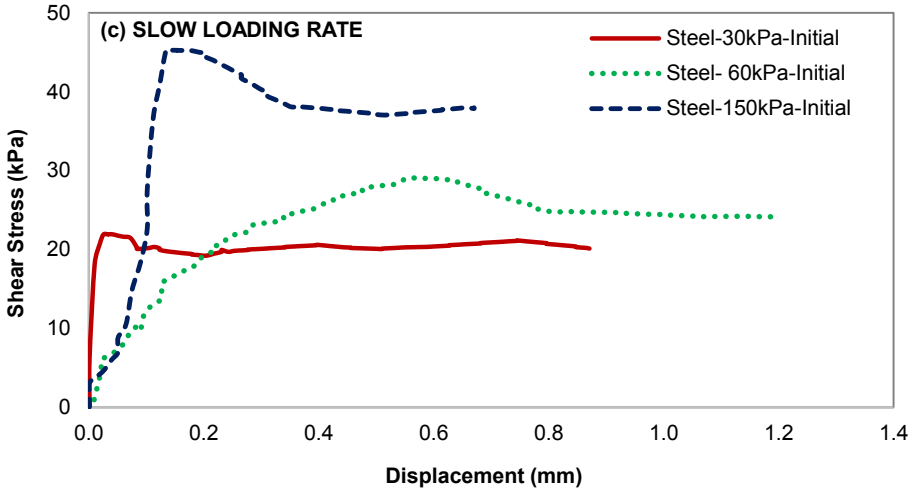

Figure 3.7: Shear Stress versus displacement curves slow loading rate

a) soil-soil tests, b) soil-concrete, c) soil-steel

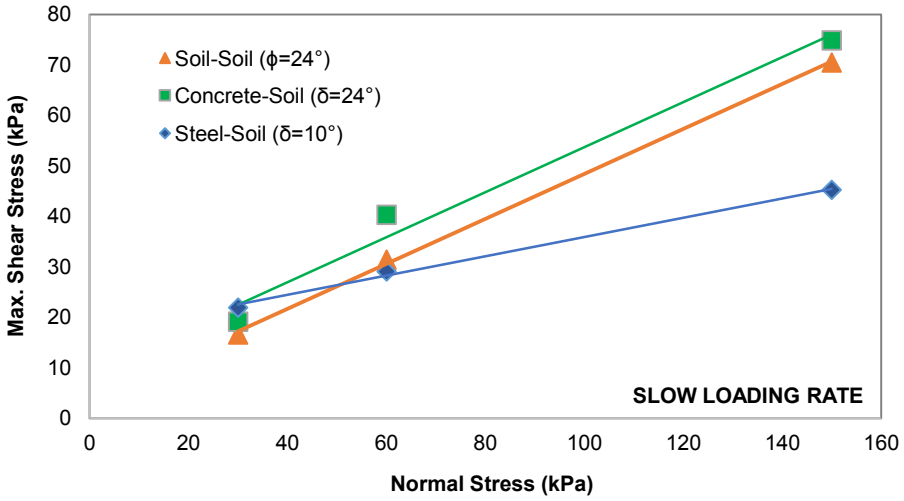

Figure 3.8: Failure envelope for soil-soil and soil-pile shear test (slow loading rate)

Table 3.2: Interface test parameters, soil-soil and soil-interface (concrete and steel)

Shearing Rate	Soil-Soil		Steel-Soil		Concrete-Soil	
	c (kPa)	ϕ (°)	c_a (kPa)	δ (°)	c_a (kPa)	δ (°)
Fast (2.5 mm/min)	52	20.7	11	11.7	15.3	10
Slow (0.05 mm/min)	5	24	16.8	10	9.1	24

Comparing the shear strength properties achieved using the two shearing rates (Table 3.2) shows that for the concrete-soil and soil-soil tests the interface friction angle is higher when the loading rate is lower. On the other hand the adhesion values are generally higher when the shearing rate is higher. The only exception on the adhesion value was the steel-clay interfaces, which the adhesion value obtained from slow loading tests was slightly higher than that measured in high rate of loading (2.5 mm/min). Correlation between the soil and the interface strength values shows that the interface friction values could vary significantly for various interface materials. Without taking into account the effect of capacity increase over time, the interface friction angle was about

40-56% of the soil friction angle (δ=0.4-0.6ϕ_{soil}) for steel and approximately 50-100% of the soil friction angle (δ=0.4-0.6ϕ_{soil}) for concrete planes, depending on the rates of loading used.

3.7 Evolution of Interface Strength over Time

In order to investigate the possible change in interface shear strength over time for different pile-soil interface systems, the interface tests were repeated over various elapsed times. The interface tests were conducted at two loading rates of 2.5mm/min (named as fast loading) and 0.05mm/min (named as slow loading) to study mechanisms involved in evolution of pile-soil interface behaviour over time.

3.7.1 Concrete Interface Shear Strength

3.7.1.1 Fast Loading Rate

Figure 3.9a shows the shear stress-displacement curves for the initial interface test as well as those repeated 1 day, 3, and 14 days after initial testing under a normal stress of 150 kPa. In fast loading rate (2.5 mm/min), the initial maximum shear stress was approximately 41 kPa for concrete-soil interface under a normal stress of 150kPa. This value increased by almost 1.6 times its initial value and reached a maximum shear stress of about 65 kPa, 14 days after initial test. The curves at each elapsed day indicate analogous shearing behaviors under fast rate of loading. Such a behavior demonstrates that the concrete interface carries a strain hardening behaviour under fast loading rate, meaning the failure stress is reached gradually before stabilizing over time. In addition, Figure 3.9 (b) illustrates the maximum shear stresses at each elapsed day for all three normal stresses. The rate of increase in maximum shear stress is slightly higher for normal stress

of 150 kPa compared to that of 30 kPa and 60 kPa. This may be attributed to the vertical pressure applied on the specimen as well as the level of excess pore water pressure generated under different confining pressures. Whitman and Healy (1962) reported an immediate increase in strength which results from a viscosity of plane surface, and in some cases, by generation of negative pore water pressure as an effect of shearing at a higher void ratio in fast loading rate.

Figure 3.9 (c) illustrates the failure envelope of the concrete interface and the result indicates an increase from the initial interface friction angle of 9.8° up to 18.7° 14 days after initial testing. This increase has probably occurred due to dissipation of excess pore water pressure after initial interface testing. A similar behaviour was reported by Ovando-Shelley (1995) for both undisturbed and remoulded specimens of Mexico Clay using direct shear apparatus. Interface strength in remoulded clays was initially less than half the interface strength of undisturbed clay specimens but it increased over time. This was related to dissipation of excess pore water pressure and reconsolidation of the soil particles at the interface level. Considering this time-dependent strength increase, the ratio between the interface friction angle, δ, and the friction angle of the soil increases from an initial value of about 50% to a final value of 90% under fast loading rate (δ=0.9 ϕ). Values of the interface friction angle for piles driven into the Leda clay are generally taken to be $0.5 \text{ to } 0.7 \times \phi_{soil}$. Implementing the pile set-up into pile design would provide much higher bearing capacity and hence will decrease the cost of pilling.

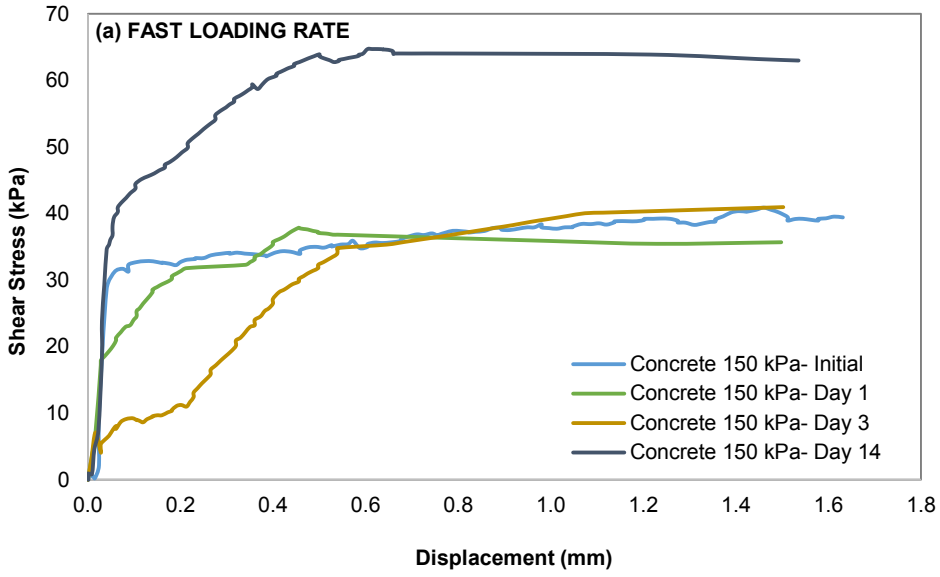
(a) FAST LOADING RATE
Shear Stress (kPa)
Displacement (mm)
Concrete 150 kPa- Initial
Concrete 150 kPa- Day 1
Concrete 150 kPa- Day 3
Concrete 150 kPa- Day 14

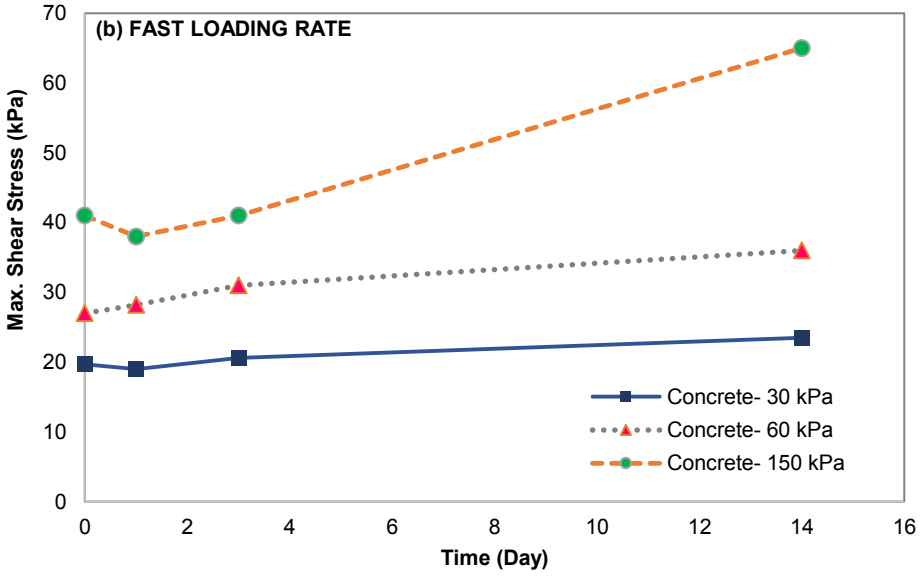
(b) FAST LOADING RATE
Max. Shear Stress (kPa)
Time (Day)
Concrete- 30 kPa
Concrete- 60 kPa
Concrete- 150 kPa

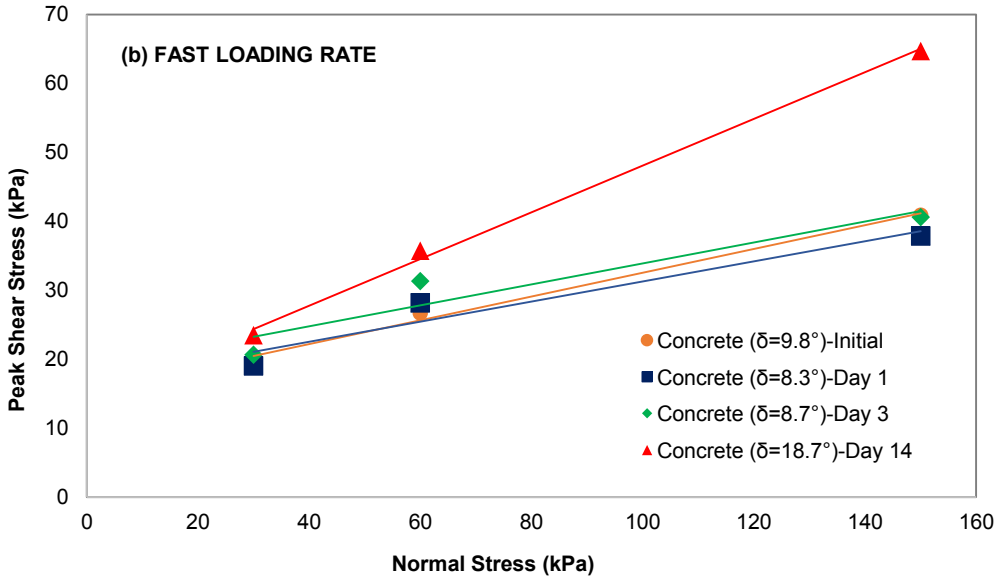

Figure 3.9 (a): Increase in interface strength of concrete-soil at normal stress of 150 kPa (fast loading rate); (b) Increase in maximum shear stress over time (fast loading rate); (c) Failure envelope at each elapsed time under fast loading rate

3.7.1.2 Slow Loading Rate

Interface shear tests were also conducted at a slower shearing rate of 0.05 mm/min and repeated 1, 3, and 14 days after initial shearing to study the progress of the interface shear strength over time and evaluate the possible effect of aging on pile set-up for concrete-soil system. The results of the shear stress versus displacement over time at constant confining pressure of 150 kPa are presented in Figure 3.10(a). The concrete-soil specimen was allowed to consolidate after initial shearing which caused to gain strength as the elapsed time increased. The maximum shear stress for concrete-soil interface under identical confining pressure of 150 kPa increased from 75 kPa at initial shearing strength up to 86 kPa 14 day after the initial test. Figure 3.10(b) illustrates the change of the interface shear stress at the three normal stresses over different elapsed times. It can be seen that the maximum shear stress generally increased over time for all normal stresses used.

As the rate of loading was small, it was assumed that this very low shearing rate would not induce any significant excess pore water pressure and, hence, this increase in shear strength could be linked to aging of the remoulded soil at the interface region. The aging of soil in driven piles is typically related to thixotropy, secondary compression, particle interference, and clay dispersion (Camp et al., 1993; Long et al., 1999; Schmertmann, 1991). In addition, aging may increase the pile–soil interface friction (McVay et al., 1999) at an approximately linear rate with the log of time (Schmertmann, 1991). Although the maximum shear stress over time increased for all these cases, however, the interface friction angle estimated over time based on the stress envelope (Figure 3.10c) has not increased significantly. This could be related to the fact that the aging might take much longer time than what was studied here. This also could be due to the disturbance of the interface sample during each interface test.

Lehane and Jardine (1994) stated that the effective stress in the soil adjacent to the pile will slowly decrease during the shearing when the pile is driven, and consequently, the interface friction angle will reduce to a residual value consistent with the interface friction angle at the fast loading rate and comparatively low level of effective stress. Table 3.3 presents the measured maximum interface friction angles and apparent adhesions at low and high shearing rate over time, which they all were estimated from the shear stress envelope. From the results, it can be seen that the maximum interface friction angle during fast shearing rate is always lower than the maximum interface friction angle at slow shearing rate. This is usually related to the excess pore water pressure and aging mechanism, respectively. On the other hand, the maximum interface friction angle at fast loading rate has been increasing over time due to the dissipation of excess pore water pressure, and reaching the steady value at slow loading rate. For instance, it can be seen that the maximum interface friction angle at the fast loading rate on day 14 reached closer to the initial

value on day 14 at the slow loading rate. Although, it did not reach the actual interface value even after consolidation and dissipation of the pore water pressure took place after initial shearing. This may be due the fact that 14 days might not be sufficient enough for dissipation of excess pore water pressure and consolidation of the remoulded clay. In addition, the apparent adhesion is estimated based on the y-intercept of the failure envelope (Figure 3.10c), which in general increases with time.

Table 3.3: Comparing the interface friction angle at different shearing rate for concrete interface

Shearing Rate	Elapsed Time	Adhesion (kPa)	Interface Friction Angle (°)
Fast (2.5 mm/min)	Initial	15.3	9.8
	Day 1	16.7	8.3
	Day3	18.7	8.7
	Day 14	14.2	18.7
Slow (0.05 mm/min)	Initial	9.1	24
	Day 1	0.5	28
	Day3	6.5	25
	Day 14	20.7	23.5

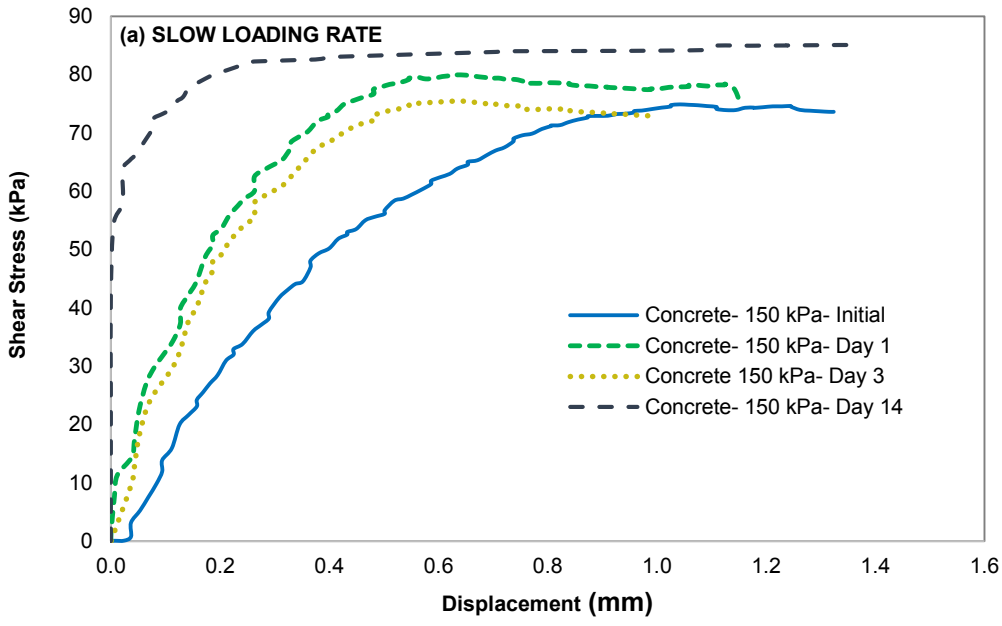

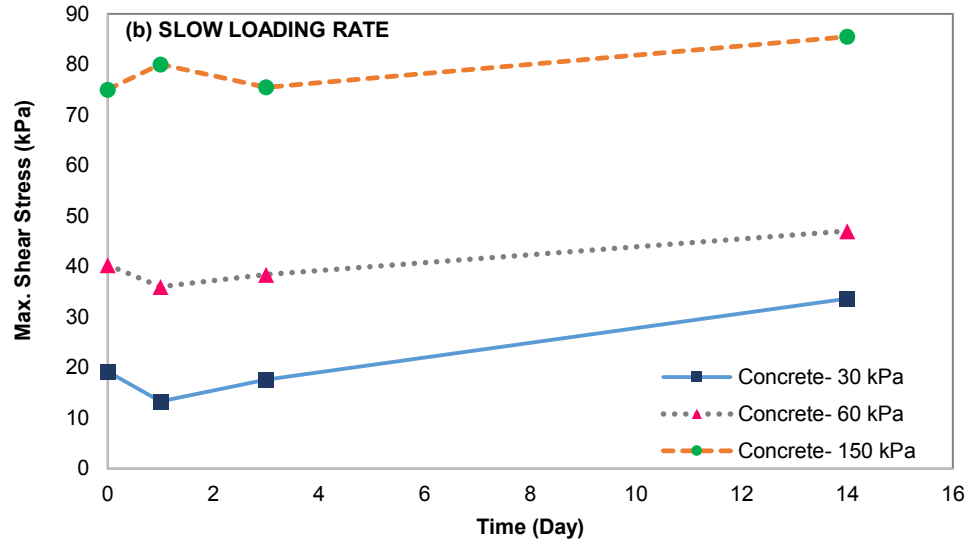

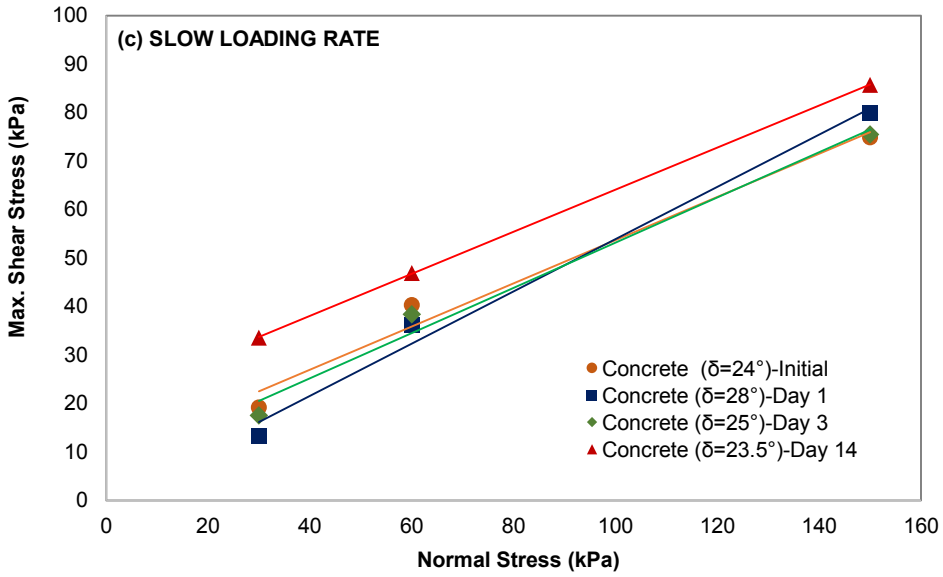

Figure 3.10: (a) Increase in interface strength of concrete-soil over time at normal stress of 150 kPa (slow loading rate); (b) Increase in maximum shear stress over time (slow loading rate); (c) Failure envelope at each elapsed time under slow loading rate

3.7.2 Steel Interface Shear Strength

3.7.2.1 Fast Loading Rate

Figure 3.11(a) presents the interface stress-strain behaviour of the steel-soil over different elapsed times for the normal stress of 150 kPa. It can be noticed that the shear stress reached a peak value at a displacement of 0.05- 0.2 mm over time and then slightly decreased to reach a volume steady residual shear stress. The initial peak shear stress was estimated at 42.5 kPa and it increased by 1.4 times and reached 60 kPa at day 14. Instantly after initial shearing, the steel-soil specimen began to consolidate which, in turn, led strength increase with time. On the other hand, this plot shows that the peak shear stress of steel interface was reached at a lower displacement range compared to that of the concrete interface under fast loading rate, which may be related to variation in their surface roughness. The results suggest that the gain in strength may be attributed due to dissipation of excess pore water pressure at the interface region over time.

Figure 3.11(b) shows the change of maximum shear stress versus elapsed time for all steel-soil specimens under various normal stresses. The shear strength also increases with time for all three normal stresses (30, 60, and 150 kPa). For instance, at a normal stress of 60 kPa, the initial peak shear stress of 18.5 kPa has increased by 1.5 times, 14 days after initial testing, reaching a peak shear stress of 25 kPa. Similarly, the rate of increase was around 1.4 times for the normal stress of 30 kPa. The average rate of change in peak shear stress was very close for all three normal stresses. These results demonstrate that due to the higher shearing rate, the effective mechanism in shear strength of the interface test is the dissipation of generated excess pore water pressure after initial shearing.

Figure 3.11(c) shows the typical shear strength envelopes for the steel-soil interface during the selected elapsed time (initial, day 1, 3, and 14) and as well the approximation of the effective interface friction angle, δ, and adhesion, c_a over time. These envelopes were obtained by fitting linear regression lines through each set of interface shear stress for their identical set of normal stresses. The interface friction angle increased from 11.7° to 16.4° after 14 days from initial test. This means that the ratio of steel-soil interface friction angle to that of the soil increased approximately 56% to 79% ($\delta=0.5\phi$ to 0.8ϕ). On the other hand, steel apparent adhesion (c_a) was at about 11 kPa initially and it reached almost 15.6 kPa after 14 days. This shows that the ratio of the steel-soil adhesion to that of the soil increased about 3-5 times its initial value.

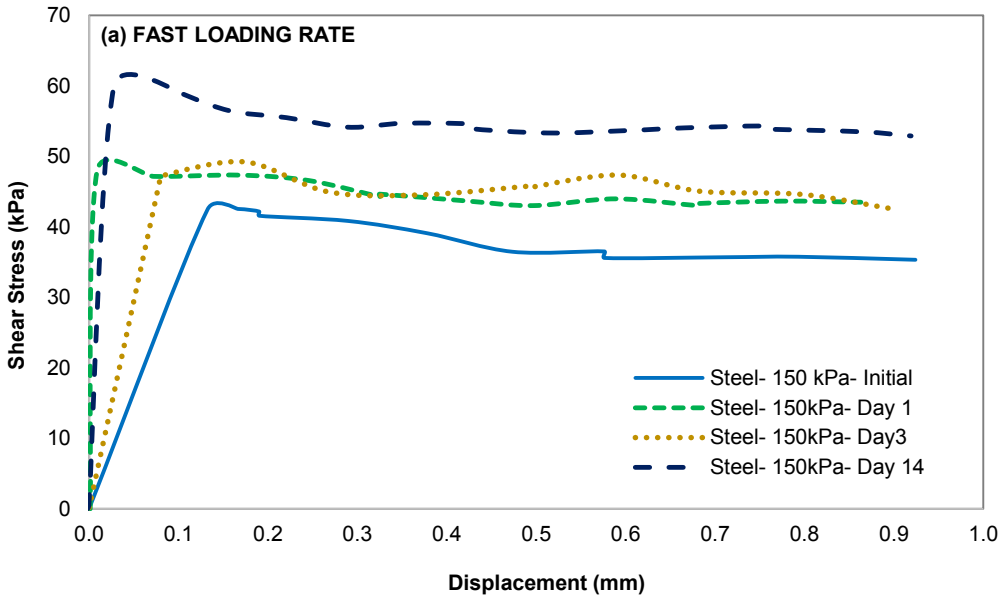

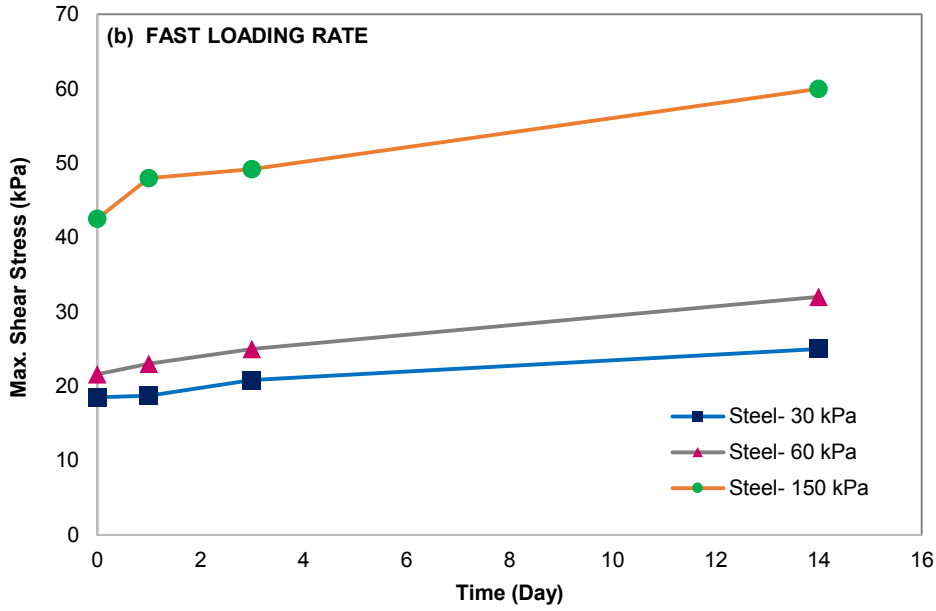

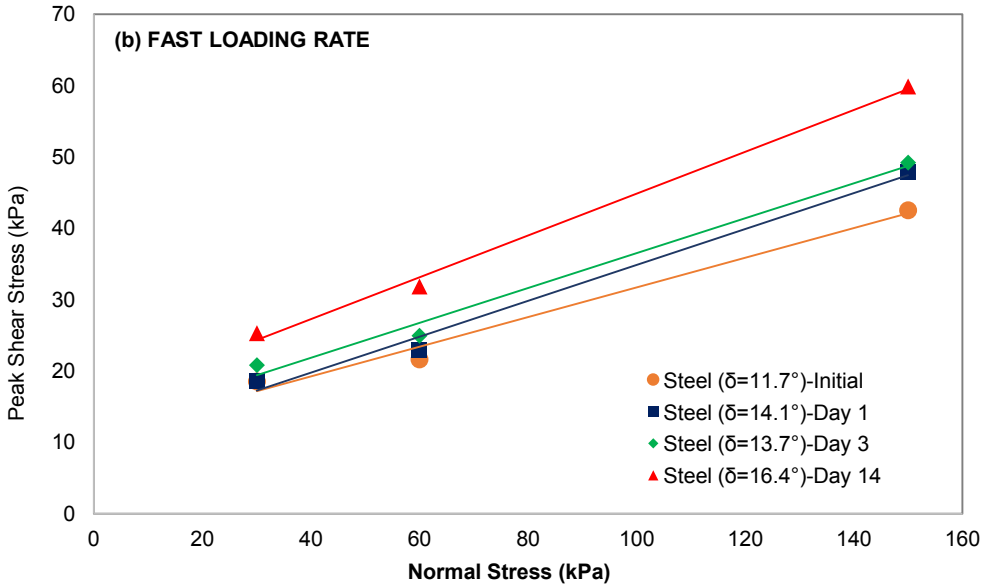

Figure 3.11: (a) Increase in interface strength of steel-soil over time at normal stress of 150 kPa (fast loading rate); (b) Increase in peak shear stress over time (fast loading rate); (c): Failure envelope at each elapsed time under fast loading rate

3.7.2.2 Slow Loading Rate

Figure 3.12 (a) illustrates the typical shear stress-displacement curves obtained for slow shearing (0.05 mm/min) under a constant normal stress of 150 kPa over time for steel-soil interface system. The interface shear tests were repeated 1, 3, and 14 days after initial shearing to study the progress of the interface shear strength over time. After initial shearing, the steel-soil interface showed a continuous increase in strength over time. The initial maximum shear stress of 45 kPa increased to 47 kPa 1 day after initial shearing, 58 kPa 3 days after initial test, and eventually increased to 69 kPa 14 days after the initial test. As the rate of shearing was very slow (0.05 mm/min), a high level of excess pore water is not expected to occur, and this significant increase in interface strength could be related to thixotropy and restructuring the disturbed clay at the interface level. A similar trend was observed for other specimens tested under normal stress of 30 and 60 kPa (Figure 3.12(b)), where the maximum shear stresses have increased by about 1.5 times their initial value.

Figure 3.12 (c) presents the failure envelope plot for the steel-soil system as well as the approximation of the effective interface adhesion, c_a, and friction angle, δ, over time. The result shows an increase in interface friction angle from 10° to 16° 14 days after initial shearing, and in addition the ratio of the interface friction angle to the soil friction angle increased from 41% to 68% in average. On a similar trend the interface adhesion has also increased from about 16kPa to 27kPa over the elapsed time tested. As mentioned earlier, this increase in interface shear strength may be related to aging and thixotropy of the disturbed clay at the interface level. On the other hand, the steel apparent adhesion (c_a) was at about 16.8 kPa initially and it reached almost 27.3 kPa at day 14. The magnitude of the steel apparent adhesion at fast loading rate is greater than the interface adhesion at slow loading rate. This can be attributed to the different mechanism involved

in both fast and slow ratings where dissipation of pore water pressure and aging mainly governs the fast and slow loadings respectively. Table 3.4 summarizes the interface shear strength properties at low and high shearing rates, which were estimated from the shear stress envelope over time.

Table 3.4: Comparing the interface friction angle at different shearing rate for steel interface

Shearing Rate	Elapsed Time	Adhesion (kPa)	Interface Friction Angle (°)
Fast (2.5 mm/min)	Initial	11	11.7
	Day 1	9.7	14.1
	Day3	12	13.7
	Day 14	15.6	16.4
Slow (0.05 mm/min)	Initial	16.8	10
	Day 1	19.8	11.3
	Day3	21.7	13.7
	Day 14	27.3	15.8

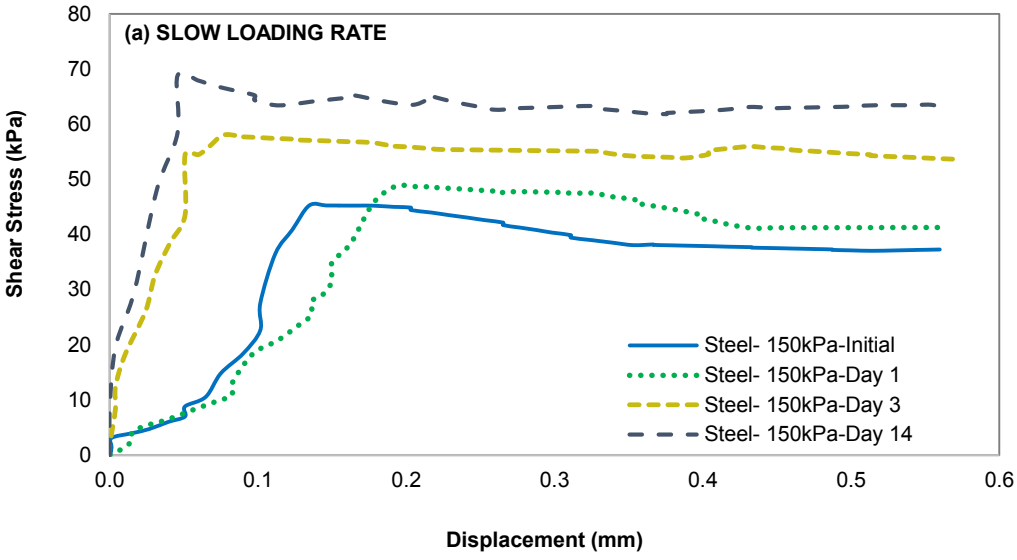

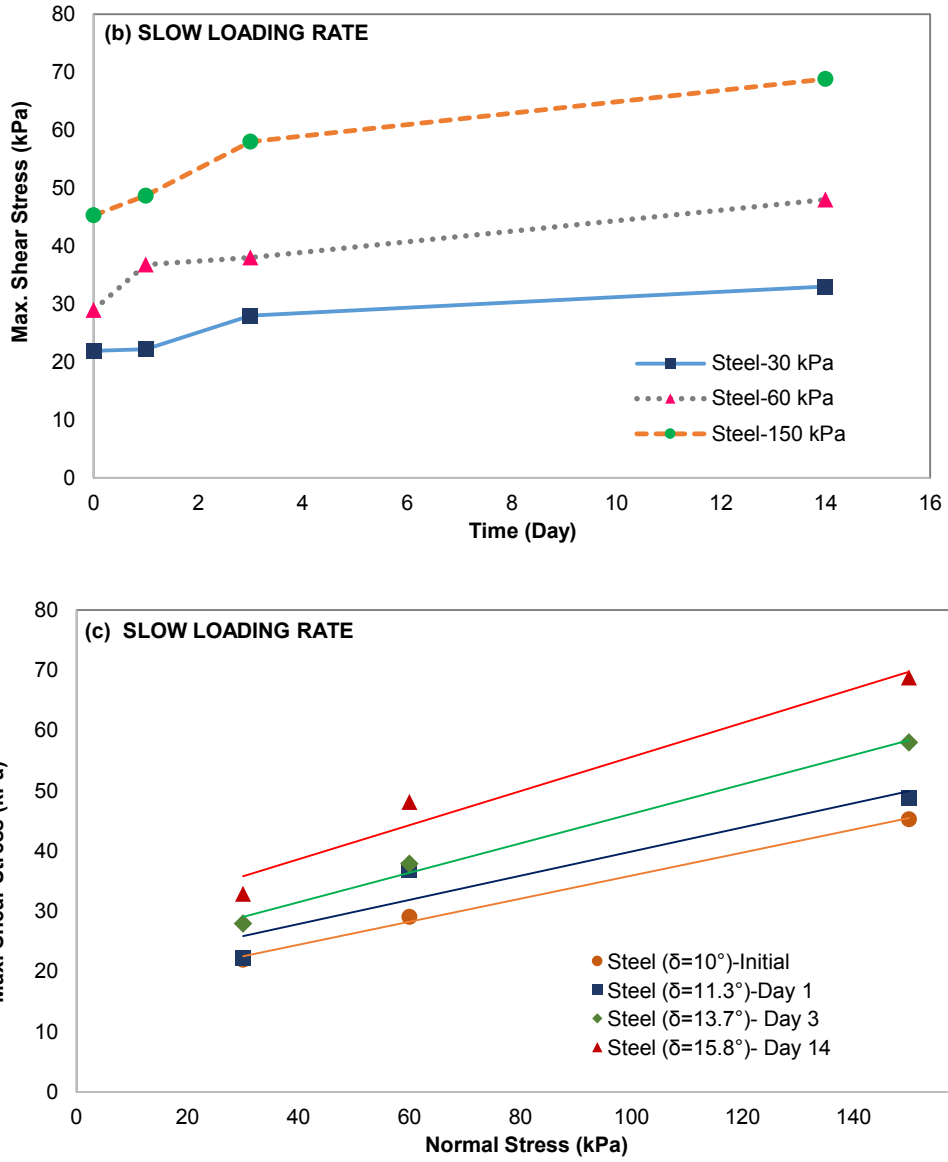

Figure 3.12: (a) Increase in interface strength of steel-soil over time at normal stress of 150 kPa (slow loading rate); (b) Increase in peak shear stress over time (slow loading rate); (c): Failure envelope at each elapsed time under slow loading rate

3.8 Effect of Loading Rate

This section compares the overall result of interface tests specifically concrete and steel for both rates of loading. Figure 3.13 demonstrates the change in maximum shear stress in two different loading rates of slow and fast over time for concrete-interface system at the normal stress of 150 kPa. The result shows that the initial shear strength of the concrete interface is higher at slow loading rate than the interface test at fast loading rate. The initial maximum shear stress of the slow loading rate was approximately 75 kPa whereas this value was at around 41 kPa for the fast loading rate. This difference in interface shear strength could be explained by the development of much higher excess pore water pressure when the interface specimens were shear at greater loading rate. This high level of excess pore water pressure leads to a reduction in effective stress at the interface level and, hence, decreases interface shear strength.

The rate of increase in interface shear strength, however, was higher for the fast loading rate compared to that of the slow loading rate. The ultimate shear stress at failure was almost 1.6 times that of the initial stress 14 days after initial test for the fast loading rate, while the increase of the shear stress was only 1.1 times for slower loading rate. The difference may be associated to contribution of higher dissipation of excess pore water pressure at fast loading whereas there is more effect of soil aging at slow loading rate. In clay with moderate to low yield stress ratio, similar to the soil studied here, the mean effective stress in the soil adjacent to the interface surface will gradually reduce during the shearing action as the interface shearing is progressed, and the interface friction angle will reduce to a residual value consistent with the high rates of shearing (Lehane & Jardine, 1994). Therefore, the ultimate interface shear strength (i.e., after dissipation of pore water pressure) should be close to the initial shear strength of the low shear rate. This seems to be the case here, as the ultimate shear strength of fast loading rate 14 days after initial

testing is 65 kPa which is closer to the initial value of 75 kPa for the slow loading rate. The difference between these two values could be related to existence of some excess pore water pressure in the pile-soil interface even 14 days after initial test.

Alternatively, Figure 3.14 illustrates the behaviour of the steel-soil interface in both loading rates over time. The result shows a marginal difference between the rate of shear strength increase of the fast and slow loading rates which it was approximately 1.1 times the initial interface 14 days after initial testing. This means the set-up mechanism through dissipation of excess pore water pressure and aging have similar effect on steel-soil interface strength increase. More detailed investigation is required to be able to draw more accurate conclusions in this regard.

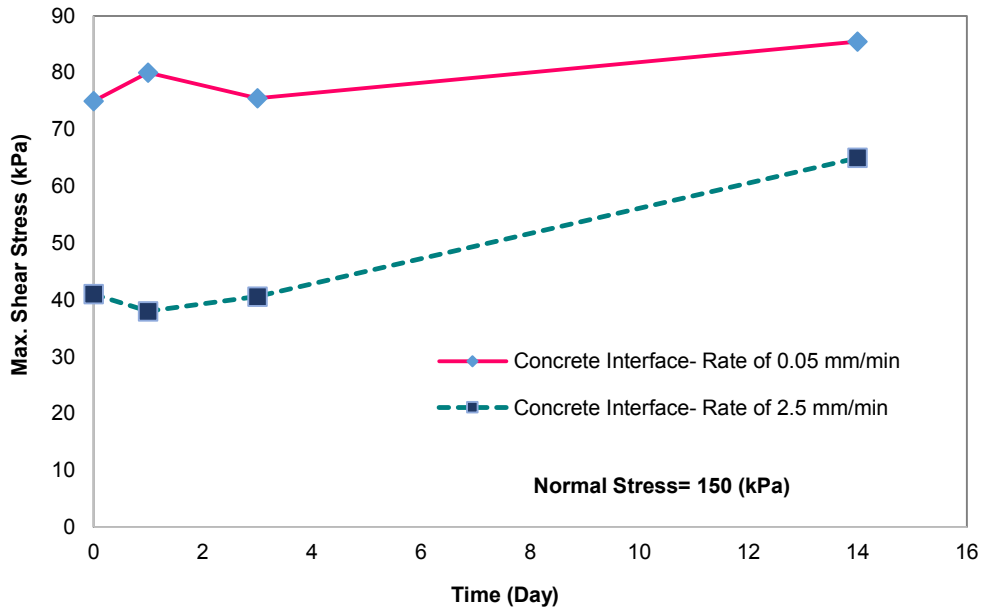

Figure 3.13: Shear stress of concrete-soil interface in two different loading rates

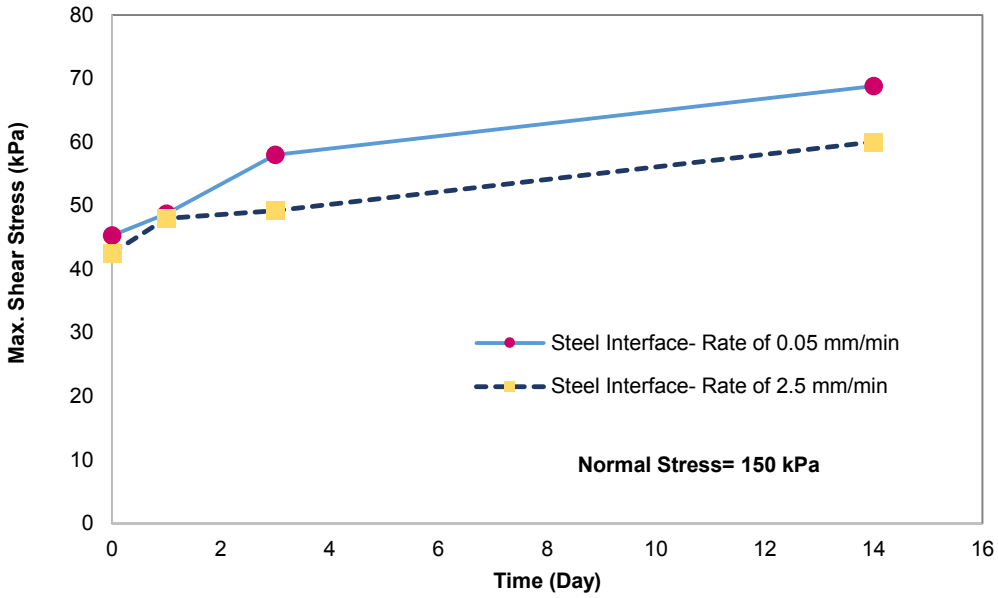

Figure 3.14: Shear stress of steel-soil interface in two different loading rates

3.9 Effect of Pile Materials on Pile Set-up

Piles driven into various types of soil specifically in clay experience an increase in capacity as a function of time due to dissipation of excess pore water pressure generated around the pile during pile driving. The rate and magnitude of this time-dependant capacity increase could be different for various types of pile foundations. Finno et al. (1989) stated that a pipe pile developed higher pore water pressures during installation compared to an H-pile, however the unit shaft resistances was estimated to be the same after 43 weeks. On the other hand, the type of the pile materials have shown different capacity over time, for instance Preim et al. (1989) reported higher capacity in prestressed concrete piles than steel pipe piles. These observations may be attributed to a higher pile-soil interface coefficient of friction.

Figure 3.15 demonstrates the maximum shear stress at failure for the concrete and the steel interface tests over time under the fast rate of loading (2.5 mm/min). In comparison, the concrete interface shear stress reached slightly higher value than steel interface shear stress after 14 days, which this can be due to possible water absorption and higher rate of excess pore water dissipation. However, the steel shear strength was slightly higher than the concrete initially, which could be related to slightly higher surface roughness of the steel surface.

Alternatively, Figure 3.16 illustrates the effect of pile materials in the result of the interface shear strength over time at slow loading rate (0.05 mm/min). The increase in shear strength for both the concrete and steel interfaces seems to be similar under low rate of loading, though both the initial and ultimate shear strength values for the concrete is higher than the steel interface. As mentioned earlier, this marginal difference can be due to variation in material properties (i.e., surface roughness, permeability) of steel and concrete as the concrete specimen may absorb interface water.

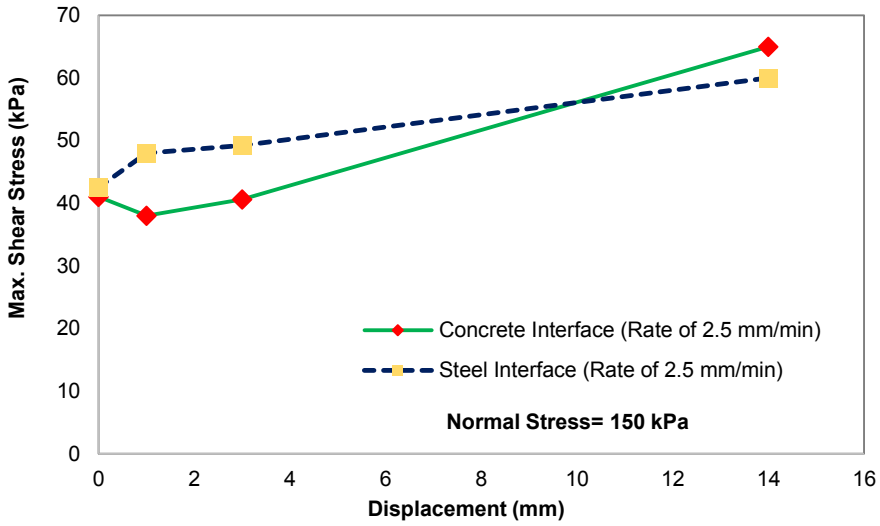

Figure 3.15: Comparing the maximum shear stress vs displacement of concrete-soil and steel-soil (fast loading rate)

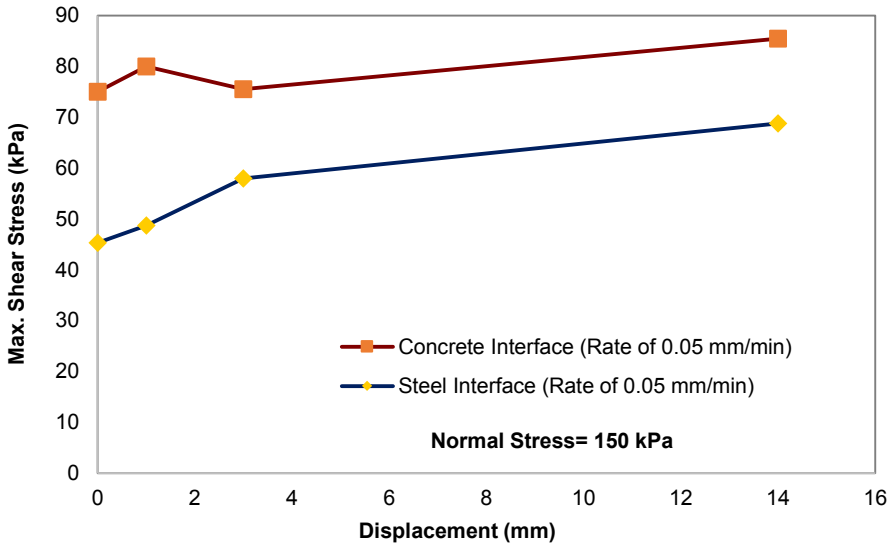

Figure 3.16: Comparing the maximum shear stress vs displacement of concrete-soil and steel-soil (slow loading rate)

3.10 Use of Interface Test Results in Pile Design

The fast loading rate used in the interface testing here can be attributed to the undrained condition, while, the slow loading rate is almost simulating the drained condition. Therefore, interface parameters obtained from these tests may be used to estimate the shaft resistance using total stress analysis (TSA) and effective stress analysis (ESA), respectively. In fast loading rate, the apparent adhesion of the concrete- and steel interface are used to calculate the adhesion coefficient (α) over time (Tables 3.5-3.6). Considering the adhesion parameters measured in the interface tests and relating it to the undrained shear strength of the soil measured using a vane shear device (Table 3.1), the adhesion coefficient, α, can be estimated (Tables 3.5-3.6). As it is noted, the α value ranges from about 0.44 to 0.53 for the interface tests performed on concrete-clay over different elapsed time. This value ranged from 0.3 to 0.44 for the steel-clay interfaces sheared at different

elapsed time. Considering the evolution of pile-soil interface over time in the design will improve the adhesion coefficient used in the design and hence will provide more realistic design parameters.

For effective stress analysis, the β parameter (i.e., $\beta = Ks.tan\delta$) can also be estimated using the interface friction angles measured in the slow interface tests. Assuming a value of one for the K_s, the β parameter used in ESA design are estimated and shown in Tables 3.5 and 3.6. This parameter has increased from a value of 0.17 for the initial steel-clay interface test to 0.28 for steel-clay interfaces tested 14 days after initial testing. The β parameter for concrete-clay interfaces ranged from 0.44 to 0.53 for different elapsed time. Similar to TSA, considering pile set-up will improve the design parameters used in ESA approach.

These data could be discussed from the perspective of difference between initial interface parameters at fast and slow rates of loading. Lehane and Jardine (1994) stated that the effective stress in the soil adjacent to the pile will slowly decrease during the shearing when the pile is driven, and consequently, the interface friction angle will reduce to a residual value consistent with the interface friction angle at the fast loading rate and comparatively low level of effective stress. In order to investigate the applicability of this hypothesis to the current study, the highest interface friction angle achieved after different elapsed times for fast loading rate can be compared with the initial interface friction angles obtained initially for slow rate interface tests. For the concrete-clay interface tests, the highest interface friction angle for fast loading was 18.7° which is close to the initial friction angle achieved in the slow loading (i.e., 24°). However, this trend was not observed in the steel-clay interface tests, where the maximum interface friction angle for the fast load tests was higher than that of initial slow test. This could be related to the shearing mode for the clay-steel interface which different failure modes discussed earlier governs the behaviour of the interface strength.

Table 3.5: Using the interface parameters at different shearing rate for concrete interface

Shearing Rate	Elapsed Time	Adhesion (kPa)	Interface Friction Angle (°)	α (TSA)	β (ESA)
Fast (2.5 mm/min)	Initial	15.3	9.8	0.437	-
	Day 1	16.7	8.3	0.477	-
	Day3	18.7	8.7	0.534	-
	Day 14	14.2	18.7	0.406	-
Slow (0.05 mm/min)	Initial	9.1	24	-	0.445
	Day 1	0.5	28	-	0.531
	Day3	6.5	25	-	0.466
	Day 14	20.7	23.5	-	0.435

Table 3.6: Using the interface parameters at different shearing rate for steel interface

Shearing Rate	Elapsed Time	Adhesion (kPa)	Interface Friction Angle (°)	α (TSA)	β (ESA)
Fast (2.5 mm/min)	Initial	11	11.7	0.314	-
	Day 1	9.7	14.1	0.277	-
	Day3	12	13.7	0.343	-
	Day 14	15.6	16.4	0.446	-
Slow (0.05 mm/min)	Initial	16.8	10	-	0.176
	Day 1	19.8	11.3	-	0.200
	Day3	21.7	13.7	-	0.244
	Day 14	27.3	15.8	-	0.283

3.11 Summary

An extensive experimental program was performed to evaluate the evolution of pile-soil interface strength at two shearing rates (fast and slow) over time using modified direct shear test for both concrete-soil and steel-soil systems. At fast loading rate (2.5 mm/min), the initial shear stress for soil-soil and pile-soil were explored and the result showed that the interface strength for the pile-soil systems were generally lower than the soil-soil interface. Among the two interfaces, the

concrete interface friction angle was significantly higher than the steel interface friction angle. The interface shear strength for both concrete-soil and steel-soil systems increased as the consolidation time after the initial shear tests increased up to 14 days. The increase in interface shear strength was attributed to the dissipation of excess pore water pressure for the fast loading rate, which resulted in increase of the interface adhesion and friction angle. For the slow loading rate of 0.05 mm/min, the increase in interface shear strength was attributed to restructuring the disturbed clay at the interface level which is often referred to as aging. Aging is related to variation in soil properties at a constant effective stress over time which may cause frictional and mechanical significances for both fine-and coarse-grained soils. Aging was shown to cause an increase of the friction angle at the soil-pile interface (McVay, 1999). Thixotropic aging effects appear mainly at very low effective stresses under slow loading rate in cohesive soils (Schmertmann, 1991).

Chapter 4: Evolution of Pile Shaft Capacity over Time in Field

4.1 Introduction

Piles driven into various types of soils, specifically in clay, experience an increase in capacity as a function of time mainly due to dissipation of excess pore water pressure generated around the pile during pile driving. This phenomenon of time-dependant capacity increase is referred to as set-up or freeze. Pile set-up occurs in almost all types of soils including organic and inorganic clays, loose to medium dense silts, sandy silts, including fine sands (Astedt and Holm, 1992; Hannigan et al., 1997). Pile set-up is of critical importance in the design of piles. In clay soils, the set-up is related to reconsolidation of the disturbed soil around the pile, and aging (Randolph et al., 1979). The time to dissipate excess pore water pressure is dependent on the coefficient of permeability of the soil along with the coefficient of consolidation, C_v.

The pile driving has shown to cause disturbance and remoulding of the soil around the pile. De Mello (1969) classified the effect of pile driving in clay into four categories; remoulding of the structure of the soil around the pile; variations in the state of stress of the soil and the pile which is referred to formation of excess pore water pressure; dissipation of excess pore water pressure; and long term increase of the strength in the soil. During pile driving, high excess pore water pressure is normally developed in the surrounding soil near the pile. This excess pore water pressure will cause reduction in the effective stresses and, hence, the shear strength of the soil for a specific period of time after driving. The amount of excess pore water pressure can approach up to twice the in-situ vertical effective stress, although there is much higher pore water pressure at

the toe of the pile and this can reach up to 3 to 4 times the effective stress (Randolph et al., 1979). In case of sensitive soils such as Leda clay, the result of pore water pressure could be greater, i.e., up to 8 times of the effective stress (Poulos and Davis 1980). The concept of pore pressure dissipation was used to explain the gain in pile capacity after driving over time by Seed and Reese (1955). However, the exact mechanisms involved in this capacity gain have not been clearly understood. Therefore this chapter investigates the set-up phenomenon in a marine sensitive clay called Leda clay by developing a series of medium-scale pile load tests in a field site located at south-east of Ottawa region, called Canadian Geotechnical Research Site No. 1.

4.2 Material Characterization

4.2.1 Test Site Characteristics

The soil used in this study is a type of marine sensitive clay called Leda clay which covers Ottawa Valley and south of Province of Quebec. This clay was formed near the end of the most recent glaciation period in the pre-historic Champlain Sea. The soil unit weight was measured to be about 15.3 kN/m^{3}and the water content of the soil was measured at about 52% (referred to ASTM D2216). From the Atterberg limit tests, the plasticity index of this Leda clay was determined at approximately 24% with a liquid limit of 51% (referred to ASTM D4318). Vane shear tests were performed according to ASTM D2573 to determine the undrained shear strength which was estimated to be about 35 kPa. The coefficient of one-dimensional consolidation was measured according to ASTM D2435/2435M and presented a value of 1.4 x10^{-8} m^2/s (summarized property index in Table 3.1).

4.2.2 Pile Properties

Three common types of pile including precast concrete, closed end steel and open ended steel pipe piles with similar diameter of 101.6 mm and embedment length of 2.0 m were used to perform pile load test (Table 4.1). The precast concrete pile was manufactured in lab using a mixture of sand, fine-grained gravel aggregate, cement and three 10M steel rebar which were placed in concrete pile in order to distribute the applied load through the pile and carry the load while driving the pile (Figure 4.1). In addition, there were two steel piles, an open-ended pipe and closed-end pipe which both have nominal size of 101.6 mm, similar to concrete pile (Figure 4.1). All three piles had a steel encasing mechanism at the pile head with the aim to apply the axial load and prevent pile destruction during driving.

All three piles have constant embedment length of 2 meter and from past studies, an appropriate spacing of three times of pile diameter (3d) was typically suggested to prevent group effects on frictional piles (Tomlinson, 1994; Franke, 1988). Accordingly, this distance is from the pile external surface up to distance of 305 mm (3d) in this field experiment (Figure 4.2). This boundary is related to the change in pore water pressure and state of stress of the clay, which this distance shows a least effective cylindrical region with approximate distance of 712 mm ($[2\times 305] + 101.6$) .

Figure 4.1: Model piles (from left to right: precast concrete pile, open-ended steel pile, and closed-end steel pile)

Figure 4.2: Spacing between model piles

Table 4.1: Model pile geometric properties

Pile Type	Outside Diameter d (mm)	Toe Area (mm^2)	Length L (mm)	Wall Thickness t (mm)
Precast Concrete	101.6	8107.3	2000	-
Closed-End Steel	101.6	8107.3	2000	-
Open-End Steel	101.6	8107.3	2000	5.47

4.3 Experimental Procedure

4.3.1 Pile Driving Technique

Pile driving was performed using a pulley which was attached on top of a tripod and drop hammer setup. The drop hammer had a weight of 88 lb (40 kg) at an average dropping distance of 400 mm which was kept constant during the pile load test (Figure 4.3). The impact energy generated by the hammer drop was about 78.5 joules per blow. Pile driving was performed at approximately 10-15 blows per minute. This rate generated a penetration of 1-2 mm/blow at shallow depths to as high as 5 mm/blow while attaining the target depth. Cumulative number of blows versus depth ratio is plotted (Figure 4.4) and the trend indicates that open-ended steel pile resisted more than closed-end steel pile which this may be due to soil plug in the open-ended steel pile.

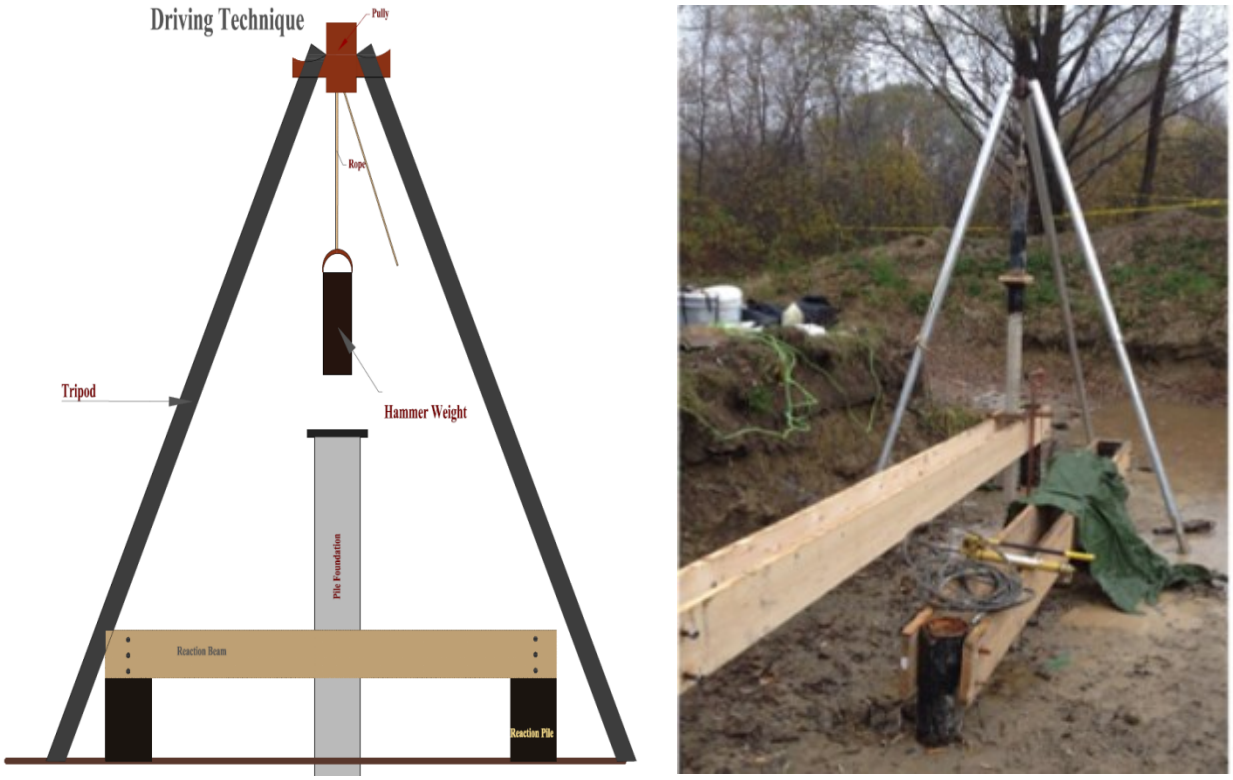

a) b)

Figure 4.3(a): Schematic drawing of pile driving, (b): Pile driving in Gloucester, Ontario

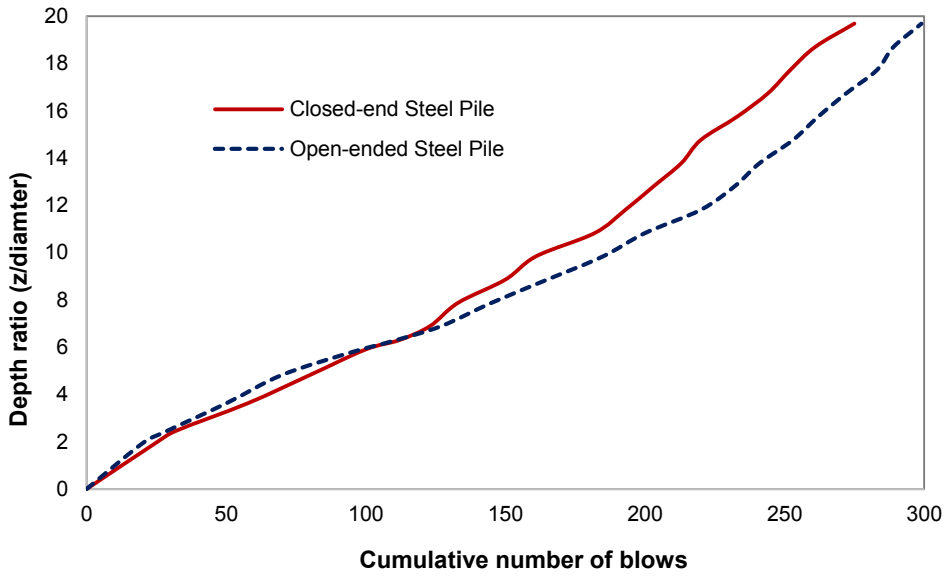

Figure 4.4: Depth ratio vs. cumulative number of blows

4.3.2 Setting the Frame to Perform Pile Load Test

A test frame was used to act as reaction beam in order to perform static load test. This frame was designed such that the load can be applied in both tension (upward) and compression (downward) directions, and designed to provide sufficient strength against applied load with minimal deflection. Reaction frames were attached to a series of reaction piles with larger diameter/embedment depth to provide resistance force. The load applied using a hydraulic jack and the applied load was measured through a load cell system, while the displacement of the pile was monitored with a displacement transducer (LVDT). Two open-ended steel reaction piles with a diameter of 152.4 mm and height of 3.0 m were driven at a distance of approximately 3.0 m, and two plywood beams with dimension of (3660 ×254×50) mm were bolted to each side of the reaction piles to form the pile load test frame (Figure 4.5a).

To facilitate the pile load testing, a steel plate was attached and welded on the top of each test pile. Subsequently, a threaded rod with bottom plate was bolted to the head plate on top of the test pile. The threaded rod was passed through the reaction frame and then a metal sheet was placed on top of the reaction frame through the threaded rod. Afterward, the hydraulic jack was positioned over the metal sheet and the load cell was placed on top of the hydraulic jack through the threaded rod then stiffened by a fastener. In addition, the displacement transducers were placed on pile head to monitor the movement of the pile. All the measurements were monitored continuously through a data logger connected to a computer to read and record the data from the load cell and displacement transducers (Figure 4.5b).

4.3.3 Pile Load Testing

The pile loading test was performed under tension to measure the pile shaft capacity according to ASTM D3689. A calibrated load cell and hydraulic jack with maximum ram height of 50 mm were used as shown in Figure 4.6. The loading procedure was designed to reach failure by applying incremental loading at 60 second intervals. This allowed the interface force to reach the equilibrium. Immediately after each test, the pressure from hydraulic jack was released to avoid excessive soil disturbance. The failure principle used to distinguish the ultimate shaft capacity over time was pile load carrying capacity at pile head displacement of 10% pile diameter as suggested by De Nicola and Randolph (1999).

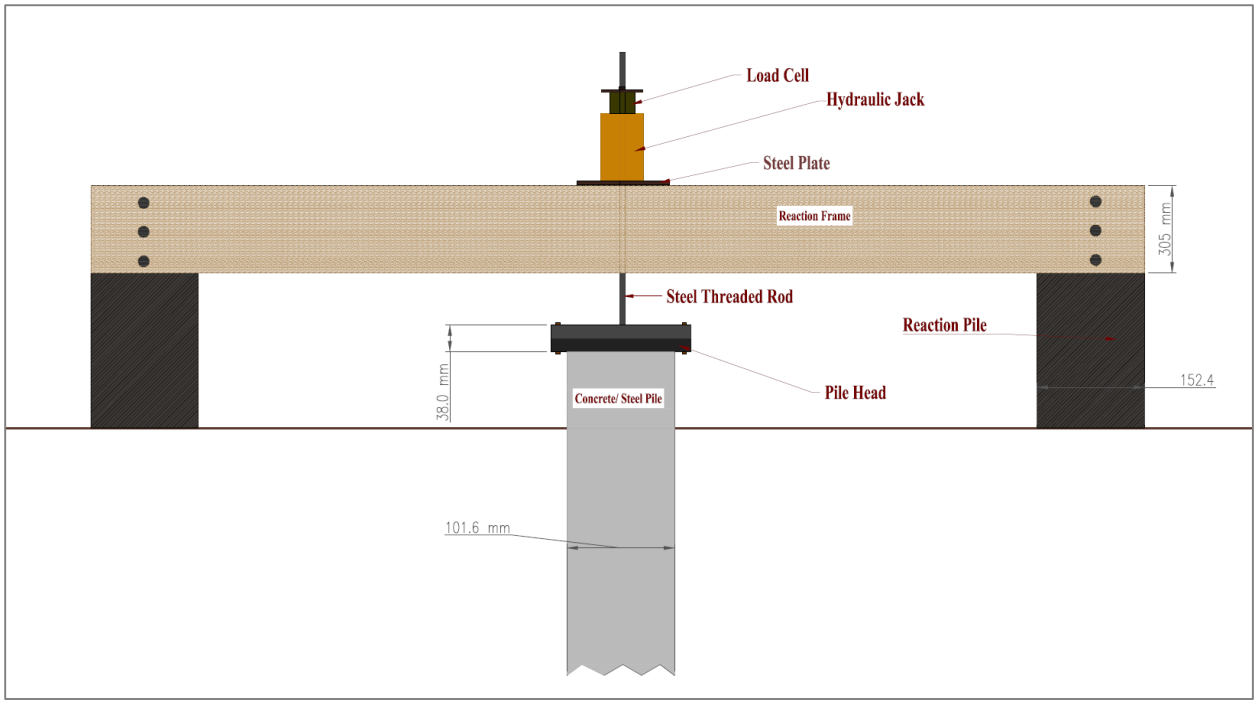

Figure 4.5 (a): Schematic drawing of setting the frame and pile load test

Figure 4.5 (b): Setting the frame and pile load test in Gloucester Site-Ottawa

Figure 4.6: Pile cap plate, load transfer threaded rod, and load cell

4.3.4 Pore Water Pressure Monitoring

Distribution of pore water pressure in the pile surrounding soil is an important factor to understand the increase in pile capacity over time. A vibrating wire piezometer with pressure capability of 0.7 MPa was installed to monitor pore water pressure around the pile tip while driving till the end of initial driving (EOID) as well as testing at different elapsed times (1, 3 ,7, 14, and 30 days). At the beginning, the sensor was attached on the surface precast concrete pile close to the toe, however this caused malfunction in reading the data due to the soil clogging at the tip of the sensor and also, it was difficult to justify that the sensor is always saturated at different elapsed day. A modified copper piping system filled with water was designed to keep the PWP sensor saturated at all the time, in addition it can protect the sensor against soil clog. The sensor was placed close to the tip of the copper pipe and a few holes were drilled on the surface of the copper pipe to facilitate water flow in and out of the piezometer. Furthermore, an extra pressuremeter was placed to measure the pressure of water inside the pipe during driving the copper pipe as shown in Figure 4.7 and 4.8. The sensor was connected to a vibrating wire reader which reads an engineering value plus the temperature at the depth. The specifications of the vibrating wire piezometer are provided in Appendix C.

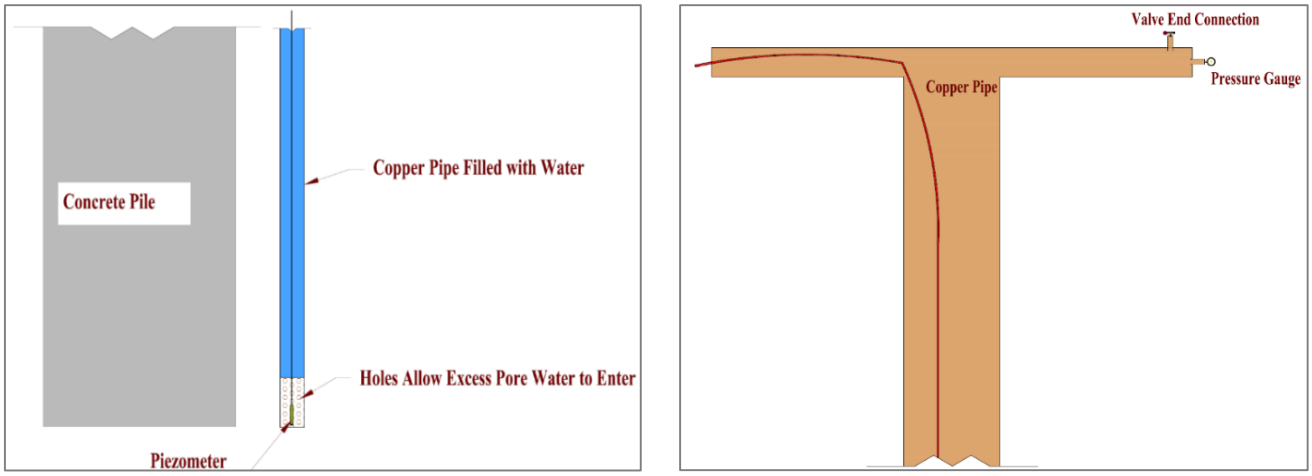

(a) (b)

Figure 4.7: Schematic drawing of: (a) Driven piezometer adjacent to the friction pile (b) PWP sensor positioned in copper pile to retain the piezometer saturated

Figure 4.8: Piezometer system adjacent to the pile in test site

4.4 Results and Discussions

The following sections present and discuss results of the pile load tests on three piles (precast concrete pile, closed-end steel pile, open-ended steel pile) to identify parameters controlling pile set-up and discuss the rate of change in pile shaft capacity over time.

4.4.1 Pile 1: Precast Concrete Pile

A 101.6 mm diameter precast reinforced concrete pile was used to study the pile set-up for concrete piles in Leda clay. The solid concrete pile was driven into the sensitive clay at a depth of 2.0 m from soil surface (i.e., 2.0 meter below the ground surface). A static tensile loading test was performed instantly after driving by using a hydraulic jack, and load cell to determine the initial pile shaft capacity. This testing was repeated over time, 1, 3, 7, 14, and 30 days after the EOID in order to observe and examine the evolution of pile shaft capacity over time (Figure 4.9). It can be seen that the shaft capacity has significantly increased from its initial value and eventually it reached a point where the rate of change was small. The initial shaft capacity for the concrete pile was measured at about 990 N, which eventually it reached 6162 N after 30 days after initial driving. The rate of increase in pile shaft capacity was higher in the earlier stages changing from day 0 to day 1 and day 3. This rate, however, was much less for the time period of 3 to 30 days after EOID. This could be related to significantly higher rate of excess pore water pressure dissipation in the earlier stages, which led to significant increase in pile shaft capacity increasing from an initial value of about 1 kN to 4.8 kN only 3 days after initial driving. This also underscores the importance of excess pore water pressure in reducing the ultimate pile capacity by reducing the effective stress at the pile-soil interface level.

Alternatively, by measuring the shaft capacity of each pile at different elapsed day, a normalized result was calculated to explore and compare the rate of set-up for precast concrete pile (Figure 4.10). The normalization was based on the maximum pile capacity at different elapsed time divided by their initial load capacity measured immediately after pile driving as shown in Table 4.2. It can be seen that the rate of increase in pile capacity was significant in the first couple days compared to the initial capacity. This rate was eventually decreased as the elapsed time increased up to 30 days. The initial changes are typically referred to the quick dissipation of excess pore water pressure and possibly greater rate of consolidation of the soil in earlier periods. While the pile is driven, an excess pore water pressure is created in the soil around the pile due to increase in total stress as the soil is disturbed and forced outward; and also partially due to the variations in mean effective stress during shearing (Randolph, 2003). However, when the change in the rate of set-up is very slow, this is correlated to the aging phase (secondary compression), since the effective stress-related set-up is adequately complete, hence, the rate of set-up is independent of effective stress during this phase.

In order to examine the change in pore water pressure during pile driving and static load testing, the pore water pressure (PWP) was monitored using a piezometer close to the pile toe. Excess pore water pressure is developed due to remoulding and disturbance of the soil by driven piles. According to the relationship between effective stress and pore water pressure, when a pile is driven into the soil, total stress is increased as the pile pushes the soil away and varies the structure of the surrounding soil. In this case, the soil generates excess pore water pressure, which in turn leads to decrease in the effective stress. The change in pore water pressure over time was recorded and the result is presented in Figure 4.11. During pile driving, the pore water pressure was fluctuating and demonstrating non-linear change in PWP, and eventually an excess pore water

pressure of 70 kPa was recorded by the sensor installed at the toe of the piezometer. The initial static load test was performed immediately after driving the pile while monitoring the change in PWP and ultimately the soil reached a maximum pore water pressure of about 70 kPa. The PWP recording was continuously repeated during every test over elapsed time of 1, 3, 7, 14, and 30 days after the EOID. The results have shown that the PWP began to decrease due to dissipation until it reached a value of 22 kPa, 30 days after the EOID. This result demonstrates that there is relationship between PWP dissipation and pile shaft capacity over time. The outcome determined that excess pore water pressure that was built by driving the pile has begun to dissipate in the surrounding soil, therefore, the effective stress increased, and the surrounding soil consolidates and then gains strength.

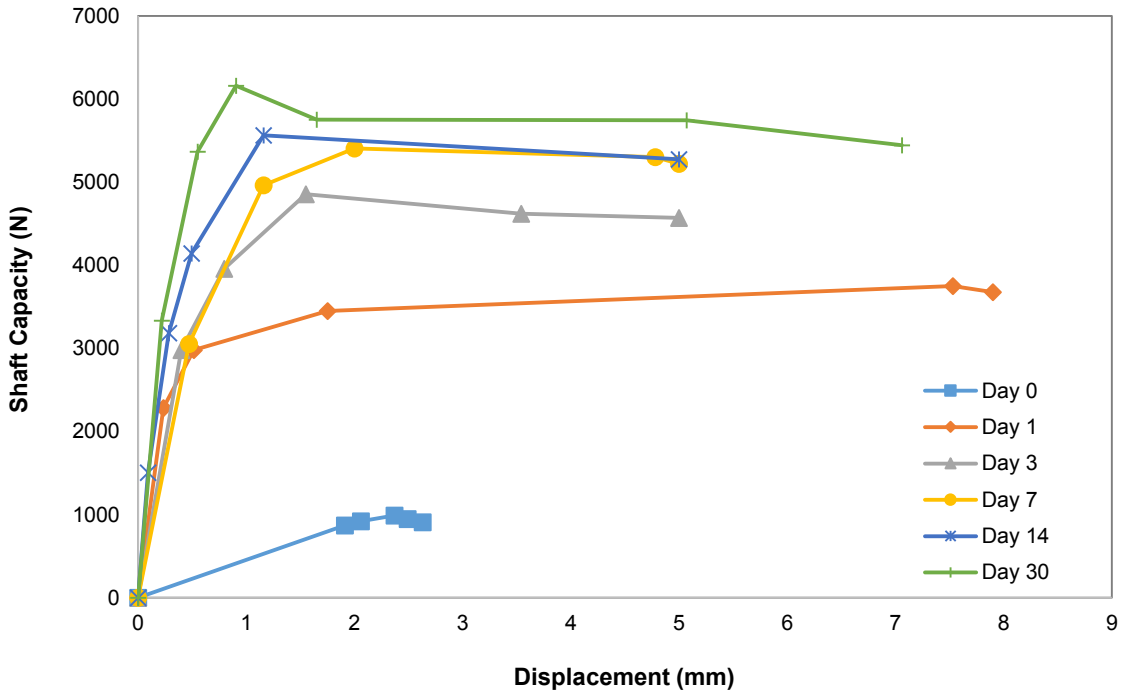

Figure 4.9: Shaft capacity vs. displacement of the precast concrete pile at elapsed time

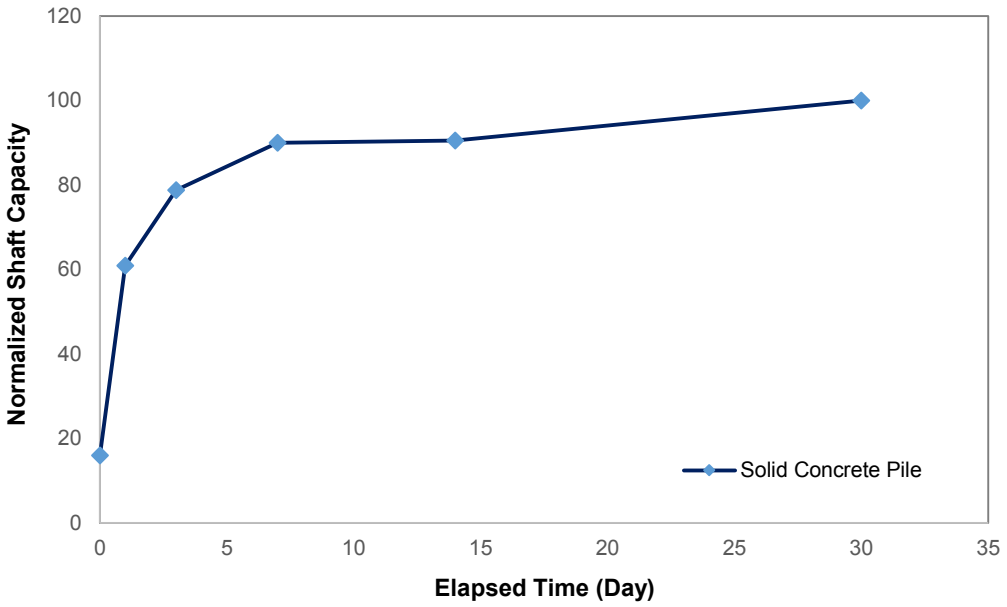

Figure 4.10: Normalized shaft capacity of precast concrete pile over time

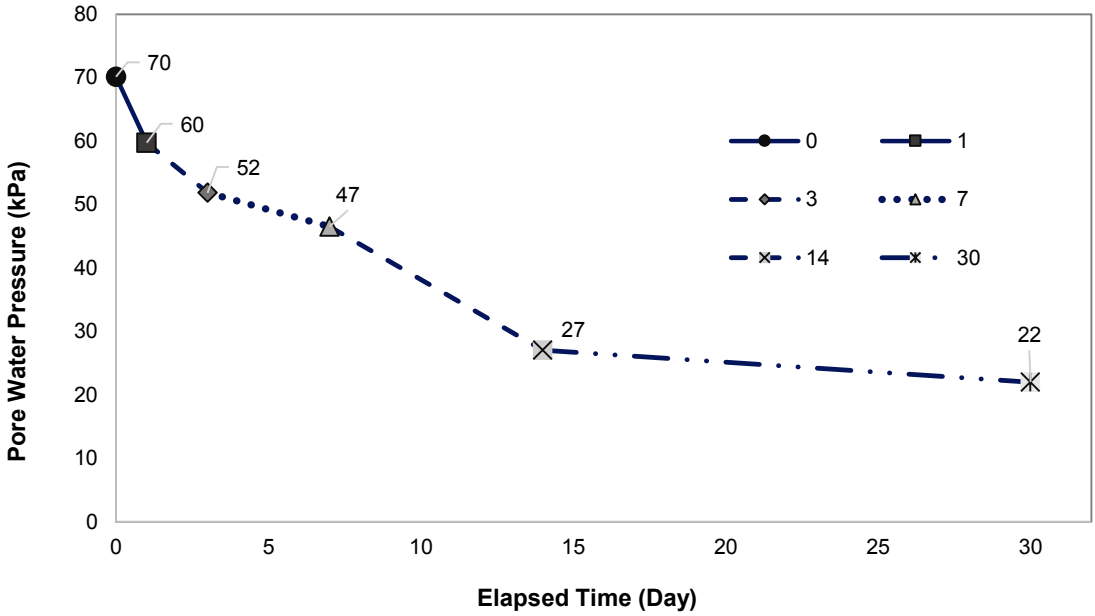

Figure 4.11: Excess pore water pressure versus elapsed time (adjacent to precast concrete pile)

4.4.2 Pile 2: Closed-end Steel Pile

A closed-end steel pile with similar dimensions was also driven into Leda clay and tested to study pile set-up and examine the effect of pile materials on set-up. The result obtained from static load tests over elapsed time is illustrated in Figure 4.12 in terms of the change in shaft capacity versus displacement over time. It can be seen that the shaft capacity increased over elapsed time as the excess pore water pressure dissipated. The initial shaft resistance for the closed-end pipe pile was measured at 945 N. This shaft capacity has slightly increased to 1.1 kN one day after the EOID. The rate of increase between day 1 and day 3 was significantly higher increasing up to 5.1 kN three days after initial testing. Similar to the concrete pile, the rate of change in shaft capacity between day 3 and day 30 was not so significant, which could similarly be related to the difference in rate of dissipation of excess pore water pressure around the pile.

Figure 4.13 shows the increase in pile shaft capacity over time considering the normalized shaft capacity to identify the rate of set-up. It can be seen that the rate of increase in pile capacity was significant during first couple of days from initial pile driving. When the pile load test was repeated three days after initial driving, the load carrying capacity was significantly increased to almost 5 times its initial capacity. This rate was eventually decreased as the elapsed time increased up to 30 days. The concept of change in pore water pressure over time can be used to explain the increase in pile capacity over time (Seed and Reese, 1955). During driving the pile, an excess pore water pressure is created in the soil around the pile due to increase in total stress as the soil is being disturbed and forced outward; and also partially due to the variations in mean effective stress during shearing (Randolph, 2003). The increase in shaft capacity is typically referred to the dissipation of excess pore water pressure and possibly greater rate of consolidation of the soil in earlier periods.

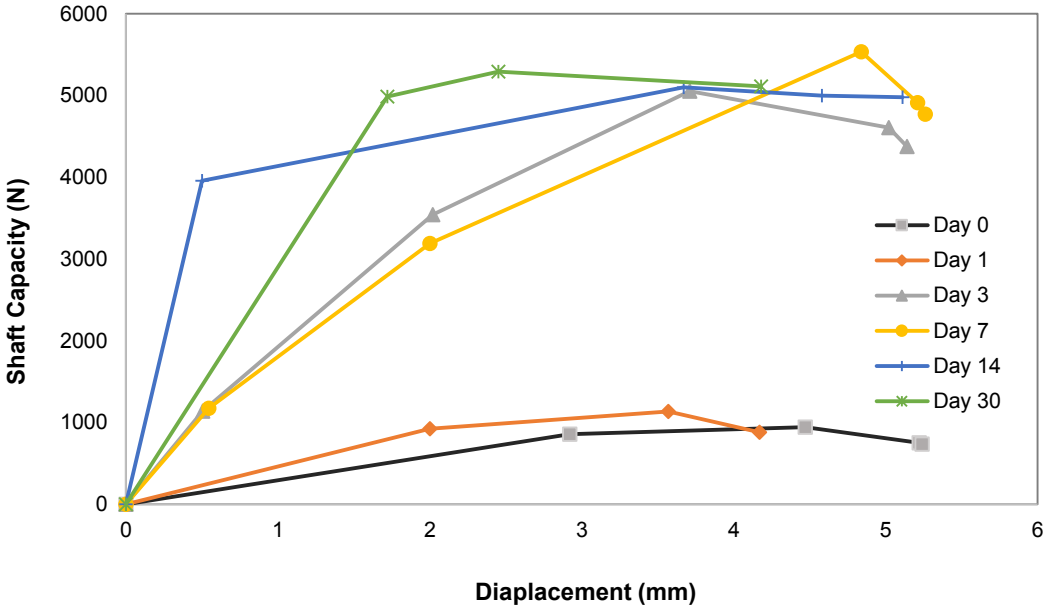

Figure 4.12: Shaft capacity vs. displacement of the closed-end steel pipe pile at elapsed time

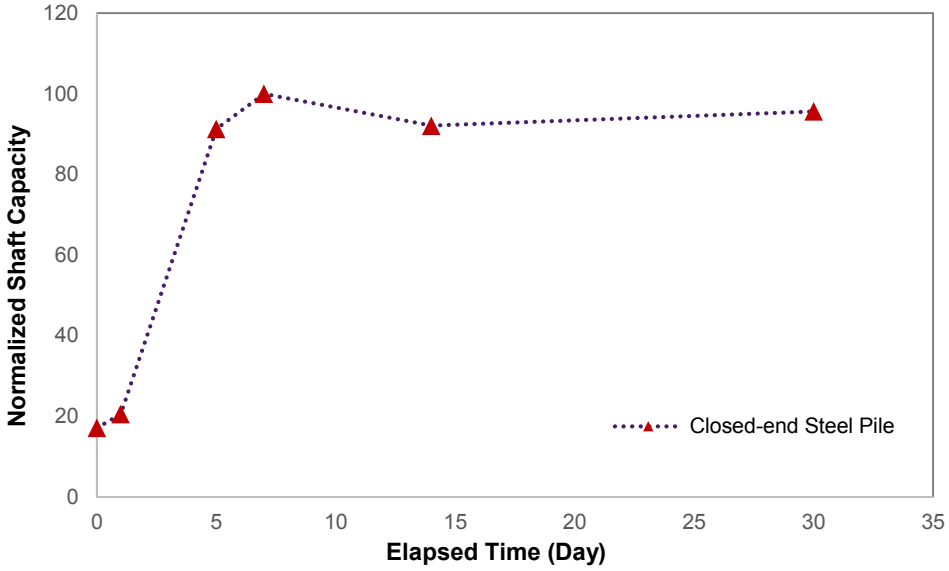

Figure 4.13: Normalized shaft capacity of closed-end steel pipe pile over time

4.4.3 Pile 3: Open-ended Steel Pile

In order to investigate the pile set-up in different types of piles, an open-ended steel pile was driven into a depth of 2.0 m in Leda clay using a hammer weight of 88 lb (40 kg) at the drop height of 400 mm. A static tensile loading test was performed instantly after driving by using a hydraulic jack, and load cell to determine the initial pile shaft capacity. This testing was repeated over time at day 1, 3, 7, 14, and 30 in order to observe and examine the evolution of the pile shaft capacity over time (Figure 4.14). The open-ended steel pile capacity was measured to be 969 N initially after driving, then it was increased to 2450 N one day after driving. The ultimate capacity of the pile was measured at 5960 N at day 7, and reached a steady state and almost constant capacity afterward. The rate of set-up was found to be similar to the other piles tested here, in which, the rate of increase in shaft capacity was higher in the earlier stages (day 1 to 7) and slowed afterwards. This may correlate to the rate of excess pore water pressure dissipation and, as mentioned in literature review, there is a period of time after the primary consolidation in which the change in the rate of set-up is very slow (secondary compression). The shaft capacity measured 14 and 30 days after the EOID slightly decreased from the maximum values measured 7 days after the EOID. This could be related to the repeated shearing and load tests on the same pile which could have further disturbed the pile-soil interface and reduced the ultimate pile capacity.

Based on the normalized data presented in Figure 4.15, it can be seen that the normalized set-up value was approximately 6 times its initial value at the EOID after 7 days of consolidation from initial pile driving (Table 4.2). This result shows the importance of considering set-up in pile designs.

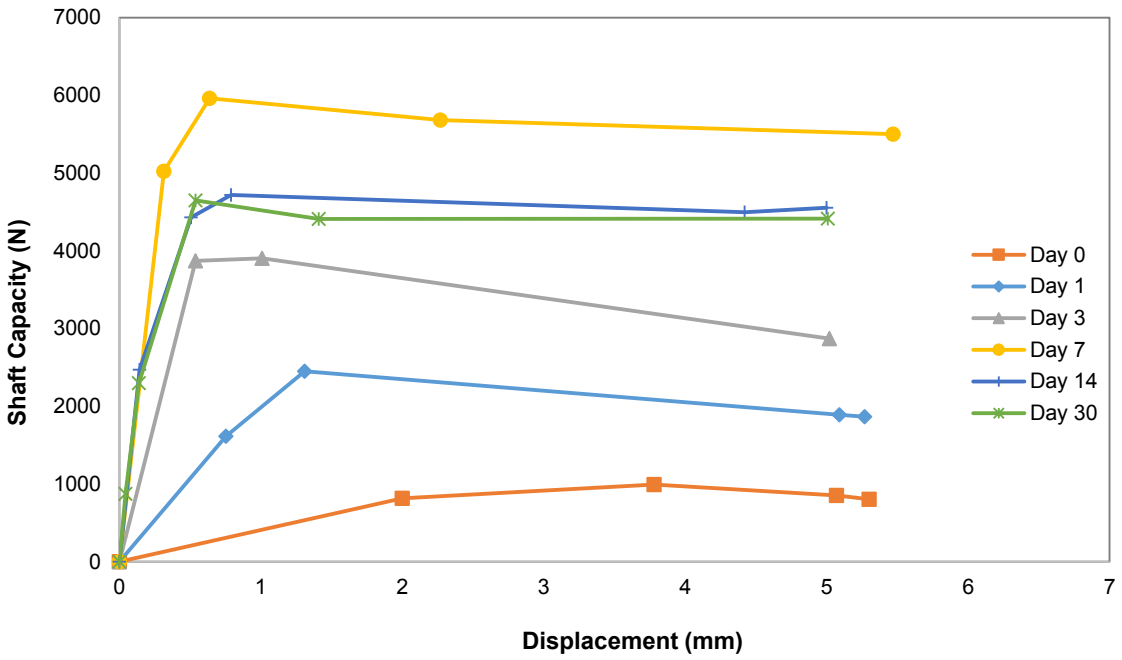

Figure 4.14: Shaft capacity vs. displacement of the open-ended steel pipe pile at elapsed time

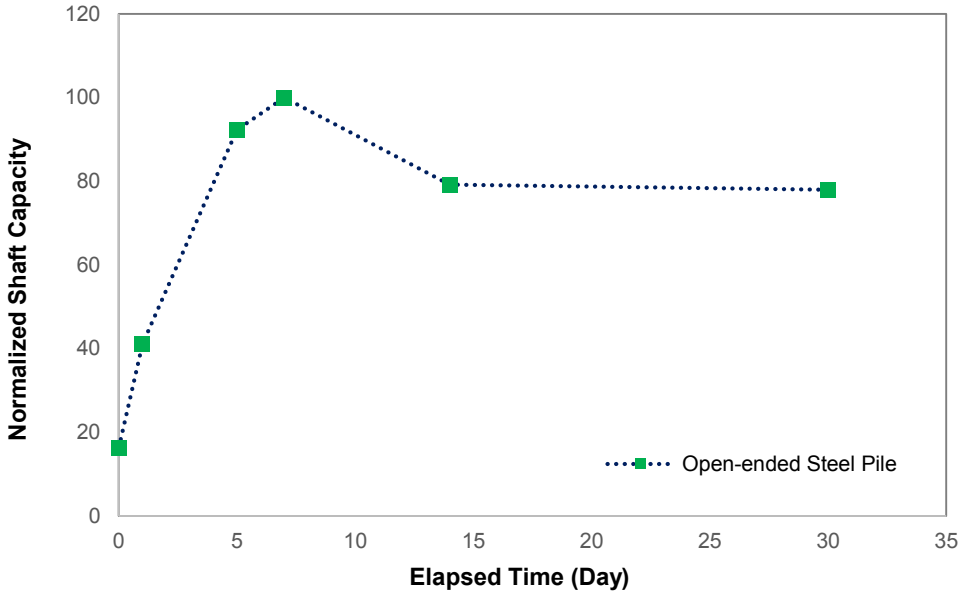

Figure 4.15: Normalized shaft capacity of open-ended steel pipe pile over time

Table 4.2: Summary of pile shaft capacities and normalized shaft capacities

Time (day)	Pile Shaft Capacity (N)			Normalized Shaft Capacity		
	Precast Concrete Pile	Open-ended Steel Pile	Closed-end Steel Pile	Percent of Concrete Pile Capacity	Percent of Open-ended Steel Pile Capacity	Percent of Closed-end Steel Pile Capacity
0	990	969	945	16.0	16.3	17.1
1	3752	2451	1135	60.9	41.1	20.5
3	4855	5500	5054	78.8	92.3	91.3
7	5548	5962	5538	90.0	100	100
14	5578	4721	5100	90.5	79.2	92.1
30	6162	4650	5295	100	78.0	95.6

4.5 Effect of Pile Type

Piles are classified based on the level of displacement they induce during their installation process. Large-displacement pile is a pile that displaces a large volume of the soil within the adjoining soil mass (e.g., closed-end pipe piles), while small-displacement piles are stated as sectional displacement of the surrounding soil such as open-ended pipe pile, and H-piles. Non-displacement piles are formed by excavation or boring method such as drilled shafts. The piles in this research can be divided into two major types, large displacement and small- displacement piles. These piles have different characteristics, i.e., the closed-end pile can cause more soil disturbance than open-ended pile. The penetration resistance of the closed-end pile was slightly higher than the open-ended pile, while slightly higher resistance was observed at some points in the open-ended pile due to soli plug.

As shown in Figure 4.16, the rate of set-up for both the small-displacement pile (open-ended steel pile) and the displacement pile (closed-end steel pile) was similar with marginal difference between them during the first week of pile load recording. This was due to the small

diameter of the piles tested here and, hence, the marginal variation in excess pore water generated by the two piles. On the other hand, the actual shaft capacity for the closed-end pile was slightly lower than the open-ended pile initially. Therefore, considering the slightly higher rate of set-up as well as higher initial shaft capacity, the open-ended pile would probably be a preferred option providing higher initial capacity and lower soil disturbance. When the pile load test was repeated three day after initial driving, the load carrying capacity for open-ended pile was higher than the shaft capacity of closed-end steel pile. The average increase in pile shaft capacity was approximately 4-5 times their initial capacity 14 days after the initial pile driving. However, the penetration resistance for the closed-end pile was considerably greater than the open-ended pile.

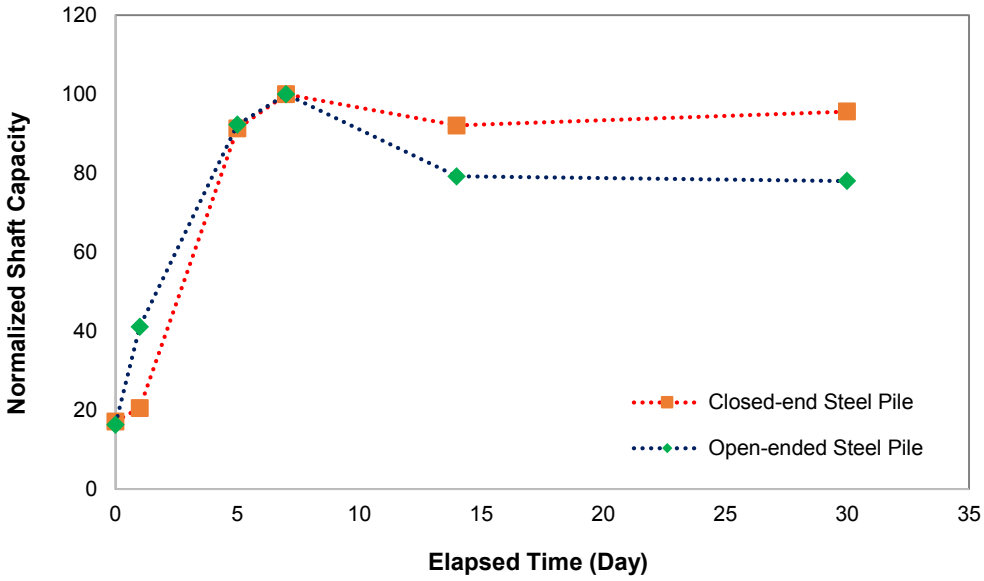

Figure 4.16: Variation of normalized shaft capacity of the closed-end and the open-ended steel pipe pile

4.6 Effect of Pile Material

It is essential to consider the effect of pile material in the rate of the pile set-up. In this section, the rate of set-up for concrete pile and closed-end steel pile is compared. The concrete pile and closed-end steel pile can be considered identical in terms of the geometry and the embedment

depth, except in material index. Figure 4.17 presents the normalized shaft capacity over time for the precast concrete pile and the closed-end steel pile. The result shows that the rate of set-up for the precast concrete pile is much greater than the closed-end steel pile within the first day of pile load test. Eventually, the rate of set-up has continued similar path for both the precast concrete pile and closed-end steel pile after couple days and ultimately, they reached a steady value with marginal difference in shaft capacity on day 30. A similar trend is reported in past studies, in which precasted or prestressed concrete piles have also shown higher resistance over time compared to other closed-end piles (Perim et al, 1989). The greater rate of pile set-up in precast concrete pile is attributed to the nature of material, as concrete has tendency of moisture absorbance compared to steel material and this may cause reduction in moisture content between the concrete shaft and the Leda clay.

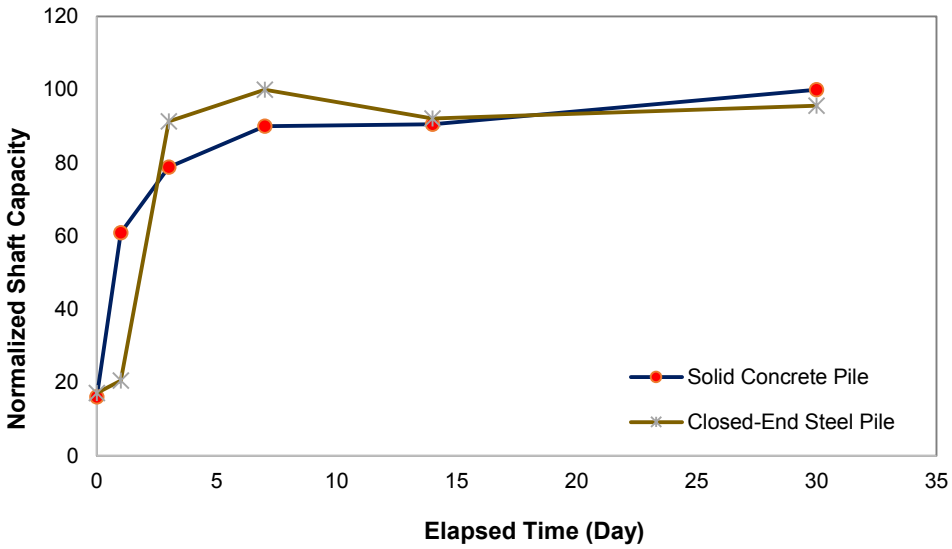

Figure 4.17: Variation of normalized shaft capacity of the precast concrete pile and the closed-end steel pipe pile

4.7 Magnitude of Pile Set-up

The lowest and highest set-up values measured here were in the range of 4-6 times the pile shaft capacity at the EOID, respectively. By measuring the shaft capacity of each pile at different elapsed time, a normalized data was used to explore and compare the rate of set-up for each pile. Several expressions were suggested and developed to predict the magnitude of pile capacity over time. Skov and Denver (1988) proposed an expression to estimate pile capacity (Q_t) at different elapsed time (t) from the pile capacity at the end of initial driving (EOID), Q_0.

$$Q_t = Q_0 [A \log (t/t_0) + 1] \qquad (4.1)$$

where A and t_0 are constant parameters based on the type of the soil, and a value of $A = 0.6$ and $t_0 = 1$ day was suggested for clay. These parameters are measured from a case study of 13 driven piles and almost 21 pile load test data. This empirical relationship could be used to evaluate A value for Leda clay from the collected data in this study. From the limited data presented here, a set-up parameter A=1.5 to 3.5, may be suggested for this clay for an elapsed time of one day to one month. The pile capacity at different elapsed time may be estimated using this parameter and equation 4.1. This approach may be used as an approximate method in the design of pile foundation to predict possible magnitude of pile set-up in marine sensitive clays and this may lead to significant saving in pile foundation costs.

4.8 Duration of Pile Set-up

According to the past studies discussed in Chapter 2 and the results of this research, the generation of excess pore water pressure during pile driving play an essential role in set-up mechanism. The

next phase in behaviour of pore water pressure in the pile-soil interface region is dissipation of the excess pore pressure which starts immediately after end of driving. This process is accompanied by changes in the stress field of the soil around the pile, where the effective stress of the soil increases as the pore water dissipation proceeds. The excess pore pressure differs around the remoulded region, where a maximum pore water pressure can be detected along the pile surface (Leifer et al., 1979). The dissipation rate is dependent on soil coefficient of permeability, pile spacing and material, and thickness of the clay layer**.** The required time for dissipation of excess pore water pressure can be predicted using Terzaghi's theory for one-dimensional consolidation.

$$T = \frac{c_v t}{H_{dr}^2} \tag{4.2}$$

where T is the time factor, t is the time of consolidation, c_v is the consolidation coefficient of the soil, and H_{dr} is the length of the drainage path perpendicular to the pile surface along the pile axis. The drainage length is typically assumed to be the width of the remoulded area around the pile, or as low as half the remoulded width for the case of concrete piles, where pore water pressure may flow from the remoulded area into both the surrounding soil and the pile itself. This remoulded length can be estimated from cavity expansion theory based on elasto-plastic analysis. By approximating the undrained shear strength and the shear modulus of the soil, the distribution of initial excess pore water pressure surrounding the pile can be predicted (Randolph et al., 1979). It is important to recognize that this equation may estimate the required consolidation time of remoulded region through an assumption that the excess pore water pressure is uniformly disturbed within the remoulded region. Using this equation, the time factor for dissipation of excess pore water pressure for both steel and concrete interfaces would be approximately 0.072. By

implementing this time factor in equation 4.2, and assuming a drainage path (e.g., 3 time pile diameter), the time required for completion of the pile set-up can be estimated.

4.9 Comparison with Past Studies

As discussed earlier in Chapter 2, the effects of soil characteristics and pile type (i.e., installation method) have shown significant influence on the rate of set-up (Axelsson, 2002; Chow et al., 1998; Svinkin et al., 1994). Several studies were published on pile set-up showing the rate and magnitude of the set-up for different piles installed in different soil strata. The majority of these researchers observed set-up within 30 days after the pile installation day, and after that, the rate of change was very slow. Ng et al. (2011) investigated pile set-up by performing pile load tests on five piles driven in cohesive soil in Iowa, and the result revealed a 52 to 66% increase in shaft resistance. Blessey and Lee (1980) performed pile load tests in southeast Louisiana, which showed an approximately 400 to 500% increase in shaft capacity several weeks after initial pile driving. McManis et al. (1988) investigated set-up on full-scale pre-stressed concrete piles in Luling Bridge near New Orleans, Louisiana and reported a 440-1150% increase in bearing capacity five weeks after initial pile driving. Most of these field experiments were performed in different type of soil and/or different pile properties, however the results of these experiments showed set-up with variation in rates which was due to their affective parameters.

The average set-up value measured in this study is compared with some of the past result for driven pile in clay (Figure 4.18). The average rate of set-up for the medium-scale piles used in this study are plotted in a modified graph from past studies. These trends are illustrating a consistent with the results of past studies. However, the marginal alteration may occur mainly due

to the soil properties, and also the level of the disturbance and remoulding during driving the piles compared to other model piles with variation in pile geometry and soil characteristics.

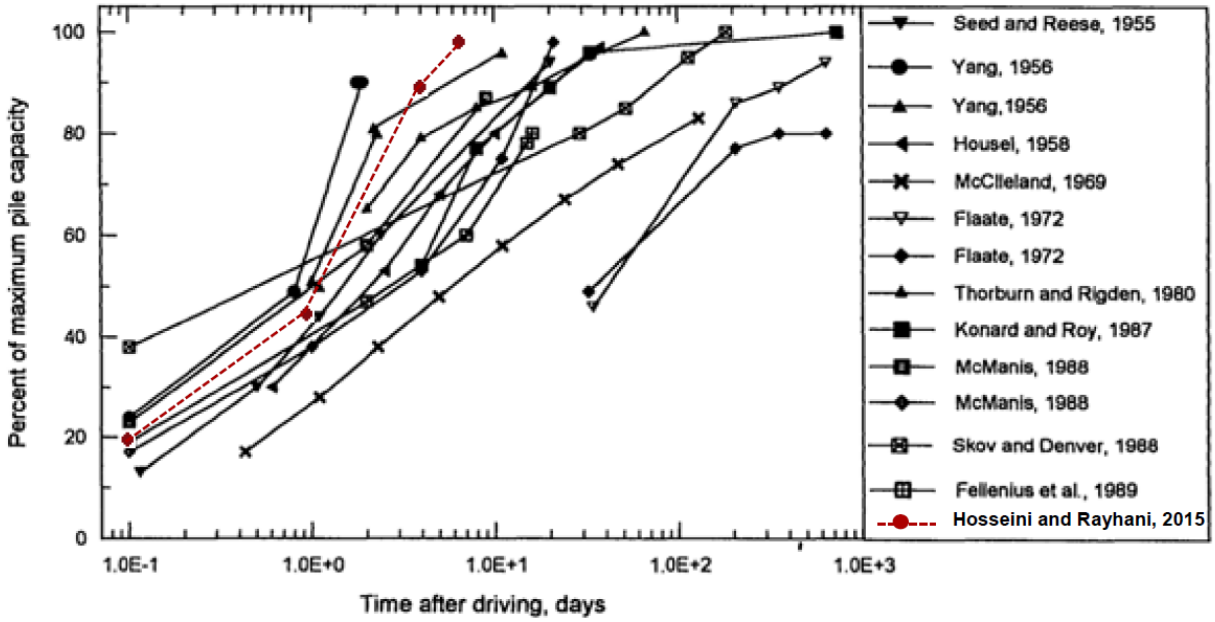

Figure 4.18: Pile capacity increase with time for piles driven into clay (modified from Titi, 1996)

4.10 Contribution of Pile Set-up in Design

4.10.1 Total Stress Analysis (α-method)

Several methods (e.g., Canadian Foundation Engineering Manual) are used in estimating pile capacity as a function of the pile geometry and the interface resistance of pile-soil for pile design. The shaft resistance (Q_s) is often calculated from the following expression:

$$Q_s = CLq_s \qquad (4.3)$$

where C is pile circumference, L is pile embedment length, and q_s is the unit shaft resistance, which is related to pile-soil interface shear strength. The unit shaft resistance is expressed in terms of the undrained shear strength (S_u) and an empirical adhesion coefficient (α) which is shown in following expression:

$$q_s = S_u \alpha \qquad (4.4)$$

The bearing capacity of piles is provided by the shaft and toe resistance. However, these model piles were tested under tensile loading, so the pile capacity only arises from the shaft resistance. The estimated shaft resistance is a simple theoretical value which is calculated and then compared with the measured shaft resistance from the field experiment. The undrained shear strength, Su= 35 kPa for the Leda clay was obtained from vane shear test and this value is used to calculate the design shaft resistance. In addition, the empirical adhesion coefficient (α) is estimated from a reverse calculation using the undrained shear strength and it is approximately 0.44 for initial shaft capacity at the EOID. The outside diameter (D) and pile embedment (L) are 101.6 mm and 2.0 m, respectively.

Table 4.3 summarizes the measured and estimated shaft resistance. The estimated shaft capacity for all three piles is almost 1.5 times the initial measured capacity which was obtained immediately after driving the piles. However, it can be seen that the capacity increased up to 5 times from their initial capacity after 30 days. The result underscores the importance of considering the pile set-up in pile design. Consequently, the implementation of the set-up in design can reduce the number of piles and/or the embedment length of the piles, which would reduce the cost of the construction.

Table 4.3: Summary of measured and estimated shaft resistance

Pile Type	Measured Shaft Resistance (N)		Estimated Shaft Resistance (N)	Rate of Increase
	Initial (Day 0)	*Day 30*		
Precast Concrete	990	6162	1479	4.2
Closed-end Steel	969	4650	1435	3.2
Open-ended Steel	945	5295	1412	3.7

Figure 4.19, illustrates the measured pile capacity of all three piles which were tested in tension and also presents the calculated pile capacity using α-method. It can be seen that the estimated shaft capacity would not consider the increase of the pile capacity over time, and this phenomenon is explained by the dissipation of the excess pore water pressure over time which is occurred due to soil remoulding and disturbance.

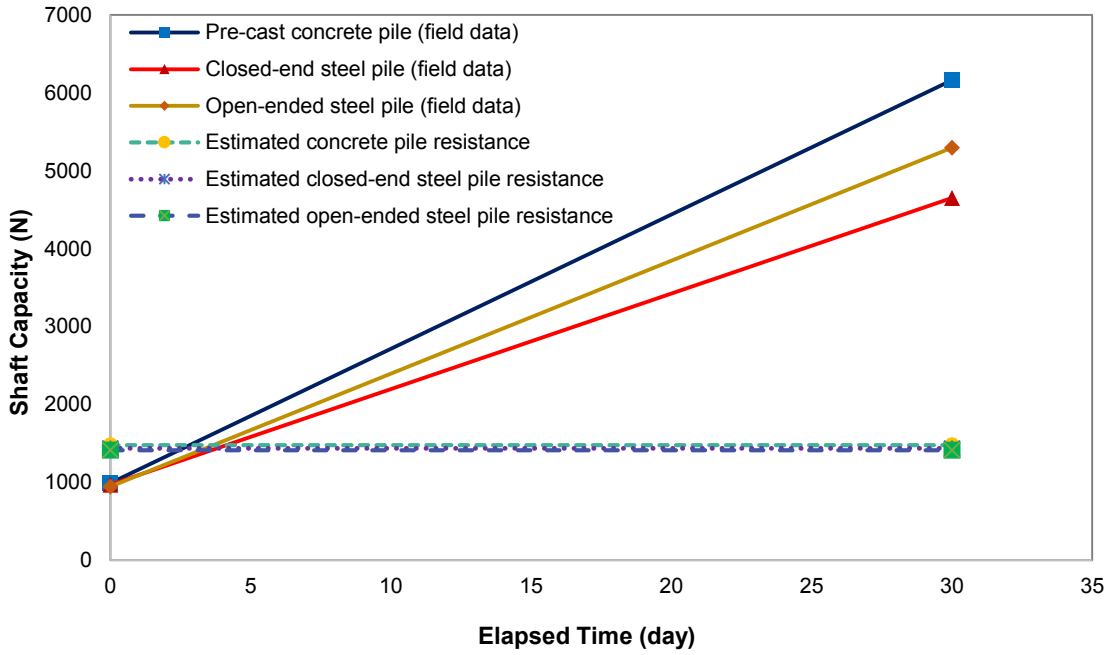

Figure 4.19: Measured and estimated pile shaft capacity

4.10.2 Effective Stress Analysis (β-method)

Using measured shaft capacity for the model piles, the range of β parameter used in the effective stress analysis of the pile in practice can be estimated. The unit shaft resistance is expressed in terms of the effective overburden pressure (σ_v') and an empirical interface coefficient (β) which is shown in following expression:

$$q_s = \beta\sigma_v' = K_s \, tan\delta \, \sigma_v' \qquad (4.5)$$

Table 4.4 presents the estimated β values over time using unit shaft resistance measured at the field and the effective stress, σ_v' (i.e., $\sigma_v' = \gamma' z = (15.3 - 9.81) \times 1 = 5.50\, kPa$). As shown, the β value is approximately at the range of 0.270 to 0.280 for all three piles when tested immediately after driving. Taking into account the evolution of pile capacity over time, the β value increased up to 1.3-1.7 after 30 days from initial driving. This further underscores the importance of considering the pile set up in design of driven piles in clay.

Table 4.4: β values estimated from measured shaft capacity

Pile	**Precast concrete pile**		**Open-ended steel pile**		**Closed-end steel pile**	
Time (day)	**β value**	**K_s**	**β value**	**K_s**	**β value**	**K_s**
0	0.282	0.63	0.276	1.57	0.269	1.53
1	1.07	2.01	0.698	3.49	0.324	1.62
3	1.38	2.96	1.57	6.44	1.44	5.90
7	1.58	-	1.70	-	1.58	-
14	1.59	3.66	1.35	4.77	1.45	5.12
30	1.76	-	1.33	-	1.51	-

These results could also be evaluated using the interface friction angles measured in interface tests discussed in Chapter 3. Considering the measured unit shaft capacities in the field tests, and implementing the initial and final interface friction angles in Equation 4.5, a range of values for the coefficient of lateral earth pressure, K_s, can be estimated. It is found that the lateral earth pressure for initial pile load tests is approximately at the range of 0.6 to 1.5 for concrete and steel piles. The lowest lateral earth pressure was observed for the precast concrete pile while the maximum value was observed for the open-ended steel pile. These values have significantly increased over time to reach a range of 3.6 to over 5.0 considering the evolution of pile-soil interface strength over time.

4.11 Comparison of Measured Pile Capacity with Interface Parameters

In this section, the unit shaft resistance in field and the estimation of the unit shaft resistance based on the interface parameters (i.e., adhesion and interface angle) are evaluated. The unit shaft resistance from interface tests is calculated using the total stress analysis (α-method) and effective stress analysis (β-method). As mentioned, the interface test was measured under two loading rate of fast and slow. The fast loading rate can simulate an undrained condition (total stress analysis) and the slow loading rate may be referred to a drained condition (effective stress analysis). Table 4.5 illustrates the summary of the measured result of unit shaft resistance in field and those estimated using the interface parameters. The unit shaft capacities estimated using the fast load interface test parameters are significantly different from those measured in the field. This could be related to the limitation of direct shear box in simulating undrained loading conditions. The unit shaft capacities estimated using the slow loading interface tests were slightly similar to those

measured in the field. However, the shaft capacities estimated over longer elapsed times are lower than those measured in the field. This could also be attributed to the limitation of direct shear test in proper simulation of the pile-soil interface strength over time.

Table 4.5: Summary of measured and estimated unit shaft resistance for field and interface tests

Time (day)	**Unit Shaft Resistance (kPa)**			**Unit Shaft Resistance using Interface Parameters (kPa)**			
	Precast Concrete Pile	Open-ended Steel Pile	Closed-end Steel Pile	Concrete Interface (α-method)	Steel Interface (α-method)	Concrete Interface (β-method)	Steel Interface (β-method)
0	1.55	1.52	1.48	15.3	11	2.45	1.00
1	5.88	3.84	1.78	16.7	9.7	2.93	1.10
3	7.61	8.62	7.92	18.7	12	2.57	1.34
7	8.70	9.34	8.68	-	-	-	-
14	8.74	7.40	7.99	14.2	15.6	2.39	1.56
30	9.66	7.29	8.30	-	-	-	-

Considering the rate of increase in interface strength, the average increase in pile shaft capacity in the field was approximately 4-5 times their initial capacity 14 days after the initial pile driving. The lowest and highest set-up values were in the range of 4-6, respectively. On the other hand, from the direct shear tests, the rate of increase in pile-soil interface resistance was about 1.5 at fast loading rate for both concrete and steel interface tests. In addition, the rate of increase was approximately 1.3 from the interface analysis of concrete-soil and steel-soil tests at slow loading rate (i.e., in average after 14 days at normal stress of 150 kPa). The lower strength gain in direct shear tests could be related to the nature of those tests, in which the pile driving process cannot be properly simulated using a direct shear apparatus. Due to the lack of such capability, the change in interface shear strength would also be limited as observed in the interface tests conducted here.

4.12 Summary

Presented herein are the summary of results of the field studies conducted on the 100 mm diameter pile segment models including precast concrete, closed-end steel pipe pile and open-ended steel pipe pile. The measurements include tensile load tests which were performed on all three model piles repeatedly at elapsed time of initial day, day 1, 3, 7, 14, and 30. The shaft capacity of all three piles initially was at about 945-990 N. While the pile load test was repeated three days after the initial driving, the load carrying capacity for all three piles was increased approximately 4.5-5.5 times in average from their initial capacity 14 days after the initial pile driving. The lowest and highest set-up values were in the range of 4-6 times, respectively. By measuring the shaft capacity of each pile at different elapsed day, a normalized chart was used to explore and compare the rate of set-up for each pile. The normalization was based on the maximum pile shaft capacity at different elapsed time divided by their initial load capacity measured immediately after pile driving. The rate of increase in pile capacity was significant in the first couple days from initial pile driving. This rate was ultimately decreased as the elapsed time increased up to 30 days; these changes could be due to quick dissipation of excess pore water pressure and possibly greater rate of consolidation of the soil in earlier periods.

Chapter 5: Conclusions and Recommendations

5.1 Conclusions

In this study, evolution of pile capacity over time for piles driven into marine sensitive clay known as Leda clay has been explored in two phases. In the first part, an extensive experimental program was performed to evaluate the evolution of pile-soil interface strength at two shearing rates (fast and slow) over time using modified direct shear tests for both concrete-soil and steel-soil systems. In the second part, a series of medium-scale pile load tests were conducted in the Canadian Geotechnical Research Site No. 1 located in Gloucester, Ontario to evaluate the pile set-up phenomenon in this Leda clay. The following findings are extracted from both the research programs.

- At fast loading rate (2.5 mm/min), the initial shear strength for soil-soil and pile-soil were explored and the result suggested that the interface strength for the pile-soil systems were generally lower than the soil-soil interface. Among the two interfaces, the concrete interface friction angle was significantly higher than the steel interface friction angle (ϕ). The interface shear strength for both concrete-soil and steel-soil systems increased as the consolidation time after the initial shear tests increased up to 14 days. The increase in interface shear strength was attributed to the dissipation of excess pore water pressure for the fast loading rate, which resulted in increase of the interface adhesion and friction angle. For the slow loading rate of 0.05 mm/min, the increase in interface shear strength was attributed to restructuring the disturbed clay at the interface level which is often referred to

as aging. Aging is related to variation in soil properties at a constant effective stress over time which may cause frictional and mechanical changes for both fine-and coarse-grained soils.

- All medium-scale piles driven in Leda clay, experienced an average increase in pile shaft capacity at approximately 4.5-5.5 times their initial capacity, 14 days after initial driving. The lowest and highest set-up values were in the range of 4-6 times, respectively. The result showed that the rate of increase in pile capacity was significant in the first couple of days from the initial pile driving. This rate was ultimately decreased as the elapsed time increased up to 30 days. These changes could be due to quick dissipation of excess pore water pressure and possibly greater rate of primary consolidation of the soil during the early periods (i.e., 1 to 7 days). However, when the change in the rate of set-up is very slow, this is correlated to the aging phase (secondary compression), since the effective stress-related set-up is adequately complete and, hence, the rate of set-up is independent of effective stress during this phase.

- Based on the classified level of displacement, both the displacement pile (closed-end steel pile) and small displacement pile (open-ended pipe) showed similar rate of set-up. This could be related to the small diameter of the piles used here. However, the small displacement pile (i.e., open ended pipe pile) showed slightly higher resistance compared to the displacement piles and this is due to soil plug; therefore using the open-ended steel pile may be a suitable option compared to the closed-end steel pile, since it involves much lower soil disturbance and vibration during driving.
- In conclusion, the precast concrete pile has shown a higher rate of set-up in comparison with the closed-end steel pile and open-ended steel pile, since the precast concrete pile

created a stronger interface bounding with Leda clay due to possible absorbance of water at the interface level.

- As per the results obtained in this study, it is important to consider the set-up in pile design, as it could significantly change the pile capacity. These results might also help in choosing an appropriate time for pile load testing in the field.

5.2 Recommendations for Future Research

The overall results of pile load tests have shown the importance of the set-up phenomenon. However, the presented results are based on a limited number of pile load tests. On the other hand, the pile size used in this research was not sufficient to draw conclusion that can be extended for set-up in displacement and non-displacement piles that can are typically used in practice. A vast experimental pile load test that involves variation of effective parameters in set-up phenomenon, such as pile size, is required in order to reach a more accurate result to create an empirical formulation for all type of piles with variety of sizes which these studies would be valuable to suggest guidelines for use in geotechnical engineering practice for marine sensitive clays such as Leda clay.

5.3 References

Afshin, A. and Rayhani, M. T., 2015. Evaluation of pile shaft capacity increase over time in Leda clay using small-scale pile-load tests. International Journal of Geotechnical Engineering, Volume 9, Issue 3, pp. 307-315.

Appolonia, D.J., 1971. Effects of foundation construction on nearby structures. Proc. of 4th Panamerican Conf. on Soil Mechanics and Foundation Eng., Puerto Rico, pp 189-235.

Asted, B., Weiner, L. and Holm, G. 1992. Increase in bearing capacity with time for friction piles in silt and sand. Proc. Nordic Geotechnical, 411-416.

ASTM D 1143. 2007. Standard test methods for deep foundations under static axial compressive load, West Conshohocken, PA, USA, ASTM.

ASTM D 2216. 2008. Standard test methods for laboratory determination of water (moisture) content of soil and rock by mass, West Conshohocken, PA, USA, ASTM.

ASTM D2435/2435M. 2011. Standard test method for one-dimensional consolidation properties of soils using incremental loading, West Conshohocken, PA, USA, ASTM.

ASTM D 2487. 2008. Standard practice for classification of soils for engineering purposes (unified soil classification system), ASTM Standard 04-08, 249–260, West Conshohocken, PA, USA, ASTM.

ASTM D 2573. 2008. Standard test methods for field vane shear test in cohesive soils, ASTM Standard 04-08, West Conshohocken, PA, USA, ASTM.

ASTM D 3080. 2011. Standard test methods for direct shear test of soils under consolidated drained conditions, West Conshohocken, PA, USA, ASTM.

ASTM D3689.2010 Standard test methods for deep foundations under static axial tensile load, West Conshohocken, PA, USA, ASTM.

ASTM D 422. 2008. Standard test method for particle size analysis of soils, ASTM Standard 04 08, 10–17, West Conshohocken, PA, USA, ASTM.

ASTM D 4318. 2008. Standard test method for liquid limit, plastic limit, and plasticity index of soils, ASTM Standard 04-08, 1–13, West Conshohocken, PA, USA, ASTM.

ASTM D4945, 2012. Standard Test Method for High-Strain Dynamic Testing of Deep Foundations, ASTM International, West Conshohocken, PA, 2012, DOI: 10.1520/D4945-12.

Attwooll, W., Holloway, D., Rollins, K., Esrig, M., Sakhai, S., Hemenway, D., 1999. Measured pile setup during load testing and production piling. Transportation Research Record: Journal of the Transportation Research Board. Vol. 1663, Paper No. 99-1140.

Axelsson, G., 1998. Long-term setup of driven piles in non-cohesive soils. Licentiate Thesis, Royal Institute of Technology, Stockholm.

Axelsson, G., 2002. A conceptual model of pile setup for driven piles in noncohesive soil. GSP 116, ASCE, 64-79.

Azzouz, A. S., Baligh, M. M. and Whittle, A. J. 1990. Shaft resistance of pile in clay. Journal of Geotechnical Engineering, 116, (GT2), 205–221.

Azzonz, A. S., and Lutz, D. G., 1986. Shaft behavior of a model pile in plastic empire clay. Journal of Geotechnical Engineering, ASCE, Vol. 112, No. GT4, pp 389-406.

Azzouz, A. and Morrison, M. 1988. Field measurements on model pile in two clay deposits. Journal of Geotechnical Engineering, 114(1), 104–121.

Baligh, M. M. 1985. Strain path method. Journal of Geotechnical Engineering, ASCE, Vol. I ll, No. GT7, pp 1108-1196.

Baligh, M. M. 1986a. Undrained deep penetration, I: shear stresses. Geotechnique, Vol. 36, No. 4, pp 471-485.

Baligh, M. M. 1986b. Undrained deep penetration, II: pore pressures. Geotechnique, Vol. 36, No. 4, pp 487-501.

Banerjee, P. K., Davies, T. G., and Fathallah, R. C., 1982. Behavior of axially loaded driven piles in saturated clay from model studies. Chapter 5 in Developments in Soil Mechanics and Foundation Engineering, Edited by P. K. Banerjee. Applied Science Publishers Ltd., England.

Bjermm, L., Brinch Hansen, J., and Sevaldson, R., 1958. Geotechnical investigation for a quay structure in Horten. N G I, No. 28, 1-17.

Blanchet, R., Tavenas, F., Garneau, R., 1980. Behaviour of friction piles in soft sensitive clays. Canadian Geotechnical Journal, Vol. 17, n 2, p 203-224.

Blessey, W.E., and Lee, P.Y., 1980. Report on Wave Equation Analysis of pile driving in the New Orleans area. Pile Driving Contractors Association of New Orleans Inc.

Bogard, J. D., and Matlock, H., 1990. Application to model pile tests to axial pile design. Proceedings, Offshore Technology Conference, Paper 6376, Houston, Texas, USA.

Bogard, J. D., and Matlock, H., 1990a. In-situ Pile Segment Model Experiments at Empire, Louisiana. Proceedings, Offshore Technology Conference, Paper 6323, Houston, Texas, USA.

Bond, A. J., and Jardine, R. J., 1991. Effects of installing displacement piles in a high OCR clay. Geotechnique, Vol. 41, No. 3, pp 341-363.

Bozozuk, M., Fellenius, B. H., and Samson, L., 1978. Soil disturbance from Pile Driving in sensitive clay. Canadian Geotechnical Journal, Vol 15, pp 346-361.

Broms, B.B., 1966. Methods of calculating the ultimate bearing capacity of piles- A Summary, Sols-Sols No. 18-19, 21-32.

Broms, B. B., 1964a. Lateral resistance of piles in cohesive soils. Journal of Soil Mechanics and Foundations Division, ASCE, 90(2), pp. 27-67.

Broms, B. B., 1964b. Lateral resistance of piles in cohesionless soils. Journal of Soil Mechanics and Foundation Division, ASCE, 90(3), pp. 123-156.

Bullock, P.J., 1999. Pile friction freeze; A Field and Laboratory Study, vol. 1. Ph.D. Dissertation, University of Florida.

Bullock, P., Schmertmann, J., McVay, M., and Townsend, F. 2005. Side shear setup. I: test piles driven in Florida. Journal of Geotechnical Geoenvironmental Engneering, 131(3), 292–300.

Bullock, P., Schmertmann, J., McVay, M., and Townsend, F. 2005. Side shear setup. II: results from Florida test piles. Journal of Geotechnical Geoenvironmental Engneering, 131(3), 301–310.

Burland, J., 1973. Shaft Friction of Piles in Clay a Simple Fundamental Approach. Proc., Ground Engineering, 6(3), pp 48-51.

Camp, W. M. and Parmar, H. S. 1999. Characterization of pile capacity with time in the cooper marl: a study of the applicability of a past approach to predict long-term pile capacity, Emre, Transportation Research Record, 1–19.

Camp III, William M., Wright, William B., and Hussein, Mohamad. 1993. The effect of overburden of pile capacity in a Calcareous Marl. Deep Foundations Institute 18th Annual Members' Conference, pp.23-32.

Canadian Geotechnical Society, 2007. Canadian Geotechnical Engineering Manual. 4th ed. Richmond, BC, BiTech Publishers Ltd.

Carter, J. P., Randolph, M.F., and Worth, C.P., 1980. Some aspects of the performance of open- and closed end piles. Numerical methods in offshore piling, London, 1980, pp. 1650170.

Chandler, R. J., 1968. The shaft friction of piles in cohesive soils in terms of effective stresses. Civil Engineering and Public Works Review, 63, pp 48- 51.

Chow, Y. K., Karunaratne, G. P., Wong, K. Y., and Lee, S. L., 1988. Prediction of load carrying capacity of driven piles. Canadian Geotechnical Journal, Vol. 25, pp 13-25.

Chow, F.C., Jardine, R.J., Brucy, F., and Nauroy, J.F. 1998. Effects of time on capacity of pipe piles in dense marine sand. Journal of Geotechnical and Geo-environmental Engineering, Vol. 124, No. 3, ASCE, pp. 254-264.

Chu, L. M. and Yin, J. H., 2006. Study on soil–cement grout interface shear strength of soil nailing. Geomechanics and Geoengineering: An International Journal, 1(4), p. 259–273.

Chung, K. Y. C., 1988. Excess pore pressure induced by pile driving in sensitive river sediment. Proceedings, 3rd. Int. Seminar on the Application of Stress-Wave Theory to Piles, Ottawa, B. H. Fellenius, Ed., pp 679-888.

Clark, J. I., and Meyerhof, G. G., 1972. The behavior of piles driven in clay I. An investigation of soil stress and pore water pressure as related to soil properties. Canadian Geotechnical Journal, Vol. 9, pp 351-373.

Clark, J. I., and Meyerhof, G. G., 1973. The behavior of piles driven in clay II. Investigation of the bearing capacity using total and effective strength parameters. Canadian Geotechnical Journal, Vol. 10, pp 86-102.

Cooke, R. W., and Price, G., 1973. Strains and displacements around friction piles. Proceedings, 8th ICSMFE, Moscow, Vol. 2, No. 1, pp 53-60.

Coop, M. R, and Wroth, C. P., 1989. Field studies of an instrumented model pile in clay. Geotechnique, Vol. 39, No. 4, pp 679-696.

D' Appolonia, D. J. and Lambe, T. W., 1971. Performance of four foundation on end-bearing piles. JSMFD, ASCE, 97(10), 1359-1377.

De Mello, V. F. B., 1969. Foundations of buildings on clay. State-of-the-Art report. Proc. 7th ICSMFE, 49-136.

De Nicola, A. and Randolph, M. F., 1993. Tensile and compressive shaft capacity of piles in sand. Journal of Geotechnical Engineering, ASCE, 119(12), pp. 1952-1973

Eide, O., Hutchinson, J. N., and Landva, A., 1961. Short and long-term test loading of a friction pile in clay. Proc. 5th Int. Conf. of Soil Mech. and Found. Eng., pp 45-54, Paris.

Esrig, M. I., Kirby, R. C., Bea, R. G., and Murphy, B. S., 1977. Initial development of a general effective stress method for the prediction of axial capacity of piles in clay. Proceedings, Offshore Technology Conference, Houston, Texas, USA.

Fellenius, B. H., and Samson, L, 1976. Testing of drivability of concrete piles and disturbance to sensitive clay. Canadian Geotechnical Journal, Vol 13, pp. 139-160.

Fellenius, B. H., Riker, R. E., O'Brien, J. A., and Tracy, G. R., 1989. Dynamic and static testing in soils Exhibiting setup. Journal of Geotechnical Engineering, ASCE, Vol. 115, No. GT7, pp. 984-1001.

Fellenius, B. 2008. Effective stress analysis and set-up for shaft capacity of piles in clay. From Research to Practice in Geotechnical Engineering: pp. 384-406.

Finno, R.J., Cosmao, T. and Gitskin, B. 1989, Results of foundation engineering congress pile load tests, Results of pile prediction symposium (R.J. Finno, ed.), Geotechnical Special Publication, No.23, Geotechnical Engineering, ASCE, pp.338-355.

Flaate, K., 1968. The bearing capacity of friction piles in clay (in Norwegian). Norway Road Res. Lab., Oslo, 38 p.

Flaate, K., 1972. Effects of pile driving on clays. Canadian Geotechnical Journal, Vol. 9, pp 81-88.

Flaate, K., and Seines P., 1977. Side friction of piles in clay. Proc. 9 Int. Conf. on Soil Mechanics and Foundation Engineering, Tokyo, Japan, Vol. 1, pp 517-522.

Fleming, W. G. K., Weltman, A.J., Randolph, M.F. and Elson, W.K., 1992. Piling Engineering. 2nd Edn, New York: Halsted Press.

Franke, E., 1988. Group action between vertical piles under horizontal loads. W.F. Van Impe, ed., A.A. Balkema, Rotterdam, Netherlands, p. 83 - 93.

Giraldo, J., and Rayhani, M.T., (2014). Load transfer of hollow fiber-reinforced polymer (FRP) piles in soft clay. Transportation Geotechnics, 1(2104): 63-73.

Guang-Yu, Z., 1988. Wave equation applications for piles in soft ground. Proc., 3rd International Conference on the Application of Stress-Wave Theory to Piles (B. H. Fellenius, ed.), Ottawa, Ontario, Canada, pp. 831-836.

Hannigan, P.J., Goble, G.G., Likins, G.E. and Rausche F., 1997. Design and Construction of Driven Piles Foundations. Publication no. FHWA-HI-97-014, WASHINGTON, DC.

Housel, W. S., and Burkey, J. R., 1948. Investigation to determine the driving characteristics of piles in soft clay. Proc. 2nd ICSMFE, Vol. 5,146-154.

Huang, S., 1988. Application of dynamic measurement on long H-Pile driven into soft ground in Shanghai. Proc., 3rd International Conference on the Application of Stress-Wave Theory to Piles (B. H. Fellenius, ed.), Ottawa, Ontario, Canada, pp. 635-643.

Kishida, H. l. and Uesegui, H., 1987. Tests of the interface between sand and steel in simple shear apparatus. Geotechnique, 37(1), pp. 45-52.

Koizumi, Y., and Ito, K., 1967. Field tests with regard to pile driving and bearing capacity of piled foundation. Soil and Foundation, VII (3), pp 30-53.

Komurka, V. E., Wagner, A. B. and Edil, T. B., 2003. Estimating soil/pile set-up, USA WHRP Report No 03-05, Wisconsin Department of Transportation.

Konard, J. M. and Roy, M., 1987. Bearing capacity of friction piles in marine clay. Geotechnique, Vol. 37, No. 2, pp 163-175.

Kraft, L. M., Focht, J. A., and Amerasinghe, S. F., 1981. Friction capacity of piles driven into clay. Journal of the Geotechnical Engineering Division, ASCE, Vol. 107, No. G U I, pp 1521-1541.

Lambe, T. W., and Horn, H. M., 1965. The influence on an adjacent building of pile driving for the M.I.T. materials center. Proceedings, 6th ICSMFE, Montreal, Vol. II, pp 280-284.

Lehane, B. M. & Jardine, R. J. 1994. Displacement–pile behaviour in a soft marine clay. Canadian Geotechnical Journal, 31 No. 2, 181–191.

Leifer, S.A., Kirby, R.C. and Esrig, M.I., 1979. Effect of radial variation in modulus on stress after consolidation around a driven pile. Proc. of the Conference on Numerical Methods in Offshore Piling, London, England, pp. 157-63.

Lemos, L. J. L. and Vaughan, P. R., 2000. Clay-interface shear resistance. Geotechnique, 50(1), pp. 55-64.

Leung, C. F., Radhakrishnan, R., and Tan, S., 1991. Performance of precast driven piles in marine clay. Journal of Geotechnical Engineering, ASCE, Vol. 117, No. 4, pp. 637-657.

Lo, K. Y., and Stermac, A. G., 1965. Induced pore pressures during pile driving operations. Proc. 6th ICSMFE, Vol. 2,285.

Long, J. H., Kerrigan, J. A. and Wysockey, M. H., 1999. Measured time effects for axial capacity of driven piling, J. Transp. Res. Board, 1663, 8–15.

Lukas, R.G., and Bushell, T.D., 1989. Contribution of soil freeze to pile capacity. Foundation Engineering: Current Principles and Practices, Vol. 2, ASCE, pp 991 -1001.

Lupini, J.F., Skinner, A.E., and Vaughan, P.R., 1981. The drained residual strength of the cohesive soils. Geotechnique, 31(2), pp. 181-213.

McCammon, N. R., and Golder, H. Q., 1970. Some loading tests on long pipe piles. Geotechnique, Vol. 20, No. 2, pp 171-184.

McClleland Engineers, 1969. Additional soil investigation. Pile Research Program, block 100, Eugene Island Area. Report to Shell Oil Company.

McManis, K. L., Folse, M. D., and Elias, J. S., 1988. Determining pile bearing capacity by some means other than the engineering news formula. Research Report No. 234, LTRC, Baton Rouge, LA.

McVay, M. C., Schmertmann, J., Townsend, F. and Bullock, P. 1999. Pile friction freeze: a field and laboratory study, Research Report No.

Meyerhof, G. G., 1976. Bearing capacity and settlement of pile foundations. Journal of Geotechnical Engineering Division, ASCE, Vol. 102, No. 3, pp 197-228.

Mitchell, J. K., 1960. Fundamental aspects of thixotropy in soils. JSMFD, ASCE, Vol. 86, No. SM3, pp 19-52.

Mitchell, J. K., 1993. Fundamentals of soil behavior. John Wiley and Sons, New York, pp 437.

Ng, K. W., 2011. Pile setup, dynamic construction control, and load and resistance factor design of vertically-loaded steel H-Piles. Graduate Theses and Dissertations. Paper 11924.

Nishida, Y., 1964. A basic calculation on the failure zone and the initial pore pressure around a driven pile. Proc. of the First Reg. Asian Conf. On Soil Mech. and Found. Eng., Tokyo, 1, pp 217-219.

Orrje, O., and Broms, B., 1967. Effects of pile driving on soil properties. Journal of the Soil Mechanics and Foundation Division, ASCE, Vol. 93, No. SM5, pp 59-73.

Ovando-Shelley, E., 1995. Direct shear tests on Mexico City clay with reference to friction pile behaviour. Geotechnical and Geological Engineering, 13, pp. 1-16.

Paikowsky, S.G. with Contributions from Birgisson from Birgisson, B., McVay, M., Nguyen, Kuo, T., Baecher, C., Ayyab, B., Stenersen, K., O'Malley, K., Chernauskas, L., and O'Neill, M., 2004. Load and Resistance Factor Design (LRFD) for Deep Foundations. NCHRP Report 507, Transportation Research Board, Washington, D.C.

Paikowsky, S.G., LaBelle, V. A., and Mynampaty, R.N., 1995. Static and dynamic time dependent pile behavior. Research Report submitted to the Mass. Highway Department, Geotechnical Section, Boston, Massachusetts.

Pandit, N. S., Chaney, R. C., and Fang, H. Y., 1983. Review of cavity expansion models in soil and its applications. Fritz Laboratory Reports. Paper 2242.

Parry, R. H. G., and Swain, C. W., 1977. Effective stress method of calculating skin friction on driven piles in soft clay. Ground Engineering 10, No. 3, pp 24-26.

Peck, R. B., 1958. A study of the comparative behavior of friction piles. Special Report 36, Highway Research Board.

Potyondy J. G., 1961. Skin friction between various soils and construction materials. Geotechnique, ll (4):831-8.

Poulos, H. G., and Davis, E. H., 1980. Pile foundation analysis and design. John Wiley and Sons Inc.

Preim, M.J., March, R., and Hussein, M., 1989. Bearing capacity of piles in soils with time dependent characteristics. Piling and Deep Foundations, Volume 1, pp. 363-370.

Randolph, M. F. 2003. Science and empiricism in pile foundation design, Geotechnique, 53, (10), 847–875.

Randolph, M. F., and Wroth, C. P., 1979. An analytical solution for the consolidation around a driven pile. International Journal for Numerical and Analytical Methods in Geomechanics, Vol. 3, pp 217-229.

Randolph, M. F., Carter, J. P. and Wroth, C. P., 1979. Driven piles in clay-the effects of installation and subsequent consolidation, Geotechnique, 29 (4), 361–393.

Rouaiguia, A., 2012. Residual shear strength of clay-structure interfaces. International Journal of Civil and Environmental Engineering, 10 (3), pp. 6-18.

Roy, M., Blanchet, R., Tavenas, F. and La Rochelle, P., 1981. Behavior of sensitive clay during pile driving. Canadian Geotechnical Journal, Vol. 18, pp. 67-85.

Satibi, S., Abed, A., Yu, C., Leoni, M., Vermeer, P.A., 2007. FE simulation of installation and loading of a tube-installed pile. Institutsbericht 29, des Instituts für Geotechnik, Herausgeber P. A. Vermeer.

Schmertmann, J. H. 1991. The mechanical ageing of soils, Journal of Geotechnical Engineering, 117, (9), 1288-1330.

Seed, H. B., and Reese, L. C., 1955. The action of soft clay along friction piles. Proceedings, ASCE, Vol. 81, Paper No. 842.

Silvestri, V., Karam, G., Tonthat, A. and St-Amour, Y., 1989. Direct and simple shear testing of two Canadian sensitive clays. Geotechnical Testing Journal, 12 (1), pp. 11-21.

Skov, R. and Denver, H., 1988. Time-dependence of bearing capacity of piles, 3rd Int. Conf. on Applications of stress wave theory to piles, ISSMFE and Canadian Geotechnical Society, Ottawa, Canada.

Soderberg, L. O., 1962. Consolidation theory applied to foundation pile time effects. Geotechnique, Vol. 12, No. 3, pp 217-225.

Sutton, V. J., and Rigden, B. P., 1979. A full scale instrumented pile test in the North Sea. Offshore Technology Conference, Houston, Texas, Paper No. 3489.

Svinkin, M. R., 1996. Setup and relaxation in glacial sand discussion. Journal of Geotechnical Engineering, ASCE, 122(4), pp. 319-321.

Svinkin, M. R. Morgano, C. M., and Morvant, M., 1994. Pile capacity as a function of time on clayey and sandy soils. Proc. of the 5th International conference on Piling and Deep foundations, Deep Foundations Institute, Englewood Cliffs, N.J., 1.11.1-1.11.8.

Svinkin, M.R., and Skov, R., 2000. Setup effect of cohesive soils in pile capacity. Proc. of Int. Conf. of Application of Stress Waves to Piles, Sao Paulo, Brazil, Balkema, pp. 107-111.

Taha, A., and Fall, M., 2013. Shear behavior of sensitive marine clay-concrete interfaces. Journal of Geotechnical Geoenvironmental Engneering, 139(4), 644–650.

Taylor, D.W., 1948. Fundamentals of Soil Mechanics. Wiley, New York.

Thorbum, S., and Rigden, W. J., 1980. A practical study of pile behavior. Proceedings, Offshore Technology Conference, Paper 3825, Houston, Texas, USA.

Titi, H. H., 1996. The increase in shaft capacity with time for friction piles driven into saturated clay. ProQuest Dissertation & Theses (PQDT).

Titi, H. H., and Wathugala, G. W. 1999. Numerical procedure for predicting pile capacity - setup/freeze. Transportation Research Record 1663, Paper No. 99-0942, Transportation Research Board, Washington, D.C., pp. 25-32.

Tomlinson, M., 1957. The adhesion of piles driven in clay soils. Proceedings 4th International Conference on Soil Mechanics and Foundation Engineering, 2, pp. 66-71.

Tomlinson, M. J., 1971. Adhesion of piles driven in clay soils. Proc. 4th Int. Conf.of Soil Mechanics and Foundation Engineering, London, 12, pp 86-71.

Tomlinson, M.J., 1994. Pile design and construction practice. Chapman and Hall Publisher, London.

Tsubakihara Y. and Kishida H., 1993. Frictional behavior between normally consolidated clay and steel by two direct shear type apparatus. Soils and Foundations, 33(2): 1-13.

Uesugi, M. and Kishida, H., 1986. Influential factors of friction between sand and dry sands. Japanese Society of Soil Mechanics and Foundation Engineering, 26(2), pp. 33-46.

Vesic, A. S., 1972. Expansion of cavities in infinite soil mass. International Journal of Soil Mechanics and Foundation Division, ASCE, 98, pp. 265-290.

Wathugala, G. W., and Desai, C. S., 1993. Constitutive model for cyclic behavior of clays. I: Theory. Journal of Geotechnical Engineering, ASCE, Vol. 119, No. GT4, pp. 714-729.

Whitman, R. V. and Healy, K. A. 1962. Shear strength of sands during rapid loading. J. Soil Mech. Found. Div., ASCE 88, No. SM2, 99-132.

Whittle, A., and Sutabutr, T., 1999. Prediction of Pile Setup in Clay. Transportation Research Record: Journal of the Transportation Research Board, Vol. 1663, No. 99-1152.

Woodward, R. J., Lundgren, R., and Boitano, J., 1961. Pile loading tests in stiff clays. Proc. 5th Int. Conf. of Soil Mechanics and Foundation Engineering, Vol. 2, pp. 177-184.

Yang, L., Liang, R., 2006. Incorporating set-up into reliability- based design of driven piles in clay. Canadian Geotechnical Journal, v 43, n 9, p 946-955.

Yang, N., 1956. Redriving characteristics of piles. Journal of Soil Mechanics and Foundation Division, ASCE, Vol. 82, SM3, Paper 1026.

Yin, Z., Karstunen, M., Chang, C., Koskinen, M., and Lojander, M., 2011. Modeling Time-Dependent Behavior of Soft Sensitive Clay. Journal of Geotechnical Geoenvironmental Engneering, 137(11), 1103–1113.

Yoshimi, Y. and Kishida, T., 1981. A Ring torsion apparatus for evaluating friction between soil and metal surfaces. Geotechical Testing Journal, 4(4), pp. 145-152.

Zeevaert, L., 1959. Reduction of point bearing capacity of piles because of negative friction. Proc. of the Pan-American Conference on Soil Mechanics and Foundation Engineering, Mexico, 3, pp. 1145-1152.

Appendix A

Interface testing lab photos and sheared interfaces

Figure A-1: Soil shearing interface

Figure A-2: Concrete- soil interface

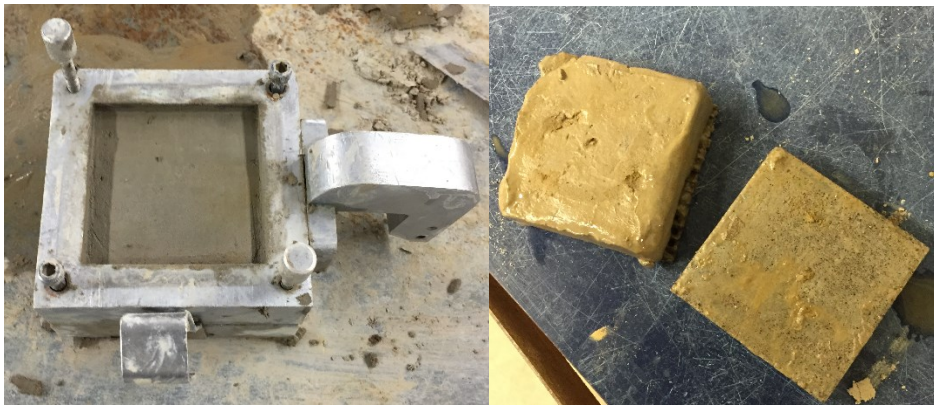

Figure A-3: Steel-soil interface

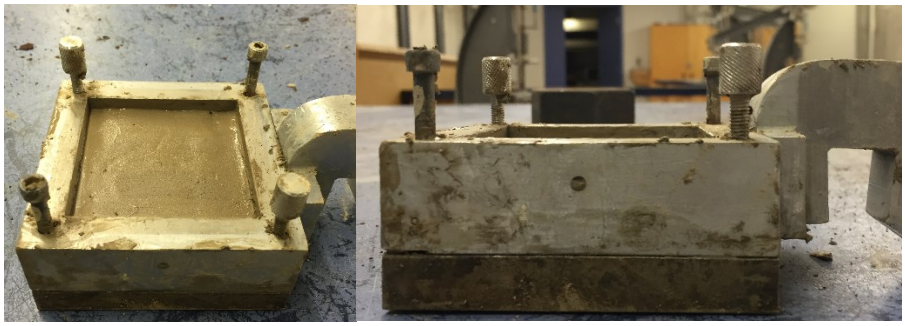

Figure A-4: Direct Shear Apparatus

Appendix B

Dataset of interface testing program

Concrete-clay direct shear test results over time (fast loading rate)

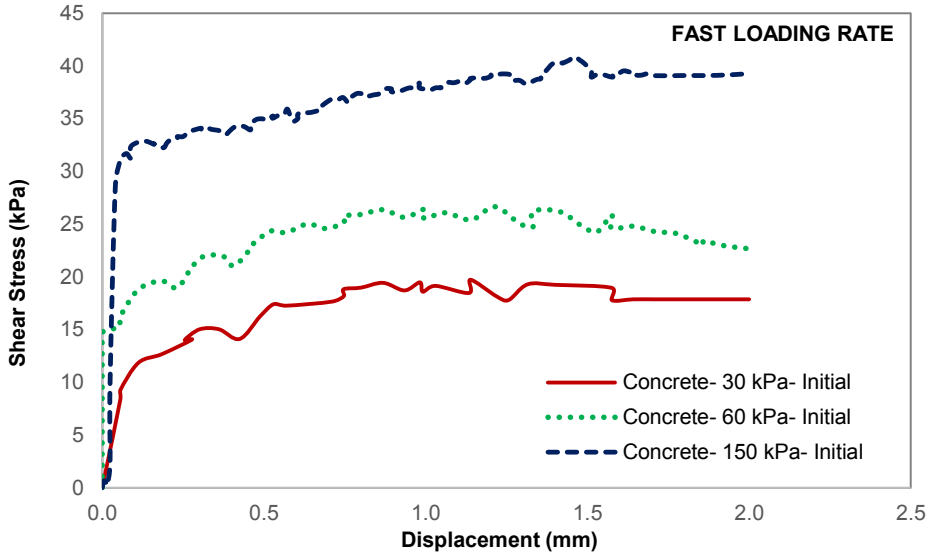

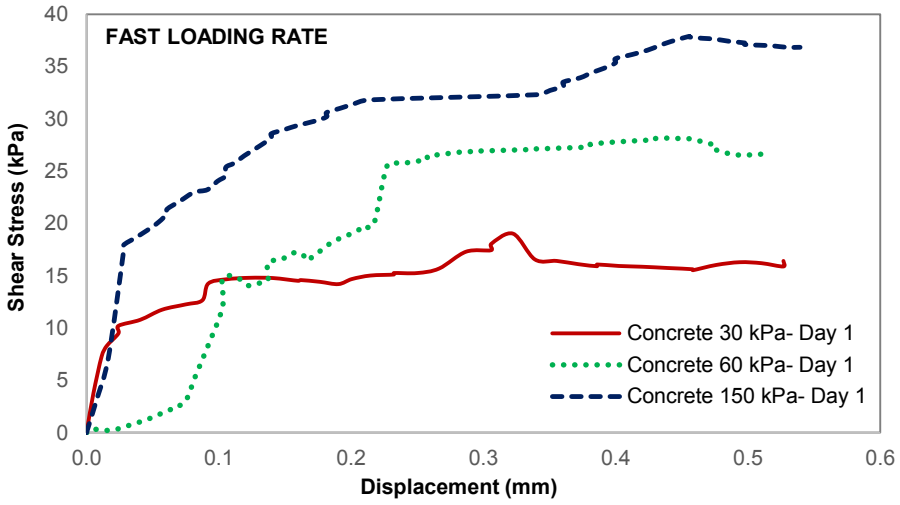

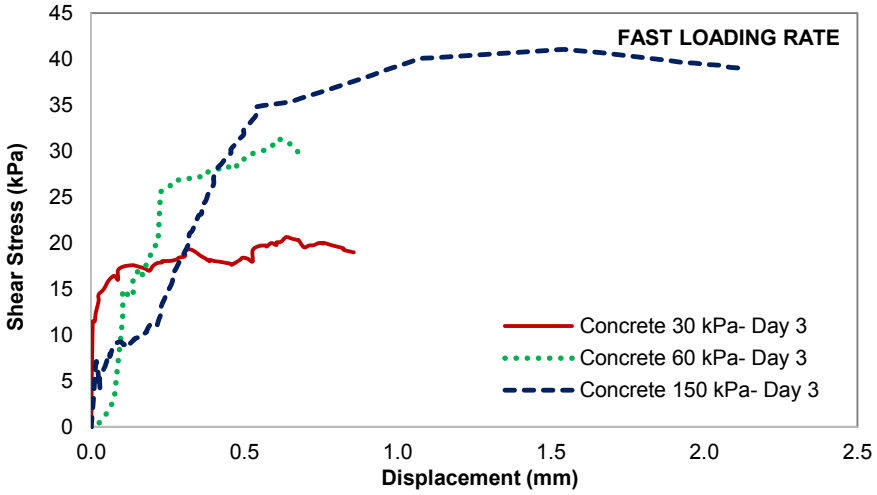
FAST LOADING RATE
Shear Stress (kPa)
Displacement (mm)
Concrete 30 kPa- Day 3
Concrete 60 kPa- Day 3
Concrete 150 kPa- Day 3
0
5
10
15
20
25
30
35
40
45
0.0
0.5
1.0
1.5
2.0
2.5

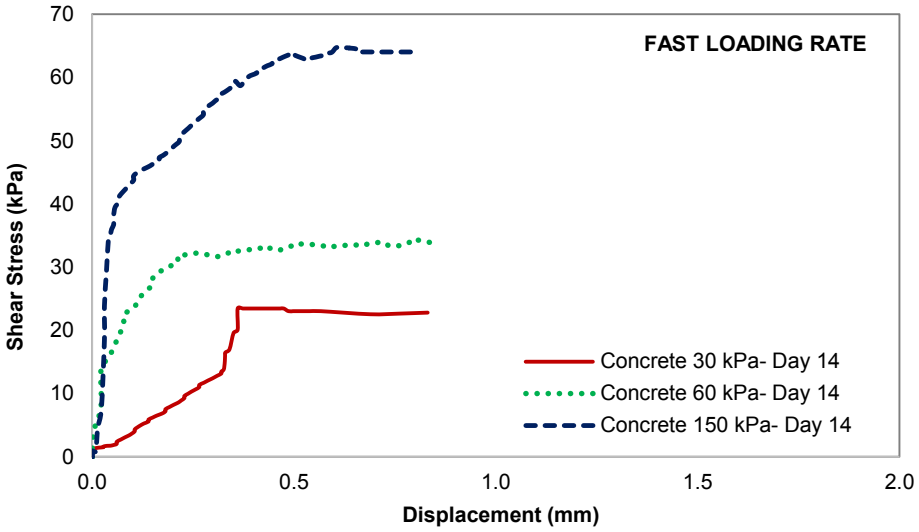
FAST LOADING RATE
Shear Stress (kPa)
Displacement (mm)
Concrete 30 kPa- Day 14
Concrete 60 kPa- Day 14
Concrete 150 kPa- Day 14
0
10
20
30
40
50
60
70
0.0
0.5
1.0
1.5
2.0

Steel-clay direct shear test results over time (fast loading rate)

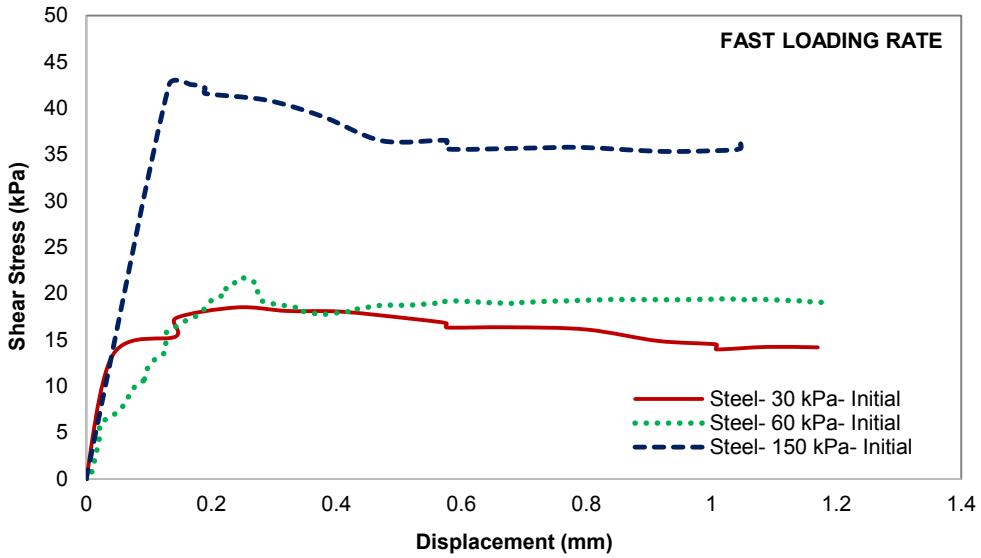

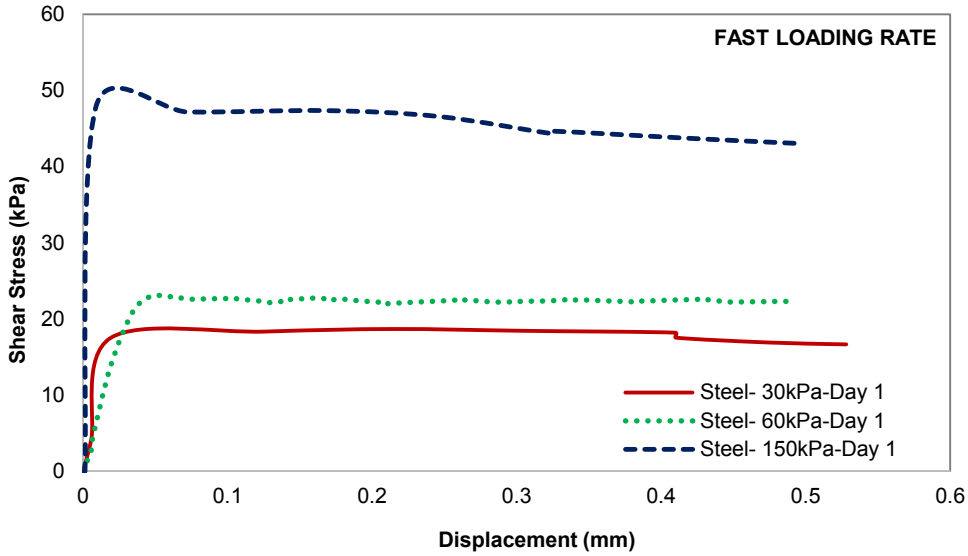

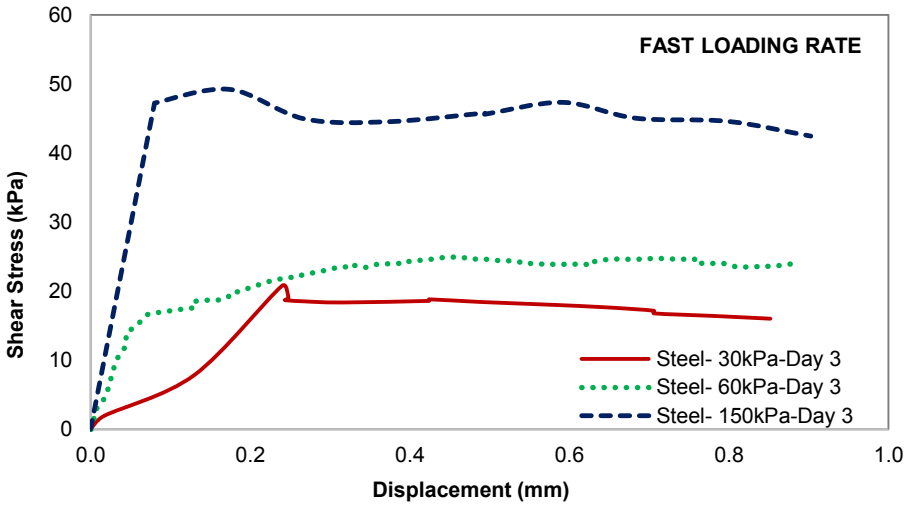
FAST LOADING RATE
Shear Stress (kPa)
Displacement (mm)
Steel- 30kPa-Day 3
Steel- 60kPa-Day 3
Steel- 150kPa-Day 3
0
10
20
30
40
50
60
0.0
0.2
0.4
0.6
0.8
1.0

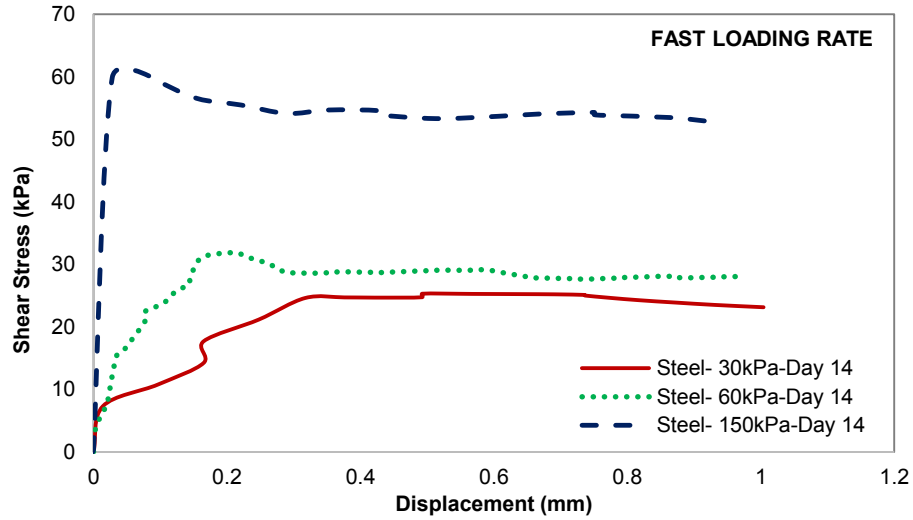
FAST LOADING RATE
Shear Stress (kPa)
Displacement (mm)
Steel- 30kPa-Day 14
Steel- 60kPa-Day 14
Steel- 150kPa-Day 14
0
10
20
30
40
50
60
70
0
0.2
0.4
0.6
0.8
1
1.2

Concrete-clay direct shear test results over time (slow loading rate)

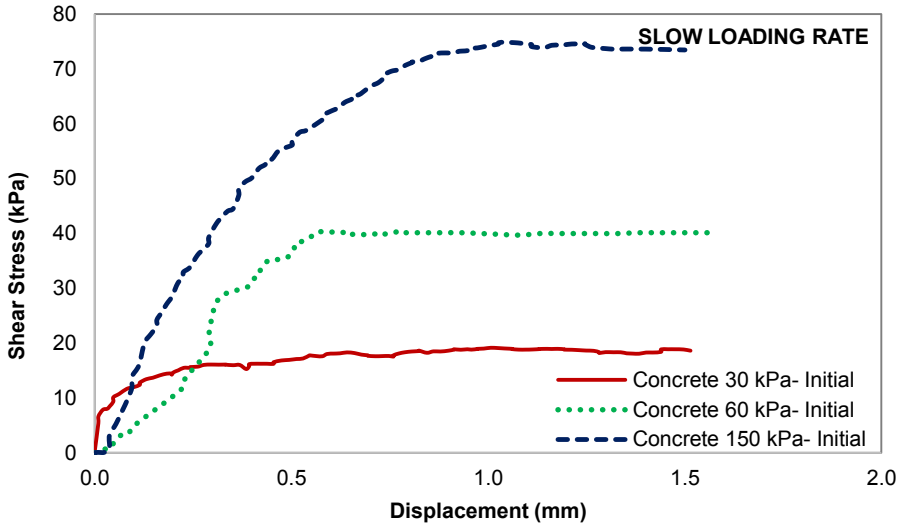

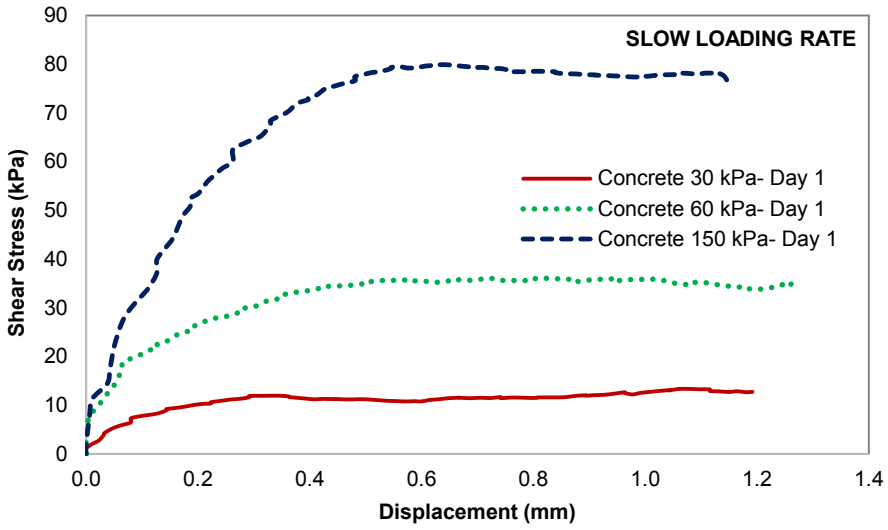

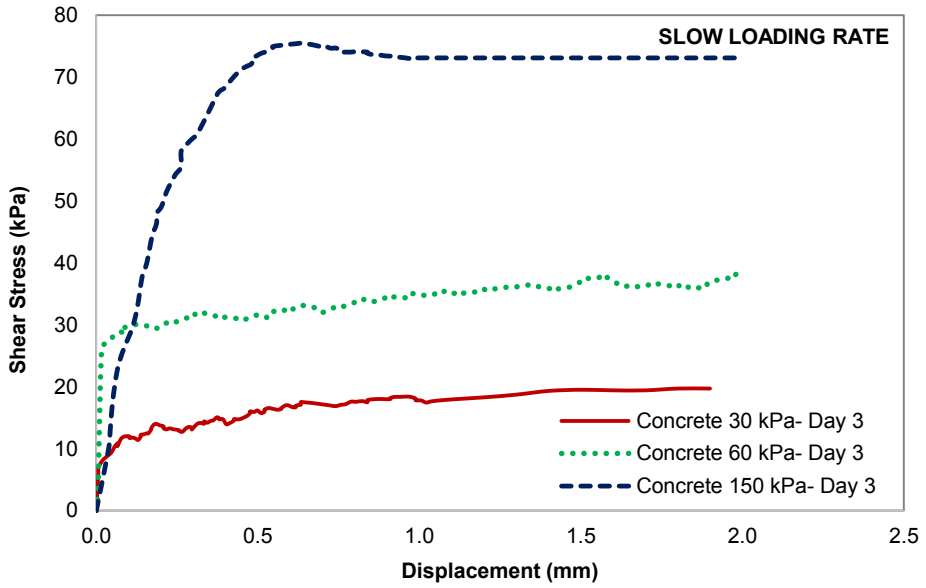
SLOW LOADING RATE
Shear Stress (kPa)
Displacement (mm)
Concrete 30 kPa- Day 3
Concrete 60 kPa- Day 3
Concrete 150 kPa- Day 3
0
10
20
30
40
50
60
70
80
0.0
0.5
1.0
1.5
2.0
2.5

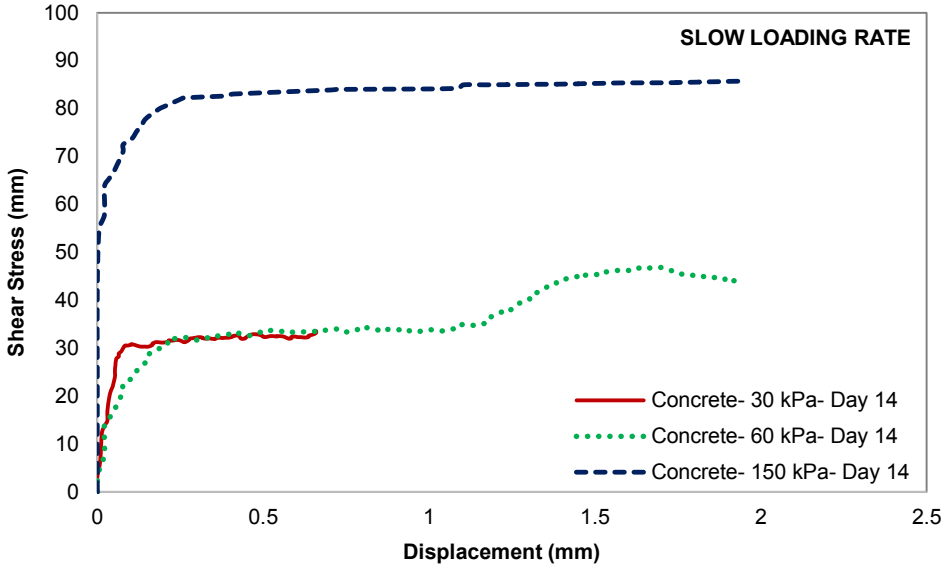
SLOW LOADING RATE
Shear Stress (mm)
Displacement (mm)
Concrete- 30 kPa- Day 14
Concrete- 60 kPa- Day 14
Concrete- 150 kPa- Day 14
0
10
20
30
40
50
60
70
80
90
100
0
0.5
1
1.5
2
2.5

Steel-clay direct shear test results over time (slow loading rate)

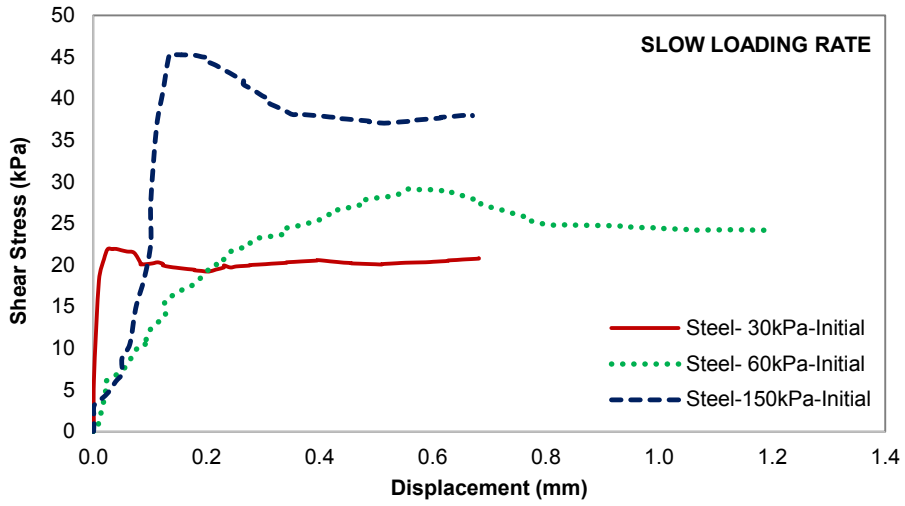

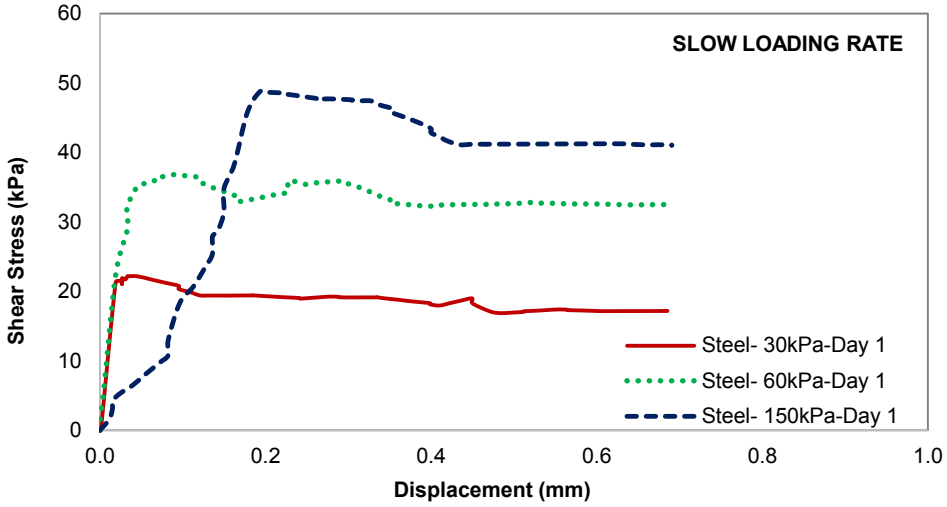

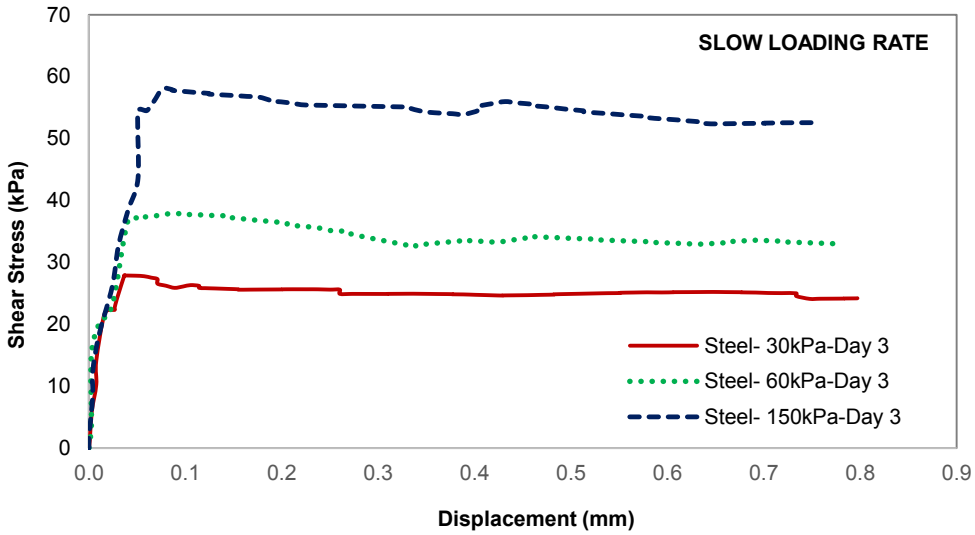
SLOW LOADING RATE
Shear Stress (kPa)
Displacement (mm)
Steel- 30kPa-Day 3
Steel- 60kPa-Day 3
Steel- 150kPa-Day 3
0
10
20
30
40
50
60
70
0.0
0.1
0.2
0.3
0.4
0.5
0.6
0.7
0.8
0.9

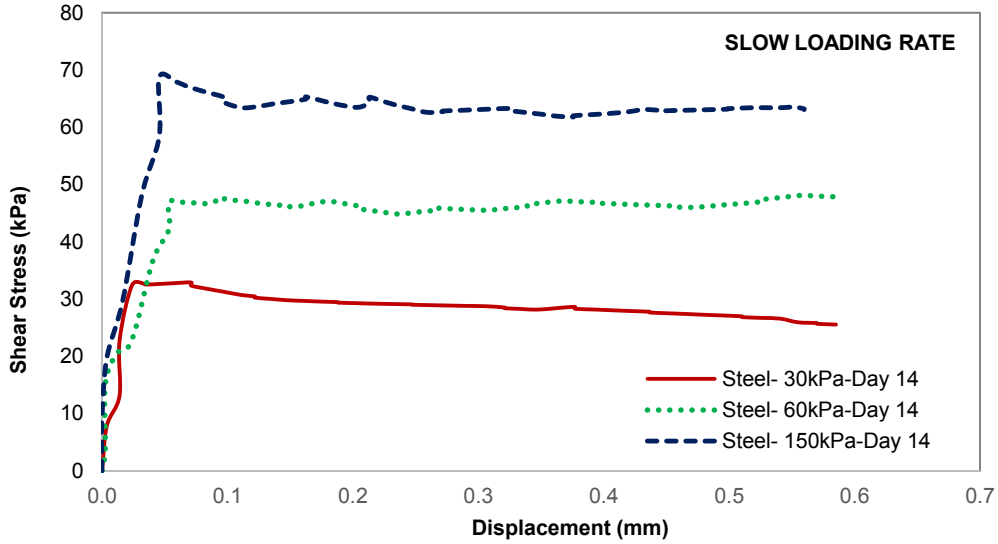
SLOW LOADING RATE
Shear Stress (kPa)
Displacement (mm)
Steel- 30kPa-Day 14
Steel- 60kPa-Day 14
Steel- 150kPa-Day 14
0
10
20
30
40
50
60
70
80
0.0
0.1
0.2
0.3
0.4
0.5
0.6
0.7

Appendix C

Figure C-1 (a): Specification of the vibrating wire piezometer

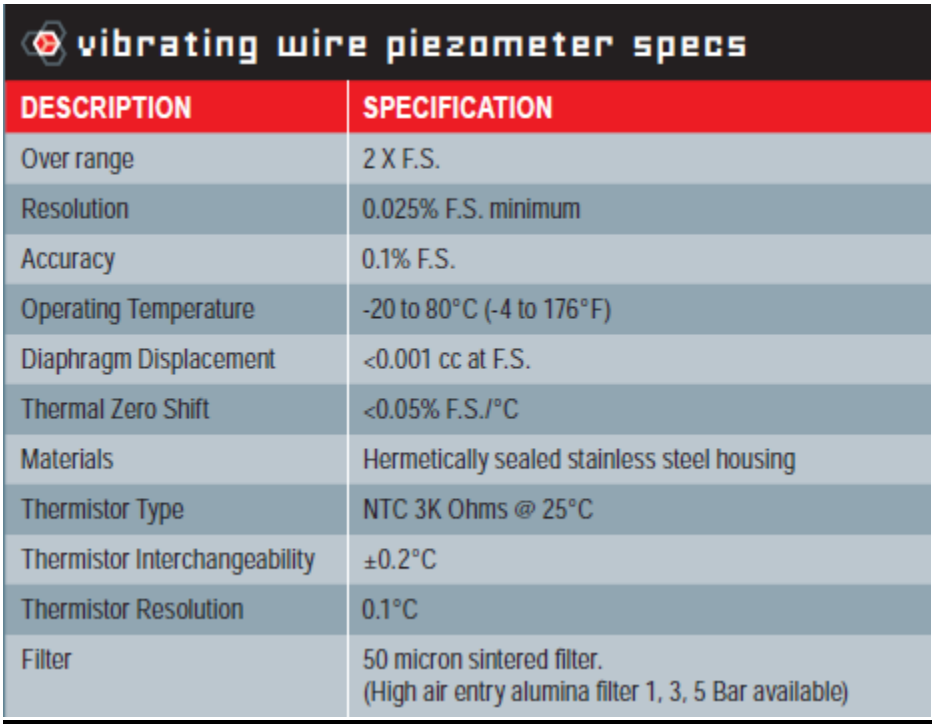

vibrating wire piezometer specs

DESCRIPTION	SPECIFICATION
Over range	2 X F.S.
Resolution	0.025% F.S. minimum
Accuracy	0.1% F.S.
Operating Temperature	-20 to 80°C (-4 to 176°F)
Diaphragm Displacement	<0.001 cc at F.S.
Thermal Zero Shift	<0.05% F.S./°C
Materials	Hermetically sealed stainless steel housing
Thermistor Type	NTC 3K Ohms @ 25°C
Thermistor Interchangeability	±0.2°C
Thermistor Resolution	0.1°C
Filter	50 micron sintered filter. (High air entry alumina filter 1, 3, 5 Bar available)

Figure C-1 (b): Vibrating wire piezometer properties

PART #	DESCRIPTION	PRESSURE RANGE	DIMENSION
VW2100	Standard model for general applications.	0.35, 0.7, 1.0, 2.0, 3.0 MPa	19 mm Ø X 130 mm

Figure C-1 (c): Standard vibrating wire piezometer

Figure C-2: Specification of the vibrating wire reader

VW2106 Vibrating Wire Readout shown with Vibrating Wire Piezometer

DESCRIPTION	SPECIFICATION
Vibrating Wire Readout Excitation Range	400 Hz to 6000 Hz, 5 V Square Wave
Vibrating Wire Readout Resolution	0.01 µs
Vibrating Wire Readout Timebase Accuracy	±50 ppm
Supported Temperature Readout Sensors	NTC3000 (standard), NTC2252, NTC10K, RTD
Temperature Readout Accuracy	±0.1°C
Temperature Readout Range	-50°C to 80°C
Display	Graphic 128 x 64 pixels large character display
Display Backlight	High efficiency LCD with auto off
Max Instrument Locations	254
Memory Capacity	11,400 custom labelled points
Location Identification String	Up to 20 characters
Download Speed	15 seconds (full memory)
Battery	3 "AA" alkaline
Battery Indicator	On-screen, low battery indicator
Operating Temperature	-20°C to 60°C
Dimensions	W 22 cm x D 19 cm x H 9.5 cm (8.75 x 7.5 x 3.75in.)
Weight	1.1 kg (2.4 lbs)